Lawrence Berkeley Laboratory
UNIVERSITY OF CALIFORNIA

Materials & Molecular Research Division

CONVOLUTION TECHNIQUES IN ANALYTICAL ELECTROCHEMISTRY

Jeffrey James Toman
(Ph.D. thesis)

June 1982

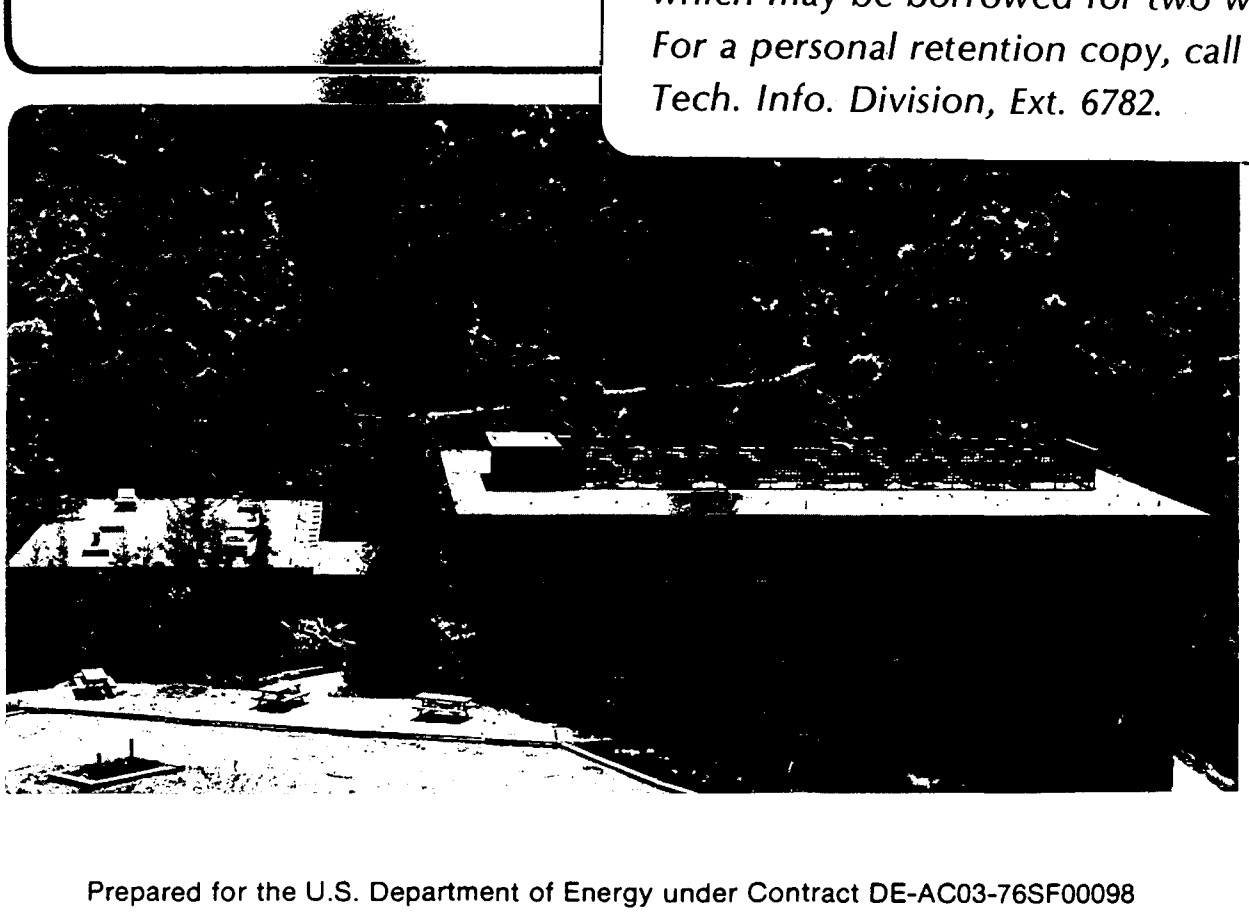

Prepared for the U.S. Department of Energy under Contract DE-AC03-76SF00098

DISCLAIMER

LBL-14429

CONVOLUTION TECHNIQUES IN ANALYTICAL ELECTROCHEMISTRY

Jeffrey James Toman

Ph.D. thesis

June 1982

Materials and Molecular Research Division
Lawrence Berkeley Laboratory
University of California
Berkeley, CA 94720

This work was supported by the Assistant Secretary of Nuclear Energy, Office of Commercial Nuclear Waste Management, Commercial Waste Management Program Division of the U.S. Department of Energy under Contract No. DE-AC03-76SF00098 through the Battelle Memorial Institute, Office of Nuclear Waste Isolation (ONWI), Columbus, Ohio.

CONVOLUTION TECHNIQUES IN ANALYTICAL ELECTROCHEMISTRY

by

JEFFREY JAMES TOMAN

Chapter 1

The application of curve fitting techniques to convolution potential sweep voltammetry, called convolutive voltammetric curve fitting, is described. Fitting functions are derived from theoretical relations among semiintegral, current, and potential. Use of these fitting functions allows the return of more mechanistic information than was previously possible. Validity of the techniques is determined by application to artificial voltammograms created by digital simulation methods. The validity of semiderivative voltammetric curve fitting in fitting waves of several kinetic mechanisms is also investigated.

Chapter 2

The usefulness of semiderivative voltammetric curve fitting (s.v.c.f.) is determined in application to real linear sweep and anodic stripping voltammograms. An experimental setup is described in

which data acquisition and experimental control are performed solely by a dedicated laboratory microcomputer. S.v.c.f. is successful in the fitting of classically reversible voltammograms, and kinetically controlled anodic stripping voltammograms, but is not successful in fitting kinetically controlled linear sweep voltammograms. Effects of perturbing influences on the method are discussed.

Chapter 3

Semiderivative voltammetric curve fitting is used for the resolution of overlapped linear sweep and anodic stripping voltammetric waves. The method is successful in the resolution of voltammograms of nearly classically reversible systems at peak separations of 40 mV. Effects of homogeneous kinetics and residual current on resolution are discussed, as well as enhancement of resolution through constraining peak widths.

Chapter 4

A new method for the numerical evaluation of the convolution integrals found in the solution of electrochemical boundary value problems is discussed. The method leads to the application of convolution techniques to more complex electrochemical systems than was previously possible. The method is derived from relations for concentration profiles of electroactive species in the Laplace

transform domain, and uses the discrete Fourier transform to create a time domain convoluting sequence. The method works in the derivation of the convoluting sequence used to evaluate the semiintegral, and is discussed in application to more complex systems.

Acknowledgement

Far too many people have assisted the author in his time in graduate school for him to be able to thank them individually; I wish to thank all of my friends for encouragement when times were bad. There are some people, though, whose names must be mentioned. Firstly, I would like to thank my research advisor Steve Brown for all of his assistance, and patience when (on occasion) it did not appear if I knew exactly what I was doing. I would like to thank all of the members of the Brown group, and especially Teri Brown, for assistance and many stimulating discussions. I would like to thank Jerry Bucher for his great help in all of my endeavors, and Norman Edelstein for financial support.

I would like to express my most sincere appreciation to my parents, for encouragement whenever things were bad. Lastly, and most importantly to me, I would like to thank my wife, Mary Adams Toman, for her incredible patience and understanding.

This work was supported by the Assistant Secretary of Nuclear Energy, Office of Commercial Nuclear Waste Management, Commercial Waste Management Program Division of the U.S. Department of Energy under Contract No. DE-AC03-76SF00098 through the Battelle Memorial Institute, Office of Nuclear Waste Isolation (ONWI), Columbus, Ohio.

Table of Contents

List of Tables

List of Figures

CHAPTER 1

CONVOLUTIVE VOLTAMMETRIC CURVE FITTING

1.1 INTRODUCTION

Linear sweep voltammetry (lsv) has several advantages as compared to other dynamic electrochemical techniques. These include a much larger dynamic range of scan rates, simpler instrumentation, and a simpler physical description of the electrochemical system. For many years, however, d.c. polarography was the dynamic electrochemical method of choice both for analytical determinations and for investigations of the physical properties of electrochemical systems. This was because the observed current-potential function in lsv, called the voltammogram, is a broad, asymmetric wave (Figure 1.1), as compared with the sigmoidally shaped polarogram.

The renaissance of electrochemistry that took place in the early 1960's resulted in electrochemical techniques that have to some extent combined the advantages of lsv and dc polarography. The renaissance was caused by the introduction of operational amplifier technology to electrochemical instrumentation; important results of this development are potential step methods such as differential pulse polarography (1-4), and square wave voltammetry (5-7), and also the potential sweep technique of ac voltammetry (8-9). The physical description of the electrochemical system for these methods is more complex than in lsv. As a consequence, except for ac voltammetry, the resultant current-potential functions for the new techniques are not describable by simple expressions such as the Heyrovsky-Ilkovic equation in dc polarography. This makes interpretation of the waveform difficult. In addition, scan rates for these techniques are still limited in

dynamic range as compared to lsv.

There is a more far-reaching rebirth in electrochemistry today, caused by the appearance of low cost laboratory microcomputer and microprocessor technology. Applications of microcomputers and microprocessors in analytical chemistry are legion; this is evidenced not only by the number of reviews of computer applications in the mainstream of analytical literature (see, for example, Refs. 10-16) but also by the appearance of journals devoted solely to applications of computers to chemical problems. Such journals include Computers in Chemistry, the Computer Techniques and Optimization volumes of Analytica Chimica Acta, and a new Chemometrics review in Analytical Chemistry, among others.

For research scientists there are at least two major motives for computerization. One is that computers, especially for complex procedures, can control experimental conditions quite precisely. This leads to increased precision in the results of complicated electrochemical techniques (17) such as linear sweep voltammetry, anodic stripping voltammetry and potentiometric stripping analysis (18-24). The second motive is that computers, when coupled with rapid analog to digital converters, have the ability to take and store large amounts of digitized data. This makes possible the routine application of sophisticated numerical techniques for the purposes of signal to noise enhancement, resolution enhancement, or both.

This work discusses the application of one such numerical technique, called convolutive potential sweep voltammetry, (or

c.p.s.v.), to the analysis of linear sweep voltammograms. Convolutive potential sweep voltammetry in many cases can effect the transformation of the broad lsv waveshape into a form as tractable as that of a dc polarogram. The transformed lsv wave is describable by a simple analytic function, which makes possible, by means of curve fitting, both signal to noise enhancement and resolution enhancement. Furthermore, because convolutive potential sweep voltammetry has a rigorous theoretical basis, physical properties of the electrochemical system are easily determinable from the transformed wave. The advantages of c.p.s.v., along with the other advantages of lsv, make linear sweep voltammetry coupled with convolutive analysis the method of choice for many analytical and physical chemistry investigations.

This work will investigate the curve fitting of lsv waves that have been transformed by means of c.p.s.v.; the technique will be referred to as convolutive voltammetric curve fitting, or c.v.c.f. C.v.c.f. is applied to simple charge transfer reactions. An exact theory for analysis of charge transfer reactions will be presented. Using this theory, information about many of the parameters of a simple electrode reaction can be deduced from a single scan; as will be shown, this exact theory allows more information to be gained from the more complicated quasi-reversible system than from the simpler reversible or irreversible charge transfer systems. In addition, a simpler, more empirical view of the theory will be presented to make possible enhancement of the resolution of overlapped peaks of non-reversible charge transfers. The usefulness of either method of analysis will be demonstrated by application to artificial lsv data

created by digital simulation.

This work will also investigate the application of c.v.c.f. techniques to electrochemical systems that also include effects due to homogeneous chemical reactions. As for the simple charge transfer, an exact theory is developed which allows information about the nature of the homogeneous chemical reaction to be deduced from a single scan; this information is gleaned from analysis of more complex electrochemical systems than have been heretofore used for analysis. As a bonus this theory results in the separation of the homogeneous kinetic effects from the electrode kinetic effects, thus allowing the return of information about both. In addition to the exact theory, the same semi-empirical treatment of the data as discussed for the simple charge transfer reaction will be applied to the systems with complicating homogeneous kinetics, with an eye towards the resolution of overlapped kinetic peaks. These approaches will be demonstrated by application to artificial lsv data for the CE and EC kinetic mechansisms. The data will be created by digital simulation.

1.2 LINEAR SWEEP VOLTAMMETRY

Convolutive potential sweep voltammetry is derived from the results of linear sweep voltammetric theory, although as stated above c.p.s.v. leads to more easily interpreted waveforms. To appreciate this, it is first necessary to review results of linear sweep voltammetric theory. In particular the discussion of the theory to

follow will stress the importance of the concept of limiting cases of kinetic behavior in the systems considered.

The literature on lsv is quite extensive (25-29). Typical applications of lsv have been to problems in quantitative analysis, the determination of stability constants, and investigations of kinetic mechanisms. Linear sweep voltammetry is more formally known as linear potential sweep chronoamperometry. Called by either name, the technique consists of varying the potential between an ideally polarizable electrode, called the working electrode, and an ideally non-polarizable electrode, called the reference electrode. The potential between these two electrodes is varied as a linear function of time, hence the name of the technique. The current between the working electrode and another polarizable electrode, called the counter electrode, is monitored as a function of the applied potential. A typical current function observed in lsv is shown in Figure 1.1.

Although lsv as a technique dates back to 1938 (30), theoretical development waited for another ten years until the work of Randles (31) and Sevcik (32). The problem of the reversible charge transfer at a planar electrode was solved independently by these two men. Another seven years passed until the treatment of the irreversible charge transfer (33), but after this time advances in the theory of linear sweep voltammetry occurred rapidly. Several reviews have been written on the theory of many electrochemical mechanisms (34-36); the book by Galus (35) is a particularly helpful reference work for

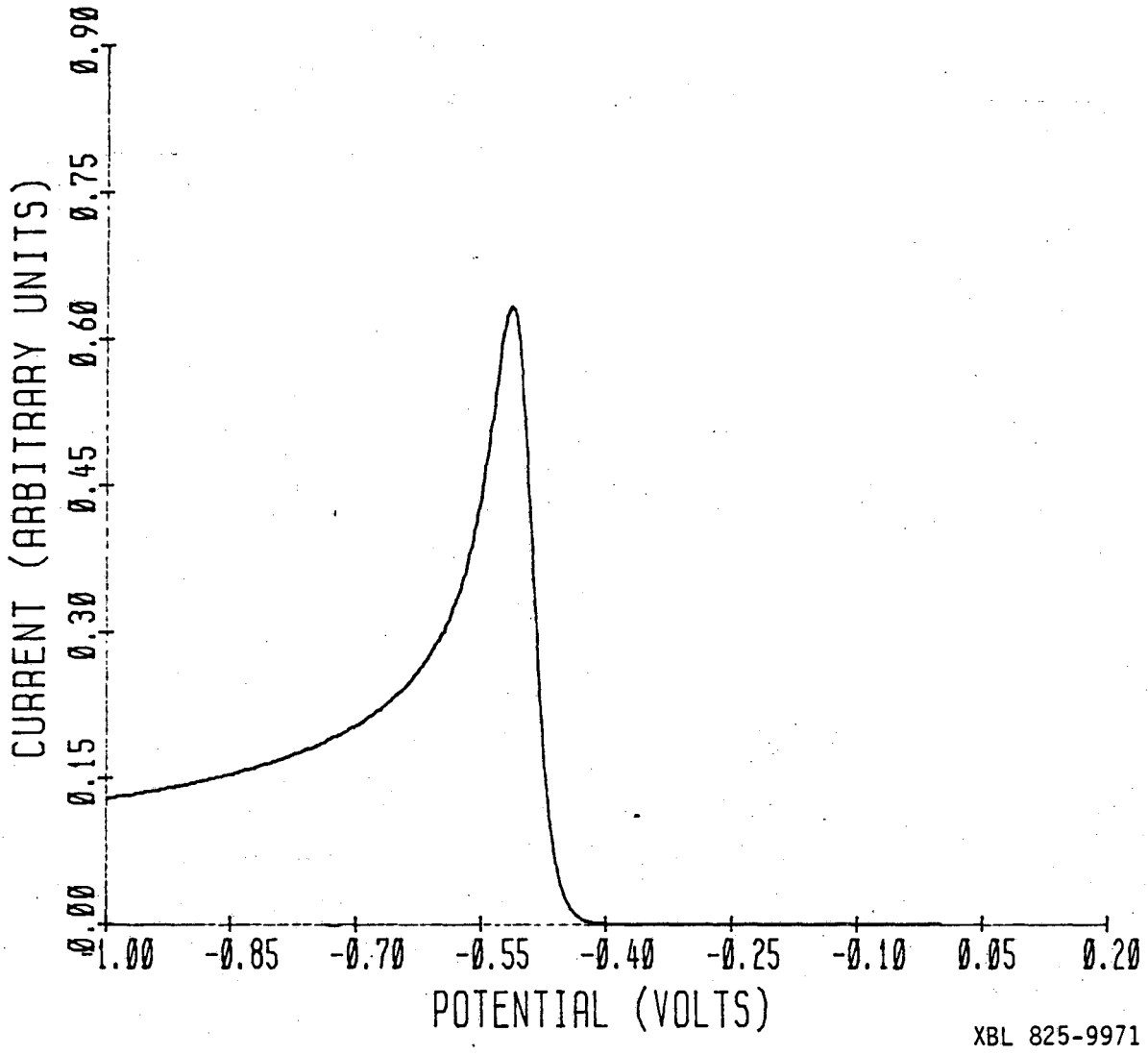

Figure 1.1: Linear sweep voltammogram of a reversible system.

discussion on the theory developed to date.

1.2.1 Charge transfer systems

The theory for the treatment of reversible, irreversible and quasi-reversible charge transfer systems without complicating homogeneous kinetics was first fully developed by Matsuda and Ayabe (37), although the paper by Nicholson and Shain (38) is often referenced with regard to this system. The system is defined by the simple charge transfer reaction

$$Ox + ne^- \overset{k^o}{=} Red \qquad (1.2.1)$$

where k^o is the charge transfer rate constant for the electrode reaction,and in general may assume any value.

The theory that predicts the behavior of any electrochemical system is derived from the solution of the boundary value problem that describes mass transport in the given system. The specification of the boundary value problem for the general charge transfer reaction is the same as that of the reversible charge transfer, except that the Nernst relation is replaced by the Butler-Volmer relation. The general solution to the boundary value problem of the simple charge transfer is that of the quasi-reversible charge transfer. In the past this solution was too complex to be of much use. This was a universal feature of the solutions to the boundary value problems. There are for most systems limiting cases of kinetic behavior in which the

solutions are simplified, and it is for these cases that useful relations have been derived.

For the simple charge transfer there are two limiting cases of kinetic behavior in which the solution may be simplified. These cases occur as k^o becomes infinitely large or small. Matsuda and Ayabe (37) describe the behavior of a charge transfer system in terms of a dimensionless charge transfer rate constant Λ, which is defined as

$$\Lambda = \frac{k^o}{\sqrt{D_{ox}\nu}} \left(\frac{RT}{nF}\right)^{1/2} \qquad (1.2.2)$$

where D_{ox} is the diffusion constant for the oxidized species, and ν is the scan rate. Figure 1.1 shows the shape of the lsv wave of a system with a reversible charge transfer.

One limiting case of behavior occurs as Λ becomes very large. For $\Lambda > 15$, the charge transfer reaction is called reversible. For the reversible charge transfer system, the peak current in amperes is given by

$$i_p = (2.69 \times 10^5)\, n^{3/2}\, A\, C^*_{ox}\, \sqrt{D_{ox}\nu} \qquad (1.2.3)$$

where n is the number of elections transferred, A is the surface area of the electrode and C^*_{ox} is the bulk concentration of the oxidized species. If A is in cm^2, D_{ox} in cm^2/s, C^*_{ox} in moles/cc, and ν in V/s, then i_p is in amperes. This equation shows the linear relation between peak height and concentration, which is useful in quantitative

analysis.

One relation for the potential at the maximum of the reversible lsv wave (the peak potential) is

$$E_p = E^r_{1/2} - 1.109 \frac{RT}{nF} \qquad (1.2.4)$$

where $E^r_{1/2}$ is the reversible half-wave potential, defined by

$$E^r_{1/2} = E^o - \frac{RT}{nF} \ln \left(\frac{D_{ox}}{D_{red}} \right)^{1/2} \qquad (1.2.5)$$

This relation is not usually employed in the analysis of the lsv waveform. A second, more useful relation is that for the difference between the potential at the peak maximum and the potential at half the peak maximum

$$E_p = E_{p/2} - 2.2 \frac{RT}{nF} \qquad (1.2.6)$$

This is the relation generally used to determine the reversibility of a reaction.

The charge transfer reaction is called irreversible as Λ becomes very small, and electrode reactions have been defined as such for $\Lambda < 10^{-2(1+\alpha)}$ (where α is the transfer coefficient, $0 < \alpha < 1$). The shape of the lsv wave for an irreversible charge transfer system is given in Figure 1.2.

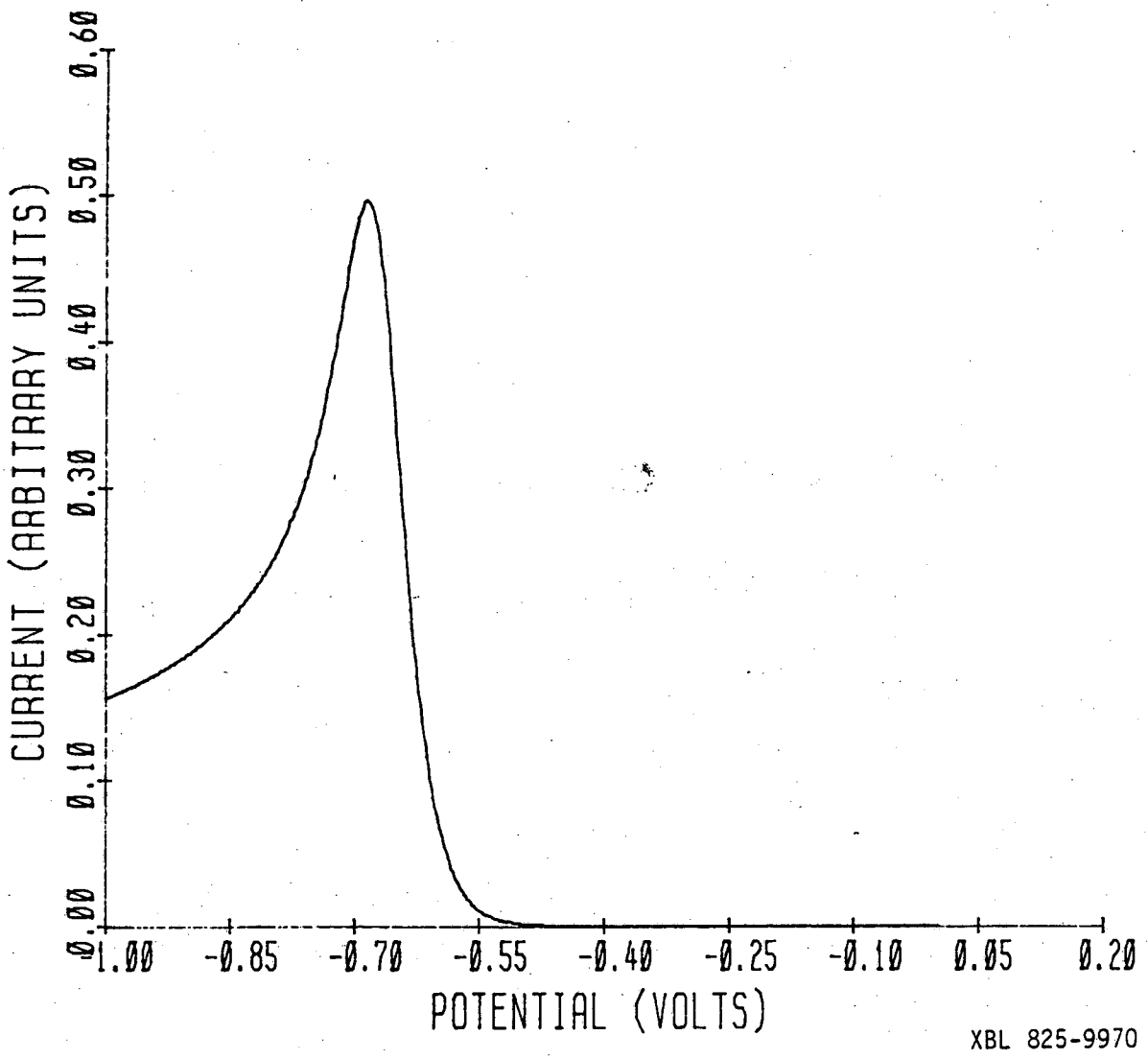

Figure 1.2: Linear sweep voltammogram of a system with irreversible electrode kinetics.

The peak current for the irreversible charge transfer is

$$i_p = (2.99 \times 10^5)\, n\, (\alpha n)^{1/2}\, A\, C^*_{ox}\, \sqrt{D_{ox} \nu} \qquad (1.2.7)$$

where i_p is in amperes if the other variables have the same units as in (1.2.3). Equation 1.2.7 is also useful for quantitative analysis. The relation between the peak potential E_p and the reversible half-wave potential $E^r_{1/2}$ is

$$E_p = E^r_{1/2} - \frac{RT}{\alpha n F} \left[0.780 + \frac{1}{2} \ln \alpha - \ln \Lambda\right] \qquad (1.2.8)$$

The peak potential is seen to have a direct dependence on the dimensionless rate constant Λ. This relation reduces to a simpler relation between E_p and $E_{p/2}$

$$E_p = E_{p/2} - 1.857 \frac{RT}{\alpha n F} \qquad (1.2.9)$$

which is often used to demonstrate the irreversibility of a reaction.

1.2.2 CE mechanism

The theory for the CE mechanism was first developed by Saveant and Vianello (39,40) and was also treated by Nicholson and Shain in their paper (38). In references 39 and 40 the mechanism is defined by a homogeneous solution reaction preceding a reversible charge transfer reaction; i.e.,

$$C \underset{k_b}{\overset{k_f}{\rightleftharpoons}} Ox$$

$$Ox + ne^- = Red \qquad (1.2.10)$$

where k_f and k_b are the homogeneous first order rate constants, and K = k_f/k_b is the equilibrium constant. This mechanism is important, among other reasons, because it describes the dissociation and subsequent reduction of a metal-ligand complex, if the dissociation reaction is assumed to be pseudo-first order (i.e., if the ligand concentration is in great excess as compared to the metal concentration, as is usually the case).

As for the charge transfer reaction, the general solution to the boundary value problem for the CE mechanism has up to now been too complex to be useful, but there are three limiting cases of kinetic behavior in which the solution is simplified, and from which useful relations have been derived. The three cases of limiting behavior are defined by limiting values of the equilibrium constant K, and by limiting values of the dimensionless homogeneous rate constant λ, which was defined by Saveant and Vianello (39) as

$$\lambda = \frac{(k_f+k_b)}{\nu}\left(\frac{RT}{nF}\right) \qquad (1.2.11)$$

The trends in kinetic behavior are best described by a zone diagram such as that of Figure 1 of reference 40.

The first case of limiting behavior occurs as $\lambda \to 0$. For $\lambda \to 0$, both k_f and k_b go to zero, and essentially there is no preceding homogeneous reaction. The solution becomes that of the reversible charge transfer, and relations describing the wave are those of Section 1.2.1. This kind of kinetic behavior is called pure diffusion-controlled behavior, and is represented by the letters DO.

The second case of limiting behavior occurs as $\lambda \to \infty$, $K \to \infty$. The homogeneous kinetics are much faster than the charge transfer reaction; one may think of the system as being comprised of a species that is itself electroactive and undergoes a reversible charge transfer. For this case the mechanism described by (1.2.10) reduces to

$$C + ne^- = Red \qquad (1.2.12)$$

The shape of the current-potential curve in this limit is that of the reversible lsv wave, as seen in Figure 1.1. The equation for peak current is that of (1.2.3) except that the bulk concentration of oxidized species C^*_{ox} is replaced by $C^*_{ox} + C^*_c$. The peak potential of the lsv wave is shifted with respect to (1.2.4); the new peak potential is given by (39)

$$E_p = E^r_{1/2} - 1.109 \frac{RT}{nF} + \frac{RT}{nF} \ln\left(\frac{K}{K+I}\right) \qquad (1.2.13)$$

This shift in peak potential is the same as that seen in polarography (41) for the same mechanism. This result can be used to determine the

equilibrium constant. This limiting type of behavior is called modified diffusion kinetic behavior, and is represented by DE.

The width of the lsv wave (in terms of $E_p - E_{p/2}$) is that given by (1.2.6). Thus systems with either DO or DE kinetics are 'reversible'. This leads to the definition of what will be called in this work 'clasically reversible' systems. A classically reversible system is any system, with a reversible charge transfer, in which the rate of mass transport is determined solely by diffusion. This can happen either because competing modes of mass transport are much slower than diffusion, as in the DO system, or much faster, as in the DE system. In this work, any mechanism, with homogeneous kinetic reactions, that is not classically reversible is affected to some extent by the homogeneous kinetics, and for this reason will be called kinetically controlled.

The last limiting case of behavior for which useful relations exist occurs as $\lambda \to \infty$, $K \to 0$. In this case there is at large negative potentials a constant flux of depolarizer to the electrode caused by conversion of C to Ox; the current-potential curve looks not like Figure 1.1, but rather like Figure 1.3. The constant flux of depolarizer causes at large negative potentials a limiting current, which is given by

$$i^* = n F A K C_c^* \sqrt{D_{ox} k_b} \qquad (1.2.14)$$

The half-wave potential of Figure 1.3 is given by

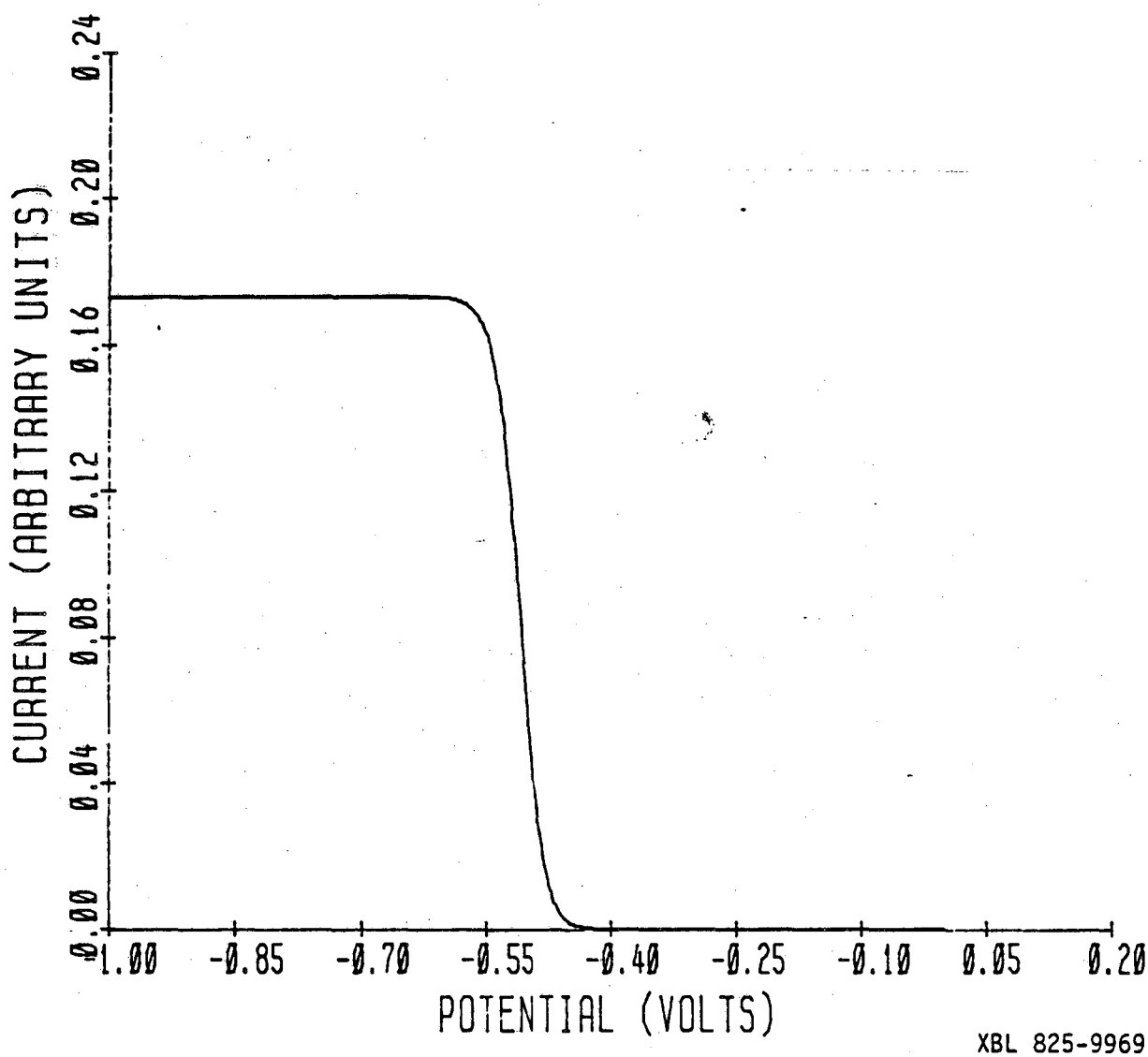

Figure 1.3: Linear sweep voltammogram of a system with CE kinetics in the pure kinetic zone of limiting behavior.

$$E_{p/2} = E^r_{1/2} - \frac{0.007}{n} - \frac{RT}{2nF} \ln\left(\frac{k_b}{\nu}\right) \qquad (1.2.15)$$

and can be used to determine k_b. This is called pure kinetic behavior, and is represented by KP.

These are the only types of kinetic behavior for which relations for quantities like i_p, E_p, etc. have been developed for the CE mechanism. As implied by the names, pure and modified diffusion systems are those systems in which mass transport is controlled solely by the rate of diffusion; pure kinetic systems are controlled solely by the rate of homogeneous chemical reaction. Intermediate to these limiting cases of behavior are systems controlled both by the rate of diffusion and rate of chemical reaction. These have not been given specific names in the literature, but are referred to simply as the KO and KE zones, the KO zone being intermediate to the DO and KP zones and the KE zone intermediate to the KP and DE zone (40). No work has been done on the analysis of systems in these zones of behavior, even though the resultant waves contain more information about the system than the other limiting cases, apparently because the analysis is too complex.

From reference to Figure 1 of reference 40, it is seen that all types of kinetic behavior can be found for a specified equilibrium constant by varying the value of λ from 0 to ∞, if the equilibrium constant is small enough. Therefore, a series of electrochemical systems, all with the same equilibrium constant, and with values of λ

ranging from very small to very large, can be taken as representative of all possible CE mechanisms. This work will consider a series of CE systems all with $K=10^{-4}$; for this equilibrium constant the behavior of the mechanism is that of pure diffusion for $\lambda \leq 0.03$; the range of the KO system is $0.03 < \lambda \leq 0.4$; the range of the pure kinetic zone is from $0.4 \leq \lambda < 6x10^{4}$; the range of the KE system is $6x10^{4} \leq \lambda \leq 2x10^{10}$; and the range for the modified diffusion zone is for $\lambda \geq 2x10^{10}$.

Other than the work of Nicholson and Shain (38) there is no work that has been done on the analysis of the CE mechanism for systems that do not have reversible electrode reactions. Nicholson and Shain consider the mechanism of (1.2.10) with an irreversible charge transfer. As for the mechanism with a reversible charge transfer, usable relations have been developed for the DO, DE and KP zones only. For the DO zone, the pertinent relations are those of (1.2.7)-(1.2.9). For the DE region, the same relations apply, except that E_p is shifted cathodically by $RT/\alpha nF \ln(K/K+1)$ with respect to E_p in (1.2.8). For the pure kinetic realm, a very complex, nearly unusable relation for the peak current is given.

No work has been done previously on the CE mechanism coupled with a quasi-reversible charge transfer.

1.2.3 EC Mechanism

The theory for the EC mechanism, which is defined by

$$Ox + ne^- = Red \qquad (1.2.16)$$

$$Red \underset{k_b}{\overset{k_f}{\rightleftharpoons}} C$$

is also treated by Saveant and Vianello (40) and by Nicholson and Shain (38) for a reversible charge transfer, and by Nadjo and Saveant (42) for a quasi-reversible charge transfer. This mechanism is interesting because it describes reactions of some organic compounds, and is of interest to those doing work in metal speciation because it describes the pseudo-first order association of a metal-ligand complex when metal is stripped out of a working electrode during anodic stripping voltammetry. The theory for this mechanism,

$$Red = Ox + ne^- \qquad (1.2.17)$$

$$Ox \underset{k_b}{\overset{k_f}{\rightleftharpoons}} C$$

is nearly the same as that of (1.2.16), and transposition is immediate. The mechanism of (1.2.16) is that which will be considered throughout this work.

The boundary value problem for this mechanism is much the same as that of the CE mechanism, and for this reason the same kind of kinetic behavior results. A diagram defining the behavior of the EC mechanism with a reversible charge transfer is that of Figure 2 of reference 40,

in which it is shown that exactly the five types of limiting behavior observed for the CE mechanism obtain for the EC mechanism, although the definition of some of the zones is changed. In fact, the diffusion controlled, or classically reversible, systems of the EC mechanism have exactly the same defining relations as the diffusion controlled systems for the CE mechanism, and exactly the same shape as the reversible lsv wave of Figure 1.1.

The behavior of the other zones differ from their analogues in the CE mechanism, however. The shape of a voltammogram in the pure kinetic zone is shown in Figure 1.4. In sharp contrast to Figure 1.3, this voltammogram looks rather like the reversible voltammogram of Figure 1.1. The peak of the voltammogram is about 10% larger than that predicted for the pure diffusion case (i.e., 10% larger than that predicted by (1.2.3)), and the peak potential is shifted cathodically by an amount (38)

$$E_p = E^r_{1/2} - \frac{RT}{nF}\left[0.780 + \ln\left(\frac{K}{K+I}\right) - \frac{1}{2}\ln\lambda\right] \qquad (1.2.18)$$

so that for a change in λ by an order of magnitude, the peak shifts by 29.5/n mv. As for the CE mechanisms, no relations exist to describe waves in the KO and KE zones of behavior for the EC mechanism.

As mentioned, Nadjo and Saveant (42) have done work on the EC mechanism coupled with a quasi-reversible charge transfer. The behavior of the mechanism is illustrated with the aid of the zone diagram of Figure 1 of reference 42. The most important feature of

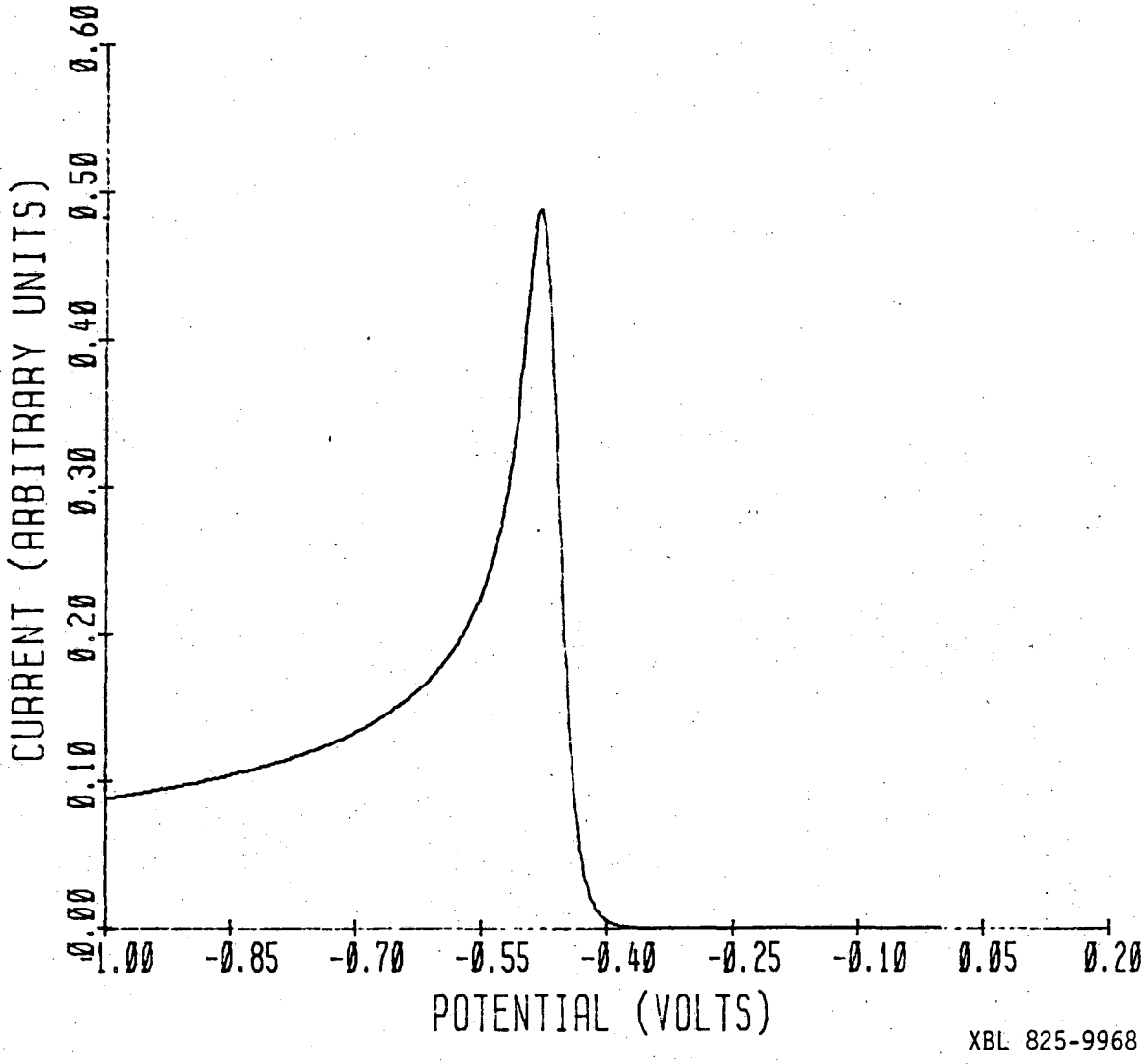

Figure 1.4: Linear sweep voltammogram of a system with EC kinetics in the pure kinetic zone of limiting behavior.

this diagram is that it shows that the definitions of charge transfer reversibility change as λ is increased. For $\lambda \gtrsim 0.1$, an increase in λ of about three orders of magnitude results in about a one order of magnitude increase in the limits of reversibility and irreversibility. Since the CE mechanism and the EC mechanism are so alike, it is expected that this behavior would also obtain for the CE mechanism coupled with a quasi-reversible charge transfer.

For a large enough equilibrium constant all types of kinetic behavior result as λ is changed from 0 to ∞. For an equilibrium constant of 10^4, assuming a reversible charge transfer, pure diffusion behavior results for $\lambda < 0.1$; behavior is in the KO zone for $0.1 < \lambda < 2$; pure kinetic behavior results for $2 < \lambda < 2\text{x}10^5$; KE behavior results for $2\text{x}10^5 < \lambda < 2\text{x}10^{10}$; and modified diffusion behavior for $\lambda \gtrsim 2\text{x}10^{10}$.

In this section it has been shown that only a relatively few relations exist to characterize voltammograms of even simple electrochemical systems. These relations usually give little information about the kinetics of the systems and when such information is given it is only for limiting cases of kinetic behavior. This is because the relations of Section 1.2 are semi-empirical in nature, derived from the observation of numerically created data. In the next section convolutive potential sweep voltammetry will be discussed. This technique, because it involves the transformation of lsv waves into a shape describable by an analytic function, allows the return of a great deal more information

about an electrochemical system, especially for systems not in limiting cases of kinetic behavior.

1.3 CONVOLUTION POTENTIAL SWEEP VOLTAMMETRY

Convolution potential sweep voltammetry is a data analysis technique about a decade old, although the technique is based on linear sweep voltammetric theory, which is of course much older. The first detailed papers on c.p.s.v. were published in 1972 and 1973 (43-45), although sketchy references to the technique were published earlier (46-48). Most of the technique has been developed by two factions; Oldham, Goto and their co-workers, and Saveant and his co-workers, although there are a number of papers by others (49-51).

Oldham, et al. are responsible for the development of the theory of what they call semiintegral and semidifferential electroanalysis. These are actually a subset of the techniques that comprise c.p.s.v.; semiintegral and semidifferential analysis are theoretically useful only for classically reversible lsv waves, although, as will be shown, they are also useful in the analysis of other electrochemical systems. They are not useful in the analysis of some homogeneous kinetic mechanisms that are not classically reversible. Works by Oldham, Goto and co-workers include a study on the analog implementation of semiintegral analysis (52); semidifferential analysis (53, 54); application of semioperator (i.e., both semiintegral and semiderivative) methods to anodic stripping voltammetry (55, 56), and applications to cyclic voltammetry (57) and staircase voltammetry

(58).

Saveant, et al. are responsible for the development of c.p.s.v., having coined the term in the first of a series of papers on the subject (44, 59-62). Convolution voltammetry is applicable to a wide variety of electrochemical systems, including systems with complex homogeneous mechanisms. Papers by Saveant and co-workers include the series already mentioned, which discusses the problems of multistep Nernstian waves, the effect of sweep rate in c.p.s.v. as applied to cyclic voltammetry, homogeneous follow-up chemical reactions, and the determination of charge-transfer kinetics deviating from Butler-Volmer behavior. Other papers include the application of c.p.s.v. to spectroelectrochemistry (63) and chronopotentiometry (64).

This section will review the results of c.p.s.v. theory for three different mechanisms: the simple charge transfer reaction, the CE mechanism, and the EC mechanism.

1.3.1 Simple Charge Transfers

Convolution potential sweep voltammetry, like linear sweep voltammetry, is based on the solutions of the boundary value problems that describe mass transport for electrochemical systems. The solutions to the boundary value problems, whenever they are possible to determine, are in the form of integral equations relating the observed current at any time to the applied potential at that time. The utility of c.p.s.v. lies in the numerical evaluation of the convolution integrals found in these solutions, which often leads to

simple expressions relating potential to convolution integrals.

For insight into the method, the boundary value problem describing the simple reduction of (1.2.1) at a hanging mercury drop electrode will be described in detail. For c.p.s.v. it is assumed that mass transport is due to semi-infinite, linear diffusion. This means that there is no mass transport due to convection or migration, and that the concentration of all species far away from the electrode surface does not change over the course of the experiment. Secondly, the assumption of linear diffusion implies that diffusion to the spherical hanging drop electrode can be approximated by diffusion to a planar surface. If these conditions are assumed, then the Fick's second law equations describing change of concentration with respect to time and distance from the electrode surface are

$$\frac{\partial C_{ox}}{\partial t} = D_{ox} \frac{\partial^2 C_{ox}}{\partial x^2}$$

$$\frac{\partial C_{red}}{\partial t} = D_{red} \frac{\partial^2 C_{red}}{\partial x^2} \qquad (1.3.1)$$

The boundary value problem is completely specified when all the boundary value conditions are specified. These boundary conditions include the assumption of semi-infinite diffusion,

$$C_{ox}(x,t=0) = C_{ox}(x=\infty,t) = C^{*}_{ox}$$
$$C_{red}(x,t=0) = C_{red}(x=\infty,t) = 0 \qquad (1.3.2)$$

and Fick's first law of diffusion.

$$D_{ox}\left(\frac{\partial C_{ox}}{\partial x}\right)_{x=0} = -D_{red}\left(\frac{\partial C_{red}}{\partial x}\right)_{x=0} = \frac{i(t)}{nFA} \qquad (1.3.3)$$

The final boundary condition has to deal with the electrode reaction rate law which specifies the concentrations of the reduced and oxidized species at the electrode surface, or x=0. The most general rate law is that for the quasi-reversible reaction; the potential-dependent charge transfer rate constant is related to the current i(E) and $C_{ox}(0,E)$ and $C_{red}(0,E)$ by

$$i(E) = nFA\, k(E) \{C_{ox}(0,E) - C_{red}(0,E) \exp [\tfrac{nF}{RT} (E-E^{o})]\} \qquad (1.3.4)$$

For an irreversible reaction the $C_{red}(0,E)$ term may be neglected so that

$$i(E) = nFA\, k(E)\, C_{ox}(0,E) \qquad (1.3.5)$$

If Butler-Volmer kinetics are assumed, then

$$k(E) = k^{o} \exp\left(\frac{-\alpha nF(E-E^{o'})}{RT}\right) \qquad (1.3.6)$$

where $E^{o'}$ is the formal potential, and is equal to E^{o} if activity coefficients for all species are one. With this assumption, (1.3.4) and (1.3.5) become, respectively,

$$i(E) = nFA\, k^{o} \left\{\exp\left(-\frac{\alpha nF}{RT}(E-E^{o})\right) C_{ox}(0,E) - \exp\left(\frac{(1-\alpha)nF}{RT}(E-E^{o})\right) C_{red}(0,E)\right\} \qquad (1.3.7)$$

and

$$i(E) = nFA\, k^{o} \exp\left(-\frac{\alpha nF}{RT}(E-E^{o})\right) \qquad (1.3.8)$$

Alternatively, if in (1.3.4), $k(E)$ is assumed to be infinite everywhere so that the charge transfer reaction is reversible, (1.3.4) reduces to

$$E = E^{o} + \frac{RT}{nF} \ln\left(\frac{C_{ox}(0,E)}{C_{red}(0,E)}\right) \qquad (1.3.9)$$

which is the well-known Nernst equation. The assumption of one of these rate law equations completes the specification of the boundary value problem.

The details of the solution to the problem are given in Appendix

II. Much of the power of c.p.s.v. lies in the fact that the final boundary condition, that of the electrode rate law, is applied only at the very end of the solution. To see that this is so, consider how the rate law is applied to the solution of the simple charge transfer. The Laplace transformation method uses only equations 1.3.1 through 1.3.3 and results in expressions for the surface concentrations of Ox and Red as

$$C_{ox}(0,E) = C^{*}_{ox} - \frac{1}{nFA\sqrt{D_{ox}\nu}} \int_{E}^{E_i} \frac{i(\gamma)d\gamma}{\sqrt{\gamma-E}}$$

$$C_{red}(0,E) = \frac{1}{nFA\sqrt{D_{red}\nu}} \int_{E}^{E_i} \frac{i(\gamma)d\gamma}{\sqrt{\gamma-E}} \qquad (1.3.10)$$

where the semiintegral is defined as

$$m(E) = \int_{E}^{E_i} \frac{i(\gamma)d\gamma}{\sqrt{\gamma-E}} \qquad (1.3.11)$$

The final expression for the simple charge transfer reaction results from the substitution of (1.3.10) into one of the electrode kinetic rate law expressions. A table of these expressions for the different rate laws is given in Table 1.1.

For the substitution of (1.3.10) into (1.3.9), the Nernst equation, the solution of the boundary value problem is (44)

Table 1.1: Semiintegral, current and potential functions for the simple charge transfer system.

Electrode Kinetics	Function
Reversible	$E = E^{r}_{1/2} + \frac{RT}{nF} \ln\left(\frac{m^{*}-m(E)}{m(E)}\right)$
Quasi-reversible, potential dependent rate law	$k(E) = \frac{\sqrt{D_{ox}\nu}\ i(E)}{m^{*}-m(E)\ [1+\exp(\frac{nF}{RT}\ (E-E^{r}_{1/2}))]}$
Quasi-reversible, Volmerian kinetics	$E = E^{o} + \frac{\alpha nF}{RT} \ln\left(\frac{k^{o}}{\sqrt{D\nu}}\right) + \frac{\alpha nF}{RT} \ln\left(\frac{m^{*}-m(E)[1+\exp(\frac{nF}{RT})(E-E^{o})]}{i(E)}\right)$
Irreversible, potential dependent rate law	$k(E) = \frac{\sqrt{D_{ox}\nu}\ i(E)}{m^{*}-m(E)}$
Irreversible, Volmerian kinetics	$E = E^{o} + \frac{\alpha nF}{RT} \ln\left(\frac{k^{o}}{\sqrt{D\nu}}\right) + \frac{\alpha nF}{RT} \ln\left(\frac{m^{*}-m(E)}{i(E)}\right)$

$$E = E^r_{1/2} + \frac{RT}{nF} \ln\left(\frac{m^*-m(E)}{m(E)}\right) \qquad (1.3.12)$$

where

$$m^* = nFA\, C^*_{ox} \sqrt{D_{ox}\nu} \qquad (1.3.13)$$

Equation 1.3.12 has the same form as the Heyrovsky-Ilkovic equation in polarography; a plot of semiintegral vs. applied potential (Figure 1.5) has the same shape as a polarographic wave. The semiintegral is a sigmoidal wave, with a limiting plateau proportional to C^*_{ox} and $\nu^{1/2}$, and with a half-wave potential equal to the reversible half-wave potential.

The derivative of the semiintegral is the semiderivative. From (1.3.12), the semiderivative is (53)

$$e(E) = \frac{\partial m(E)}{\partial E} = \frac{nFm^*}{4RT} \operatorname{sech}^2\left\{\frac{nF}{2RT}(E-E^r_{1/2})\right\} \qquad (1.3.14)$$

A plot of semiderivative vs. potential is shown in Figure 1.6; for a reversible charge transfer the semiderivative is a symmetric, narrow peak, beginning and ending at the baseline. The height of the semiderivative peak is proportional to C^*_{ox} and $\nu^{1/2}$. The potential of the peak maximum is

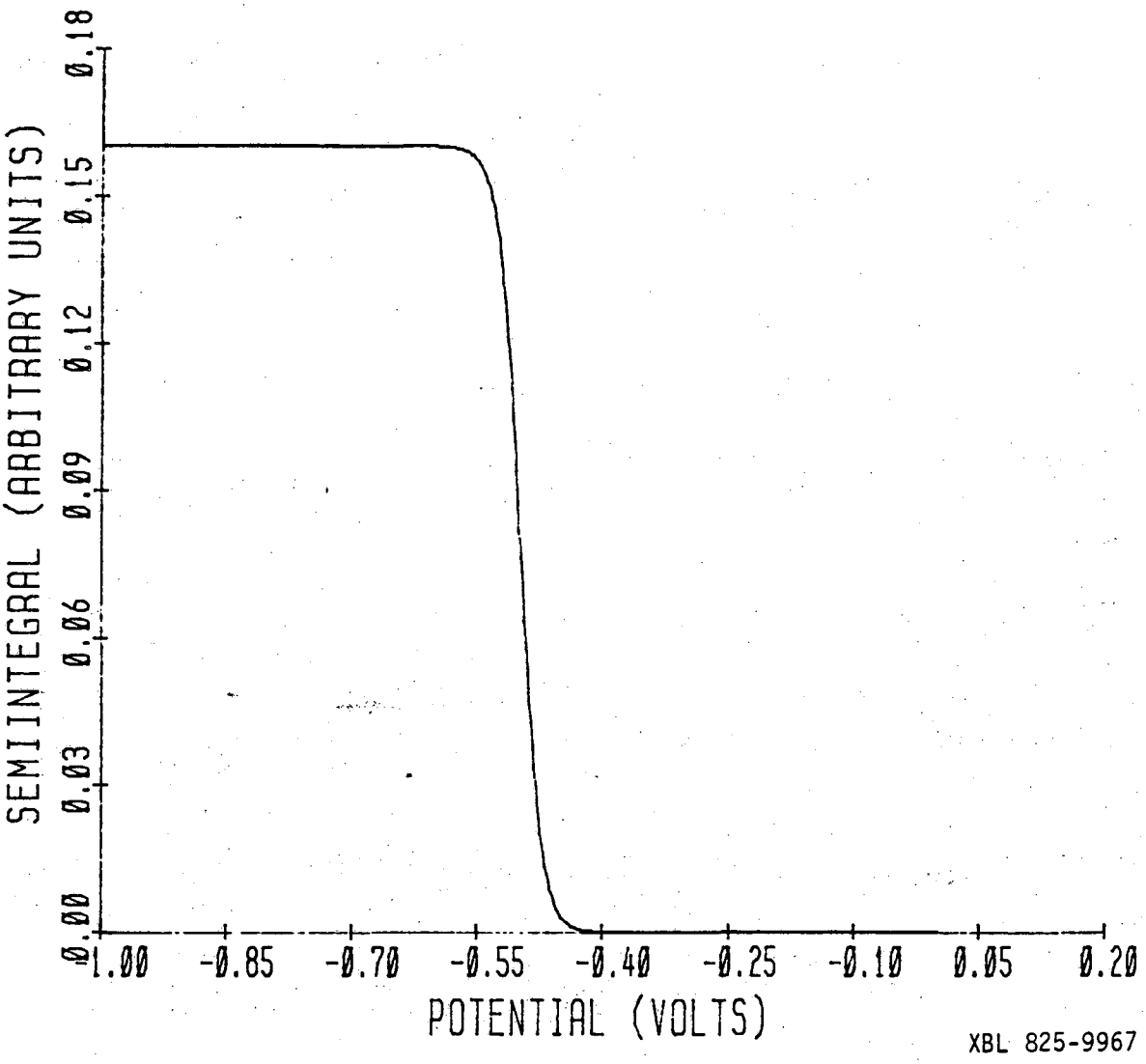

Figure 1.5: Semiintegral of the reversible system of Figure 1.1.

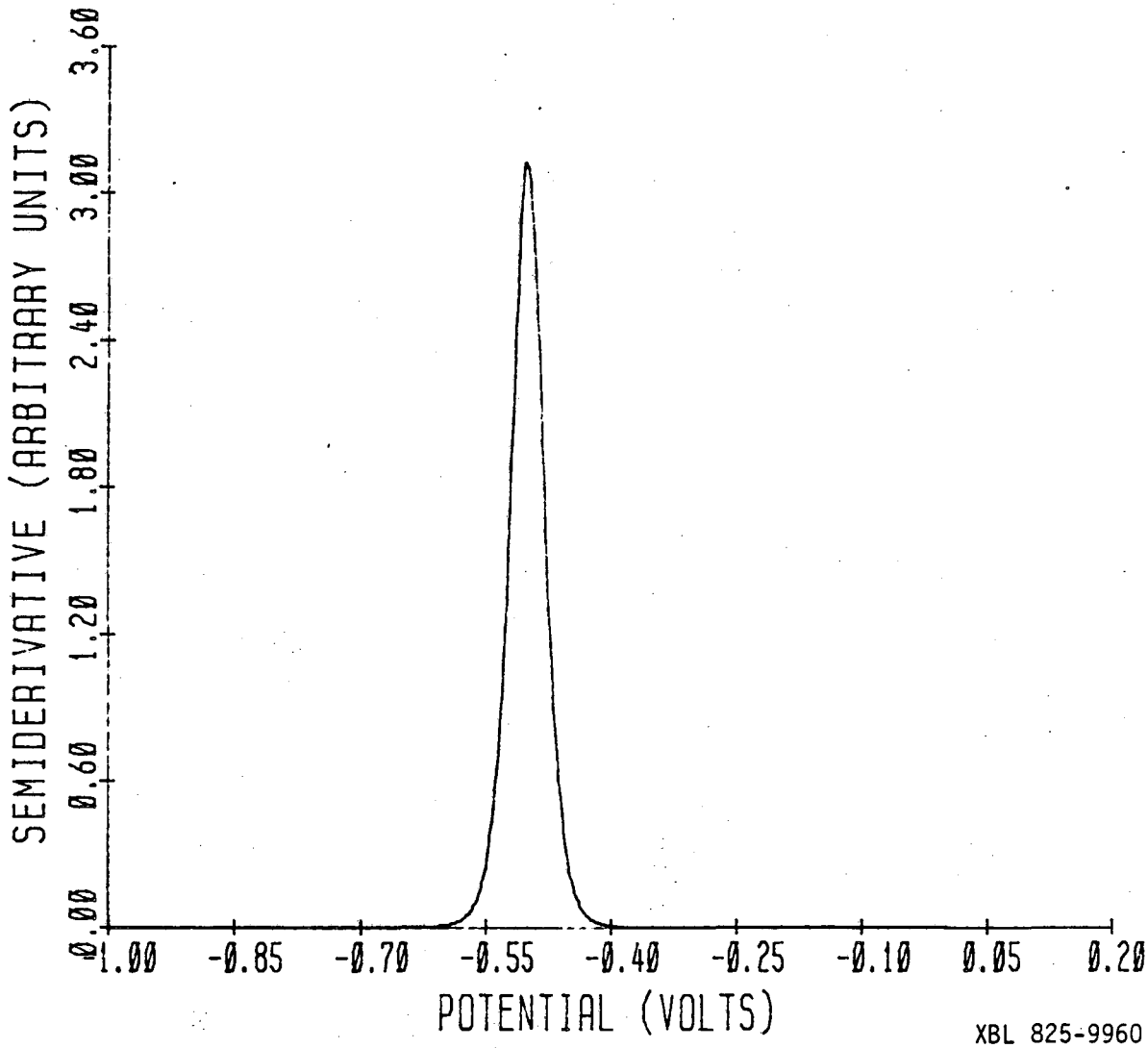

Figure 1.6: Semiderivative of the reversible system of Figure 1.1.

$$E_p = E^r_{1/2} \qquad (1.3.15)$$

while the full width at half of the peak maximum is, assuming T = 25°C,

$$FWHM = \frac{90.6}{n} \text{ mV} \qquad (1.3.16)$$

For the quasi-reversible charge transfer, upon substitution of (1.3.10) into (1.3.4), the current, semiintegral and potential function is (44)

$$k(E) = \frac{\sqrt{D_{ox}\nu}\ i(E)}{m^* - m(E)\ [1+\exp(\frac{nF}{RT}(E-E^r_{1/2}))]} \qquad (1.3.17)$$

while that for the irreversible charge transfer is (44)

$$k(E) = \frac{\sqrt{D_{ox}\nu}\ i(E)}{m^* - m(E)} \qquad (1.3.18)$$

It is seen that semiintegral analysis is a powerful tool for the examination of the rate-potential relationship for any simple charge transfer. By means of either (1.3.17) or (1.3.18) the potential dependent rate law can be gained directly, if $E^r_{1/2}$ is known. These expressions have been used by Saveant and Tessier (62) in an investigation of the reduction of tert-nitrobutane in both

acetonitrile and dimethylformamide.

Goto and Oldham (65) have derived an analytical expression for the semiintegral of an irreversible charge transfer as a function of the potential as

$$m(E) = -\frac{nF}{RT} C^*_{ox} A \sqrt{D_{ox}\nu} \sum_{j=1}^{\infty} (-1)^j \frac{\exp(jz)}{\sqrt{j!}} \qquad (1.3.19)$$

where

$$z = \frac{\alpha nF}{RT} (E-E^r_{1/2}) + \ln \Lambda \qquad (1.3.20)$$

Dalrymple-Alford et al. (54) were able to extend this work to derive an expression for the semiderivative of an irreversible charge transfer. The expression itself is not very useful, but from this a plot of semiderivative vs. potential was made. The semiderivative of an irreversible charge transfer is shown in Figure 1.7; it is seen that this looks much like a sech^2 function.

Dalrymple-Alford et al. also developed relations for the peak potential of the irreversible semiderivative

$$E_p = E^r_{1/2} + 0.055 \frac{RT}{\alpha nF} + \frac{RT}{2\alpha nF} \ln \left(\frac{nF}{RT}\right) + \frac{RT}{\alpha nF} \ln \Lambda \qquad (1.3.21)$$

and for the peak width at 25^oC

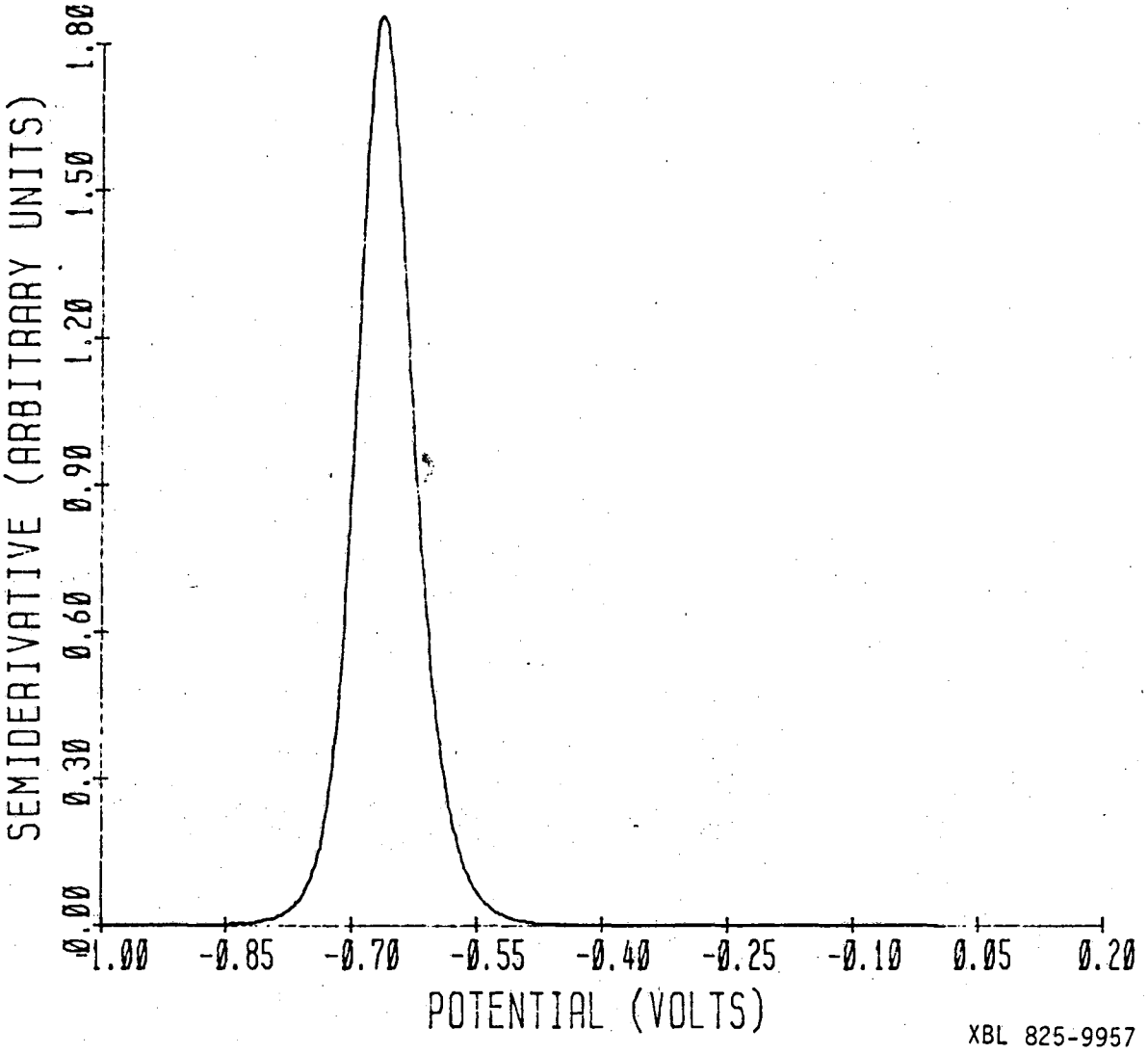

Figure 1.7: Semiderivative of the irreversible system of Figure 1.2.

$$FWHM = \frac{75.5}{\alpha n} \text{ mV} \qquad (1.3.22)$$

1.3.2 CE Mechanism

The theory of c.p.s.v. for the CE mechanism derives directly from the original treatment of the mechanism by Saveant and Vianello (39). The partial differential equations that describe this system are

$$\begin{aligned} \frac{\partial C_c}{\partial t} &= D_c \frac{\partial^2 C_c}{\partial x^2} + k_b C_{ox} - k_f C_c \\ \frac{\partial C_{ox}}{\partial t} &= D_{ox} \frac{\partial^2 C_{ox}}{\partial x^2} - k_b C_{ox} + k_f C_c \\ \frac{\partial C_{red}}{\partial t} &= D_{red} \frac{\partial^2 C_{red}}{\partial x^2} \end{aligned} \qquad (1.3.23)$$

and the boundary conditions are those of the reversible charge transfer, with an additional boundary condition

$$C_c(x,t=0) = C_c(x=\infty,t) = C_c^* = \frac{C_{ox}^*}{K} \qquad (1.3.24)$$

As with the solution of the boundary value problem for the simple charge transfer, the solution to the differential equation system is achieved with the help of the Laplace transform method. (See Appendix

II.) The solution is in terms of the concentrations of Ox and Red, and is (39)

$$C_{ox}(0,E) = C^{*}_{ox} - \frac{1}{nFA\sqrt{D\nu}} \int_{E}^{E_i} \left\{ \frac{K}{K+1} + \frac{\exp\left[-\lambda\left(\frac{nF}{RT}\right)(\gamma-E)\right]}{K+1} \right\} \frac{i(\gamma)d\gamma}{\sqrt{\gamma-E}}$$

$$C_{red}(0,E) = \frac{1}{nFA\sqrt{D\nu}} \int_{E}^{E_i} \frac{i(\gamma)d\gamma}{\sqrt{\gamma-E}} \qquad (1.3.25)$$

and, as before, the final solutions are found with the application of one of the electrode boundary value conditions to (1.3.25). The solution to the boundary value problem for the mechanism with a reversible charge transfer is, upon substituting (1.3.25) into (1.3.9),

$$E = E^{o} + \frac{RT}{nF} \ln\left(\frac{m^{*}-m(E,\lambda)}{m(E)}\right) \qquad (1.3.26)$$

where

$$m(E,\lambda) = \int_{E}^{E_i} \left\{ \frac{K}{K+1} + \frac{\exp\left[-\lambda \frac{nF}{RT}(\gamma-E)\right]}{K+1} \right\} \frac{i(\gamma)d\gamma}{\sqrt{\gamma-E}} \qquad (1.3.27)$$

The solution of (1.3.26) is not very helpful because of the difficulty of calculating $m(E,\lambda)$. Fortunately, for almost all of the systems discussed before $m(E,\lambda)$ need not be calculated explicitly, although it has not been shown that such a calculation is not

feasible. Table 1.2 shows the simplification of $m(E,\lambda)$ in the zones of kinetic behavior discussed earlier. Substituting the relations of Table 1.2 into (1.3.26), and rearranging, one obtains the equations of Table 1.3. Equations for the general case and the KO zone are not shown because there is little or no simplification of $m(E,\lambda)$ in these cases.

For the DO zone, the exponential term in (1.3.27) goes to 1, and (1.3.25) becomes, upon rearrangement, (44)

$$E = E^{o} + \frac{RT}{nF} \ln \left(\frac{m^{*}-m(E)}{m(E)} \right) \qquad (1.3.28)$$

This equation is the same as (1.3.12); this is in agreement with the lsv findings, that as $\lambda \to 0$ the behavior becomes that of the reversible charge transfer. All of the pertinent relations for peak width, height, etc. are those of the reversible charge transfer.

In another case of limiting behavior, the DE zone, the exponential term may be ignored in comparison to K/K+1. The semiintegral-potential relation is (44)

$$E = E^{o} + \frac{RT}{nF} \ln \left(\frac{K}{K+1} \right) + \frac{RT}{nF} \ln \left(\frac{m^{*}-m(E)}{m(E)} \right) \qquad (1.3.29)$$

where

$$m^{*} = nFA \left(C_{c}^{*} + C_{ox}^{*} \right) \sqrt{Dv} \qquad (1.3.30)$$

Table 1.2: Simplification of the $m(E,\lambda)$ integral for different limiting cases.

Zone	Limiting value of parameter	Simplified $m(E,\lambda)$
General	Any	$\int_E^{E_i} \left\{ \frac{K}{K+1} + \frac{\exp\left[-\lambda \left(\frac{nF}{RT}\right)(\gamma-E)\right]}{K+1} \right\} \frac{i(\gamma)d\gamma}{\sqrt{\gamma-E}}$
DO	$\lambda \to 0$	$\int_E^{E_i} \frac{i(\gamma)d\gamma}{\sqrt{\gamma-E}}$
KO	$K \to 0$	$\int_E^{E_i} \frac{\exp\left[-\lambda\left(\frac{nF}{RT}\right)(\gamma-E)\right] i(\gamma)d\gamma}{\sqrt{\gamma-E}}$
KP	$K \to 0$ $\lambda \to \infty$	$\frac{\nu^{1/2}}{(k_f+k_b)^{1/2}}\, i(E)$
KE	$\lambda \to \infty$	$\frac{K}{K+1} \int_E^{E_i} \frac{i(\gamma)d\gamma}{\sqrt{\gamma-E}} + \frac{\nu^{1/2}}{(k_f+k_b)^{1/2}} \frac{i(E)}{(K+1)}$
DE	$\lambda \to \infty$ $K \to \infty$	$\frac{K}{K+1} \int_E^{E_i} \frac{i(\gamma)d\gamma}{\sqrt{\gamma-E}}$

Table 1.3: C.v.c.f. functions for the CE mechanism with a reversible charge transfer.

Zone	Limiting value	Function
DO	$m^* = nFA\sqrt{D\nu}\, C^*_{ox}$	$E = E^r_{1/2} + \frac{RT}{nF} \ln\left(\frac{m^*-m(E)}{m(E)}\right)$
KP	$i^* = nFA\sqrt{D\nu}\, (C^*_{ox} + C^*_c) K\lambda^{1/2} \left(\frac{RT}{nF}\right)^{1/2}$	$E = E^o - \frac{RT}{2NF} \ln\left(\frac{k_f+k_b}{\nu}\right) + \frac{RT}{nF} \ln\left(\frac{i^*-i(E)}{m(E)}\right)$
KE	$m^* = nFA\sqrt{D\nu}\, (C^*_{ox} + C^*_c)$	$E = E^o + \frac{RT}{nF} \ln\left(\frac{K}{K+1}\right) + \frac{RT}{nF} \ln\left\{\frac{m^* - \left(\frac{RT}{nF}\right)^{1/2} \frac{i(E)}{K\lambda^{1/2}} - m(E)}{m(E)}\right\}$
DE	$m^* = nFA\sqrt{D\nu}\, (C^*_{ox} + C^*_c)$	$E = E^o + \frac{RT}{nF} \ln\left(\frac{K}{K+1}\right) + \frac{RT}{nF} \ln\left(\frac{m^*-m(E)}{m(E)}\right)$

The semiderivative of the lsv wave for this limiting case of kinetic behavior is (66)

$$e(E) = \frac{nFm^*}{4RT} \operatorname{sech}^2 \left\{ \frac{nF}{2RT} (E-E^o) - \frac{1}{2} \ln \left(\frac{K}{K+1} \right) \right\} \qquad (1.3.31)$$

Equations 1.3.29 and 1.3.31 are the same as those of equations 1.3.12 and 1.3.14, respectively, except for a difference in m^* and the ln (K/K+1) term. As for the lsv waves, in the modified diffusion case of limiting behavior the semiintegral and semiderivative waves are described by the relation that describes the reversible charge transfer waves, except that the modified diffusion waves are shifted cathodically. The semiderivative peak potential is given by

$$E_p = E^o + \frac{RT}{nF} \ln \left(\frac{K}{K+1} \right) \qquad (1.3.32)$$

while the peak width of the semiderivative is given by (1.3.16).

The next limiting case of kinetic behavior is the pure kinetic zone. As for the non-reversible charge transfer, analytic expressions for zones other than the diffusion controlled zones must involve both semiintegral and current. For the KP zone, the following relation for semiintegral, current and potential can be derived from the treatment of Imbeaux and Saveant (44)

$$E = E^{o} - \frac{RT}{2nF} \ln\left(\frac{k_f+k_b}{\nu}\right) + \frac{RT}{nF} \ln\left(\frac{i^{*}-i(E)}{m(E)}\right) \qquad (1.3.33)$$

where i^{*} is the limiting current at large negative potentials.

The last zone to be considered is the KE zone. Although it has not been stated previously, the semiintegral, current and potential function for this zone is just a combination of the relation in the KP and DE zones,

$$E = E^{o} + \frac{RT}{nF} \ln\left(\frac{K}{K+1}\right) + \frac{RT}{nF} \ln\left\{\frac{m^{*} - \left(\frac{RT}{nF}\right)^{1/2} \frac{i(E)}{K\lambda^{1/2}} - m(E)}{m(E)}\right\} \qquad (1.3.34)$$

where m^{*} is given by (1.3.30).

1.3.3 EC Mechanism

The solution of the boundary value problem for the EC mechanism is similar to that of the CE mechanism. For the EC mechanism, the concentration profiles are given by

$$C_{ox}(0,E) = C^{*}_{ox} - \frac{1}{nFA\sqrt{D\nu}} \int_{E}^{E_i} \left\{ \frac{1}{K+1} + \frac{K}{K+1} \exp\left[-\lambda \left(\frac{nF}{RT} \right) (\gamma - E) \right] \right\} \frac{i(\gamma)d\gamma}{\sqrt{\gamma - E}}$$

$$C_{red}(0,E) = \frac{1}{nFA\sqrt{D\nu}} \int_{E}^{E_i} \frac{i(\gamma)d\gamma}{\sqrt{\gamma - E}} \qquad (1.3.35)$$

so that the final semiintegral, current, and potential functions are found by substitution into one of the electrode boundary conditions (1.3.4) through (1.3.9). This is not necessary; if one defines K' = 1/K and substitutes into (1.3.35), this latter equation has the same form as (1.3.10) with K' instead of K. Thus the analysis of the EC mechanism with c.p.s.v. is essentially the same as that of the CE mechanism.

1.4 CONVOLUTIVE VOLTAMMETRIC CURVE FITTING

Section 1.3 discusses ways in which analytic expressions involving current, semiintegral and potential can be derived for certain electrochemical systems. Because simple analytic expressions can be derived, it is expected that curve fitting techniques would be of great utility when combined with c.p.s.v. theory. The technique of fitting current, semiintegral and potential data with a function derived from c.p.s.v. theory is called convolutive voltammetric curve fitting, or c.v.c.f. In the special case where a sech^2 fitting function is used to fit semiderivatives of voltammetric data, the

technique is referred to as semiderivative voltammetric curve fitting, or s.v.c.f.

In this section the s.v.c.f. and assorted c.v.c.f. techniques will be derived and discussed for the three mechanisms considered in the last section. S.v.c.f. will be derived for those systems for which it is valid from theory. The technique will then be discussed in its application to systems for which the method is not theoretically valid, but for which the shape of the voltammogram is close enough to that of the classically reversible voltammogram so that the error involved in using s.v.c.f. is small. C.v.c.f. fitting functions will be presented in terms of $sech^2$ functions, and methods will be outlined for the use of these fitting functions in the determination of kinetic parameters for different systems.

1.4.1. Simple Charge Transfers

Equation 1.3.14 implies that the shape of semiderivatives of reversible charge transfer systems should be that of a hyperbolic secant squared function. The s.v.c.f. technique should be able to fit semiderivatives of such systems with no error at all. As will be seen in Chapter 3, this works to great advantage in the resolution of overlapped reversible lsv waves.

This example also serves to demonstrate that s.v.c.f. is of little use in obtaining kinetic information about a system. Since mass transport in this system is wholly diffusion controlled, it is impossible to gain any information about the kinetics of this system

via this kind of electrochemistry. For the systems considered in this work s.v.c.f. is completely valid only for systems in which mass transport is diffusion controlled, so that it is impossible to use s.v.c.f. to obtain any kinetic information about such systems.

For quasi-reversible charge transfer systems, if Butler-Volmer charge transfer kinetics are assumed, and if $D = D_{ox} = D_{red}$, then for the quasi-reversible charge transfer the relation (44)

$$\exp\left(-\frac{\alpha nF(E-E^o)}{RT}\right) = \left(\frac{\sqrt{Dv}}{k^o}\right)\frac{i(E)}{m^*-m(E)[1+\exp(\frac{nF}{RT}(E-E^o))]} \qquad (1.4.1)$$

can be derived from (1.3.17), and for the irreversible charge transfer from (1.3.18) one can derive

$$\exp\left(-\frac{\alpha nF(E-E^o)}{RT}\right) = \left(\frac{\sqrt{Dv}}{k^o}\right)\frac{i(E)}{m^*-m(E)} \qquad (1.4.2)$$

There are two approaches to the use of (1.4.1) in the analysis of quasi-reversible charge transfer systems. The first approach to the analysis of (1.4.1) is the following. Solving for the $\exp[(nF/RT)(E-E^o)]$ term, and taking the natural log of both sides, one obtains

$$E = E^o + \frac{RT}{nF}\ln\left\{\frac{m^* - \frac{\sqrt{Dv}}{k^o}\exp\left(\frac{\alpha nF}{RT}(E-E^o)\right)i(E)-m(E)}{m(E)}\right\} \qquad (1.4.3)$$

For $k \to \infty$, (1.4.3) is seen to reduce to (1.3.12), the relation for the reversible charge transfer.

For other values of the electrode kinetic rate constant, for $E >> E^{o}$, i(E) is zero, and the i(E) term in (1.4.3) is essentially zero. For $E << E^{o}$, $\exp(nF(E-E^{o})/RT)$ is zero, and the i(E) term is again essentially equal to zero. This implies that the semiintegral of a non-reversible Volmerian charge transfer reaches a limiting value m^{*} at very negative potentials. This will become important in discussions about the analysis of the CE and EC mechanisms. Secondly, it implies that if the constant factor of the i(E) term is small enough, the semiintegral of a non-reversible charge transfer could be approximated by (1.3.12), and the the semiderivative by (1.3.14), with little error. That the semiderivative of an irreversible charge transfer is $sech^{2}$ in shape is shown by Figure 1.7, and implied by the work of Goto, Oldham and Dalrymple-Alford, discussed in Section 1.3.1.

This is important because it implies that s.v.c.f. can be used to fit semiderivatives of quasi-reversible and irreversible charge transfer systems with only small error. As mentioned above, one might be able to resolve lsv waves of non-reversible charge transfer systems using s.v.c.f.

In the second approach to the analysis of quasi-reversible charge transfers, taking the natural log of both sides of (1.4.1), upon rearrangement one obtains

$$\ln\left\{\frac{m^{*}-m(E)\ [1+\exp\ (\frac{nF}{RT}\ (E-E^{o}))]}{i(E)}\right\}\ =\ \frac{\alpha nFE}{RT}\ -\ \frac{\alpha nFE^{o}}{RT}\ -\ \ln\left(\frac{k^{o}}{\sqrt{D\nu}}\right)\qquad(1.4.4)$$

This means that, for the correct E^{o}, a plot of E vs. the log term of the l.h.s. should be a straight line with slope = $\alpha nF/RT$, and intercept equal to $-\alpha nFE^{o}/RT - \ln(\ k^{o}\ /\sqrt{D\nu}\ ) = -\alpha nFE^{o}/RT - \ln\ \Lambda - (1/2)\ln(nF/RT)$. This gives an easy way to determine α and Λ, the two parameters of the electrode reaction, provided that the correct E^{o} is known.

If E^{o} is not known, one way to determine it is to find the E^{o} that gives the 'straightest' straight line, i.e., find the E^{o} that gives the smallest variance to a linear least squares fit of the plot of E vs. the l.h.s. of (1.4.4). This is the approach outlined in Section 1.6, in which it is shown to be possible, using (1.4.4), to obtain values of E^{o}, α and Λ for an electrode reaction from a single scan.

1.4.2 CE Mechanism

Equations 1.4.3 and 1.3.31 imply that in the limiting cases of diffusion controlled behavior of this mechanism that s.v.c.f. can be used to fit voltammograms with no error at all. For systems that are kinetically controlled the outlook for fitting semiderivatives with sech^{2} functions is not good. The shape of the voltammogram in the limiting case of pure kinetic behavior is very different from the

shape of the voltammogram of the classically reversible system, (Figure 1.3 as compared to Figure 1.1), and it is doubtful that the semiderivative of the pure kinetic wave will be even close to $sech^2$ in shape.

The application of c.v.c.f. techniques to these kinetically controlled limiting cases of behavior is much more interesting. For the pure kinetic zone, from (1.3.33), a c.v.c.f. fitting function analogous to (1.3.14) and (1.3.31) can be derived.

$$f(E) = \frac{4m^2(E)\,(i^*-i(E))^2}{\left[m^2(E)+(i^*-i(E))^2\right]^2} = \operatorname{sech}^2\left\{\frac{nF}{RT}\,(E-E^o) + \frac{1}{2}\ln\left(\frac{k_f+k_b}{\nu}\right)\right\} \tag{1.4.5}$$

This function has a maximum at the potential

$$E_p = E^o - \frac{RT}{2nF}\ln\left(\frac{k_f+k_b}{\nu}\right) \tag{1.4.6}$$

has a peak height of 1, and a width of

$$FHWM = \frac{45.3}{n}\ mV \tag{1.4.7}$$

If E^o is known, it becomes possible to obtain λ from (1.4.5).

For the KE zone, from (1.3.34) a c.v.c.f. fitting function

$$f(E) = \frac{4m^2(E)\left[m^* - \left(\frac{RT}{nF}\right)^{1/2}\frac{i(E)}{K\lambda^{1/2}} - m(E)\right]^2}{\left[m^2(E)+\left(m^* - \left(\frac{RT}{nF}\right)^{1/2}\frac{i(E)}{K\lambda^{1/2}} - m(E)\right)^2\right]^2}$$

$$= \operatorname{sech}^2\left\{\frac{nF}{RT}(E-E^o) + \ln\left(\frac{K+1}{K}\right)\right\} \qquad (1.4.8)$$

can be derived. This function has a maximum at the potential given by (1.3.32), and has a peak width given by (1.3.16).

Equations (1.3.34) and (1.4.8) illustrate one of the advantages of c.p.s.v. as applied to the CE mechanism. As is the case for the quasi-reversible charge transfer, more information about the electrochemical system is contained in the voltammogram of a system in the KE zone than in the DO, DE, or KP zones. Up to now, however, the information has been indecipherable because of the complexity of the wave. Using c.p.s.v. and some elementary curve fitting techniques, one may obtain the information from more complex systems such as the KE zone. Considering (1.3.34), it is seen that at large negative potentials the numerator of the last term must go to zero, i.e., for a sufficiently negative potential one has

$$m^* = m(E) + \left(\frac{RT}{nF}\right)^{1/2}\frac{i(E)}{K\lambda^{1/2}} \qquad (1.4.9)$$

This offers a way to obtain the value of $K\lambda^{1/2}$ from a single scan. By using a fitting function

$$f(E) = m(E) + Ai(E) \tag{1.4.10}$$

and varying A so as to make f(E) a constant at very negative potentials, one obtains an estimate of $K\lambda^{1/2}$ as

$$K\lambda^{1/2} = \left(\frac{RT}{nF}\right)^{1/2} A^{-1} \tag{1.4.11}$$

If E^o is known, then it becomes possible to determine both K and λ from a single scan. This is a consequence of the fact that more information is contained in the voltammogram of the more general KE zone than of the less general KP zone.

Saveant and Vianello treat only the CE mechanism with a reversible charge transfer; however, there is no reason why any of the electrode boundary conditions (1.3.4) through (1.3.8) cannot be applied to this mechanism, making possible the analysis of CE mechanisms with irreversible and quasi-reversible charge transfers.

For example, substituting (1.3.25) into (1.3.4), the equation for the general quasi-reversible charge transfer, one obtains upon rearrangement

$$k(E) = \frac{\sqrt{D\nu}\, i(E)}{m^* - m(E)\left[\frac{K}{K+1} + \exp\left(\frac{nF}{RT}(E-E^o)\right)\right] - \frac{1}{K+1} m(E,\lambda)} \tag{1.4.12}$$

This equation bears a strong resemblance to (1.3.17), and implies that

if one knows K, λ, and E^o that one may obtain the electrode response for this system also. This is another one of the advantages of c.v.c.f.; the technique allows one to separate the effects due to homogeneous kinetics from those due to electrode kinetics.

To further illustrate the advantage of this separation, consider a CE mechanism that is in the KE limiting case of homogeneous kinetic behavior. Next suppose that the charge transfer is Volmerian; with these assumptions, (1.4.12) becomes

$$\exp\left\{\frac{nF}{RT}(E-E^o) + \ln\left(\frac{K+1}{K}\right)\right\} = \frac{m^*-m(E) - \left(\frac{RT}{nF}\right)^{1/2}\frac{i(E)}{K\lambda^{1/2}} - \frac{\sqrt{D\nu}}{k^o}\, i(E)\exp\left(\frac{\alpha nF}{RT}(E-E^o) + \ln\left(\frac{K+1}{K}\right)\right)}{m(E)} \tag{1.4.13}$$

As discussed in Section 1.4.1, for $E << E^o - RT/\alpha nF \ln(K+1/K)$ the last term in the numerator of (1.4.13) disappears. Then for very negative potentials (1.4.13) reduces to (1.3.34). The value of $K\lambda^{1/2}$ may be determined for this mechanism just as it is for the mechanism with a reversible charge transfer.

One may go a step further. Rewriting (1.4.13) as

$$\ln\left\{\frac{m^{*}-m(E)-\left(\frac{RT}{nF}\right)^{1/2}\frac{i(E)}{K\lambda^{1/2}}-\exp\left(\frac{nF}{RT}(E-E^{o})+\ln\left(\frac{K+1}{K}\right)\right)m(E)}{i(E)}\right\}$$

$$=\frac{\alpha nFE}{RT}-\frac{\alpha nFE^{o}}{RT}+\ln\left(\frac{K+1}{K}\right)-\ln\left(\frac{k^{o}}{\sqrt{D\nu}}\right) \qquad (1.4.14)$$

it is seen that this latter equation has a strong similarity to (1.4.4). Since $K\lambda^{1/2}$ is now known, exactly the same approach used for the analysis of simple quasi-reversible charge transfers may be applied to the return of electrode kinetic parameters for systems with complicated homogeneous kinetics. If E^{o} is known, for example from analysis of a system run at a low scan rate, then it may be possible to determine K, λ, k^{o}, and α from a single scan! Undoubtedly in practice this will rarely be possible, but (1.4.14) illustrates how with a bit of ingenuity (and luck) c.v.c.f. can result in a dramatic increase in the amount of information returned from a voltammogram.

1.4.3 EC Mechanism

In Section 1.3.3 it was stated that the c.p.s.v. theory for this mechanism was exactly that of the CE mechanism, with the equilibrium constant for the homogeneous reaction $K = 1/K'$. Thus the c.v.c.f. techniques described in Section 1.4.2 can be applied with equal facility to the appropriate limiting cases of kinetic behavior of the EC mechanism, and will not be described here.

The correspondence also implies that, as for the CE mechanism, in

diffusion controlled limiting cases of kinetic behavior s.v.c.f. should fit voltammograms of this mechanism with no error. Unlike the CE mechanism, however, it is possible that s.v.c.f. might be effective in fitting voltammograms of kinetically controlled limiting cases of behavior for this mechanism. As shown in Section 1.2.3, the voltammogram for the KP zone of the EC mechanism (see Fig. 1.4) looks like that of a reversible charge transfer. It might prove feasible to apply s.v.c.f. fo the fitting of non-diffusion controlled systems of the EC mechanism. The success of this application will be discussed in Section 1.7.

1.5 NUMERICAL METHODS

The effectiveness and range of validity of the convolutive voltammetric curve fitting and semiderivative voltammetric curve fitting procedures were determined by application to artificial lsv data. A great deal of time was spent on the development of computer programs to accomplish these three tasks of simulation, transformation, and curve fitting. A good understanding of the concepts behind the programs is essential for a successful evaluation of the work; for this reason the ideas behind the simulation, semioperator and curve fitting programs will be discussed in detail.

1.5.1 Digital Simulation of Lsv Data

In digital simulation, the behavior of continuous systems is mimicked by approximations involving discrete quantities. For

example, many physical systems are described by continuous ordinary or partial differential equations. Oftentimes the systems of equations are so complex as to defy attempts at an analytical solution. In these cases the differential equations can be approximated by the use of difference equations. With the aid of a computer the difference equations can be solved and an approximation to the solution is made, which can (within the physical limitations of the computer) be made arbitrarily close to the real solution.

There is an extensive list of electrochemical systems to which digital simulation have been applied. This is because the solutions to the boundary value problems are almost always either in terms of integral equations, which must be evaluated numerically, or the solutions to the boundary value problems cannot be determined at all. Simulation methods of one type or another were used to get the results stated before for the simple charge transfer (31-33,37,38) and the CE mechanism (38-40); other systems simulation methods have been applied to are the EC mechanism (38,40,67), the ECE mechanism (68-71), and many, many others (See, for example, Ref. 72).

For systems involving charge transfer kinetics alone, or for systems with slow homogeneous kinetics, the simulation method used was the explicit finite difference method discussed by Feldberg and others (73-75). This method involves the creation of a grid of volume elements representing the concentration of species in solution at specified distances from the electrode surface. The values of concentration are changed iteratively with increasing time increments

by means of difference equations derived from differential equations describing the change of concentration with respect to diffusion, charge transfer reaction and whatever homogeneous kinetics may be present in the system.

The relations describing the changes in concentration with time are derived from the Fick's law equations defining the electrochemical system. The differential equations are converted to difference equations by considering the differential as the limiting value as an increment goes to zero, and then removing the limit. For example, for the reversible charge transfer reaction given as (1.2.1), the Fick's second law equation for the oxidized species

$$\frac{\partial C_{ox}}{\partial t} = D_{ox} \frac{\partial^2 C_{ox}}{\partial x^2} \qquad (1.5.1)$$

becomes

$$\Delta f_{ox} = f_{ox}(\chi,\tau+1)-f_{ox}(\chi,\tau) = D_M\{f_{ox}(\chi+1,\tau)-2f_{ox}(\chi,\tau)+f_{ox}(\chi-1,\tau)\} \qquad (1.5.2)$$

where the difference equation is in terms of dimensionless variables. The dimensionless concentration f_{ox}, defined by $f_{ox} = C_{ox}/C^*_{ox}$, represents the concentration of Ox during the τ^{th} iteration (where l is the total number of iterations) for the χ^{th} volume element away from the electrode surface. The factor D_M is called the model diffusion constant and is defined by $D_M = \frac{D_{ox}\Delta t}{(\Delta x)^2}$, and is usually

chosen to be slightly less than 0.5. The factor Δt is the change in time (in seconds) for one iteration, and Δx is the distance between adjacent volume elements. Equation 1.5.2 is predictive; knowing f_{ox} at χ,τ allows one to determine f_{ox} at $\chi,\tau+1$. In this way the change in concentration due to diffusion can be determined. The extension of this treatment to the concentration changes in the reduced species is obvious.

Equation 1.5.2 is incorrect for the volume element next to the electrode surface, i.e. for $\chi = 1$. For this element in addition to diffusion changes there is a change in concentration due to the charge transfer reaction. If Butler-Volmer kinetics are assumed, the potential dependent dimensionless forward and backward charge transfer rate constants are

$$r_{hf} = \Lambda \exp\left(-\frac{\alpha nF(E-E^0)}{RT}\right) \qquad r_{hb} = \Lambda \exp\left(\frac{(1-\alpha)nF(E-E^0)}{RT}\right) \tag{1.5.3}$$

and the change in concentration in the first volume element is given by

$$\Delta f_{ox} = D_M \left\{ f_{ox}(\chi=2,\tau) - f_{ox}(\chi=1,\tau) - \frac{z(\tau)}{(D_M \ell)^{1/2}} \right\} \tag{1.5.4}$$

where $z(\tau)$ is the dimensionless flux

$$z(\tau) = \frac{2(D_M \ell)^{1/2} \left[r_{hf} f_{ox}(\chi=1,\tau) - r_{hb} f_{red}(\chi=1,\tau)\right]}{\left[2(D_M \ell)^{1/2} + r_{hf} + r_{hb}\right]} \qquad (1.5.5)$$

The current, the usual quantity desired from the simulation, is found as

$$i(\tau) = nFA C^*_{ox} \sqrt{D_{ox} t_k} z(\tau) \qquad (1.5.6)$$

where t_k is the duration (in seconds) of the experiment, so that $\Delta t = t_k/l$.

Proceeding from what was just done, it would seem reasonable that in simulating systems with homogeneous kinetics, one would include terms like $k_f f_{ox} \Delta t$ in (1.5.2). For example, for the CE mechanism of (1.2.10), the difference equation analogous to (1.5.2) would be

$$\Delta f_{ox} = D_M \{f_{ox}(\chi+1,\tau) - 2f_{ox}(\chi,\tau) + f_{ox}(\chi-1,\tau)\} + k_f f_c(\chi,\tau)\Delta t - k_b f_{ox}(\chi,\tau)\Delta t \qquad (1.5.7)$$

One would simply replace (1.5.2) by this equation in doing the simulation.

In practice, however, this is usually not done. Instead the concentration changes due to homogeneous kinetics are done after the diffusion and charge transfer reaction changes. This is permissable provided that Δt is small, which it must be for an accurate

simulation.

For the CE mechanism, if one separates the homogeneous kinetics from the diffusion and charge transfer effects, the resultant difference equation is

$$\Delta f_{ox} = k_f f_c(\chi,\tau)\Delta t - k_b f_{ox}(\chi,\tau)\Delta t \qquad (1.5.8)$$

One does the simulation by applying (1.5.8) subsequent to (1.5.2), so that each iteration consists of two steps, first finding the concentration change due to diffusion and charge transfer and then finding the concentration change due to homogeneous kinetics.

Equation 1.5.8 can be, and often is, used to do simulations, especially for very complicated homogeneous kinetics. Unfortunately, for first order kinetics the solution is accurate only for $\Delta t < 0.1/(k_f+k_b)$. This means that for large rate constants Δt must be very small, which in turn means that a very large number of iterations must be used to do the simulation. The explicit finite difference method is impractical for very fast kinetics, because the computer time needed to do the simulation becomes excessively large.

This situation can be improved by considering the differential equations that describe the change in concentration due to only homogeneous kinetics. For the CE mechanism the equations are

$$\frac{\partial f_c}{\partial t} = k_b f_{ox} - k_f f_c$$

$$\frac{\partial f_{ox}}{\partial t} = k_f f_c - k_b f_{ox} \qquad (1.5.9)$$

These can be solved exactly for Δf_{ox} (and $\Delta f_c = -\Delta f_{ox}$) as

$$\Delta f_{ox} = \frac{k_b f_c(\chi,\tau) - k_f f_{ox}(\chi,\tau)}{k_f+k_b} \left(1-\exp[-(k_f+k_b)\Delta t]\right) \qquad (1.5.10)$$

where $f_c(\chi,\tau)$ and $f_{ox}(\chi,\tau)$ are the concentrations of C and Ox after the diffusion-charge transfer step. Equation 1.5.10 enables the use of about five times larger rate constants. Note that for Δt small, (1.5.10) reduces to (1.5.8).

For very fast kinetics this improvement is not enough. For this reason the numerical integration method of Nicholson and Shain (38) was employed for the simulation of systems with rapid kinetics. In this method, the partial differential equations and boundary conditions describing the CE mechanism with a reversible charge transfer are first solved to get an integral equation in time:

$$1 - \int_0^{at} \frac{\psi(z)dz}{\sqrt{at-z}} = \frac{K+1}{K}\,\theta S_\lambda(at) \int_0^{at} \frac{\psi(z)dz}{\sqrt{at-z}} + \frac{1}{K}\int_0^{at} \frac{\exp[-\lambda(at-z)]\psi(z)dz}{\sqrt{at-z}}$$

(1.5.11)

where $a = nF\nu/RT$, $\theta = \exp[(nF/RT)(E - E^O)]$, E_i is the initial

potential, and $S_\lambda(at) = \exp(-at)$.

The solution desired is the value of $\psi(at)$. Suppose that the entire interval from 0 to at is divided into n subintervals each of length $\delta = at/n$; from this it is seen that the value of $\psi(n\delta)$ is desired, where n is some integer. Furthermore suppose that all the $\psi(k\delta)$, $k = 1,2,\ldots,n-1$ are already known. The substitution $z = k\delta$ is made into all the integrals of (1.5.11) and these now have the form

$$\int_0^{at} \frac{f(at-z)\psi(z)dz}{\sqrt{at-z}} = \sqrt{\delta} \int_0^{n} \frac{f((n-k)\delta)\psi(k\delta)dk}{\sqrt{n-k}} \qquad (1.5.12)$$

These integrals cannot be evaluated in this form because a singularity exists at n = k. This singularity is removed by integration by parts, and the resulting integral is in the form of a Riemann-Stieltjes integral (76), where it is assumed that the integral of $f((n-k)\delta)/\sqrt{n-k}$ exists, and $g((n-k)\delta)$ is that integral. The Riemann-Stieltjes integral may be recast as a finite sum

$$\int_0^{n} g((n-k)\delta)d\psi(k\delta) = \sum_{k=1}^{n} g((n-k)\delta)\,[\psi(k\delta)-\psi((k-1)\delta)] \qquad (1.5.13)$$

After substituting the corresponding sum for all the integrals of (1.5.12), the resulting equation is solved for $\psi(n\delta)$. As all the $\psi(k\delta)$ are known, the value of $\psi(n\delta)$ follows immediately. The process is extended to determine $\psi((n+1)\delta)$, and continued until the desired termination.

For the simulation of the EC mechanism with a reversible charge transfer the following equation, also from Nicholson and Shain, was used

$$1 - \int_{.0}^{at} \frac{\psi(z)dz}{\sqrt{at-z}}$$

$$= \frac{1}{K+I}\,\theta S_{\lambda}(at) \int_{0}^{at} \frac{\psi(z)dz}{\sqrt{at-z}} + \frac{K}{K+I}\,\theta S_{\lambda}(at) \int_{0}^{at} \frac{\exp[-\lambda(at-z)]\psi(z)dz}{\sqrt{at-z}} \qquad (1.5.14)$$

For the simulation of the CE mechanism with a quasi-reversible charge transfer, Nicholson and Shain do not give an integral equation. One is easily constructed, however, from (1.3.10) and (1.3.4). Making the same substitutions as did Nicholson and Shain, one derives

$$1 - \left(1 + \frac{K+1}{K}\,\theta S_{\lambda}(at)\right) \int_{0}^{bt} \frac{\psi(z)dz}{\sqrt{bt-z}} =$$

$$\frac{K+1}{K}\, e^{u-bt}\, \psi(bt) + \frac{1}{K} \int_{0}^{bt} \frac{\exp[-\lambda(bt-z)]\psi(z)dz}{\sqrt{bt-z}} \qquad (1.5.15)$$

where $b = \alpha nF\nu/RT$, and $e^{u} = (\sqrt{\pi\alpha}/\Lambda)\exp((\alpha nF/RT)(E - E^{o}))$. From these two equations, algorithms for a solution in terms of $\psi(n\delta)$ can be obtained in the same manner as above.

One other technique was tested for the simulation of fast

homogeneous kinetic systems; this is the orthogonal collocation technique (77-79). In this method the space part of the solution to the partial differential equation is approximated by a sum of orthogonal Laguerre polynomials of order N. In this way the system of M partial differential equations can be reduced to a system of MN first order ordinary differential equations, which can be solved using a standard differential equation solving technique such as a Runge-Kutta or Hamming predictor-corrector technique. (For information on these differential equation solving methods, see Ref. 80, for example.) Work done by us using this method showed little improvement in computation time over the explicit finite difference method, however, even though this method had been touted as a time saver. For large rate constants the order of the approximating polynomial must be very large, which leads to great increases in computer time.

1.5.2 Semiintegration and Semidifferentiation

The artificially created data files were numerically transformed, either by simple semidifferentiation or by the application of one of the c.v.c.f. functions. In either case, the input file must be either semidifferentiated or semiintegrated. The algorithm to perform semioperations originally used by this group (66) was based upon semiintegration employing the method of Huber (81) as discussed by Nicholson and Olmstead (82), followed by differentiation to get the semiderivative if desired. It was discovered that this process is in error (83), and subsequently semioperations were done using the Gl

algorithm of Oldham and Spanier (84)

$$\frac{d^q i}{dE^q} = \frac{N^q}{|E_i - E_f|^q \, \Gamma(-q)} \sum_{j=0}^{N-1} \frac{\Gamma(j-q)}{\Gamma(j+1)} i_j \qquad (1.5.16)$$

where i_j is the j^{th} current point, Γ is the Euler gamma function, N is the number of points in the current file, and q = 1/2 for semidifferentiation, q = -1/2 for semiintegration. This operation is a convolution of the current with another file, and it is from this operation that convolution voltammetry gets its name.

1.5.3 Curve Fitting

After the artificial lsv data files have been created and transformed by the convolution methods, the files were used as input to a curve fitting program. In all cases the c.v.c.f. technique involves fitting a $sech^2$ function to the transformed data. For this reason the curve fitting process is properly called non-linear regression analysis. There are a number of review articles on the application of both linear and non-linear regression analysis to chemistry (85-87) as well as a great number of statistics texts describing regression methods (See, for example, Refs. 88 and 89). Two different non-linear regression methods were investigated for this work, the sequential simplex method and Marquardt's method.

The theory behind non-linear regression analysis is, except for the nature of the fitting function, exactly the same as regression

analysis with a linear fitting function. It is assumed that some measurable response Y is describable by the sum of a model function f and an error term

$$Y = f(\underline{x},\underline{a}) + \varepsilon \qquad (1.5.17)$$

where $\underline{x}$ is a vector of observations such that $\underline{x} = (x_1,x_2,\ldots,x_n)$ and $\underline{a}$ is a vector of parameters $\underline{a} = (a_1,a_2,\ldots,a_p)$. If the error ε is assumed to be independent and uncorrelated between measurements, as is the case for random error, then the best values of the parameters a_i can be found by minimizing the error sum of squares

$$S(\underline{a}) = \sum_{i=1}^{n} \{Y_i - f(x_i,\underline{a})\}^2 \qquad (1.5.18)$$

with respect to $\underline{a}$. In linear regression it is possible to find the best a_i by setting all the $\frac{\partial S}{\partial a_i}$ equal to zero and solving the system of simultaneous equations. For non-linear fitting functions, however, the system of equations is too complex to be solved, and other approaches to minimizing $S(\underline{a})$ must be taken.

One approach is that of the sequential simplex method. The sequential simplex method (90) is not really a curve fitting method, but is rather a general optimization method, whether optimization towards a minimum or a maximum. Suppose the fitting function contains p parameters to be fit. Initially a p+1 verticed equilateral figure (a 'simplex') is created in a p+1 dimensioned response space, where p

dimensions are the parameters to be fit, and the other dimension is the response variable, in this case the error sum of squares. The simplex works to optimize the response by replacing the vertex with the worst response with a new vertex. The new vertex is placed somewhere along the line connecting the old, worst vertex and the centroid of the simplex and extending through both of these points. After the new vertex is found, the response for this vertex is determined, and the process is repeated; i.e., the new worst response is determined and that vertex is then changed. The optimization process is continued until a limiting number of iterations is reached, or until some convergence criterion in the response is reached.

The motivation behind the simplex method is that a movement away from the worst response is in the end a movement towards the best response. Unfortunately, however, this movement can occur very slowly. By using a more statistically oriented regression method that works by moving towards the best response it is often possible to achieve a fit more rapidly than by using the simplex.

Marquardt's method (88,89) is actually a compromise between two other non-linear regresssion methods, Taylor's method and the method of steepest descents. In Taylor's method the non-linear fitting function $f(\underline{x},\underline{a})$ is approximated by a Taylor series expansion

$$f(\underline{x},\underline{a}) = f(\underline{x},\underline{a}_o) + \sum_{i=1}^{p} \left(\frac{\partial f(\underline{x},\underline{a})}{\partial a_i} \right)_{\underline{a}=\underline{a}_o} (a_i - a_{io}) \qquad (1.5.19)$$

which is truncated after the first order terms. The vector $\underline{a}_0$ is the vector of initial guesses of the parameter vector $\underline{a}$. By this means the problem becomes one of linear regression analysis; using standard linear regression techniques, a correction vector $\underline{b}_0$ can be determined such that $\underline{a}_1 = \underline{a}_0 + \underline{b}_0$ is a revised best estimate of the optimum value of $\underline{a}$. From this corrected value $\underline{a}_1$ a new correction vector $\underline{b}_1$ may be determined, and then a new best estimate $\underline{a}_2$. The process is continued until some convergence criterion is reached. The Taylor method works well for cases in which the initial guess $\underline{a}_0$ is close to the optimum value $\underline{a}$. For initial guesses far away from $\underline{a}$, the higher order terms not included in (1.5.19) cause the technique to converge slowly, or not at all.

The method of steepest descent is complementary to Taylor's method; it works well for $\underline{a}_0$ far from $\underline{a}$, but poorly for $\underline{a}_0$ near $\underline{a}$. In the method of steepest descent the gradient vector $\underline{c} = -\nabla \cdot S(a)$ is used as a correction vector; this makes sense, because this is the direction of the greatest local improvement of the response. The response is found for points $\underline{a}_0 + \lambda \underline{c}_0$ for increasing values of λ until the response begins to decrease. The point with the best response is chosen as $\underline{a}_1$, and the process begun anew with the determination of the $\underline{c}_2$ vector at the point $\underline{a}_1$. Near the optimum response the response curve is quite flat, and small errors in the input data often cause the direction of the gradient to be significantly away from the direction of the best response, and thus convergence near $\underline{a}$ generally takes a long time with this method.

The Marquardt method uses as a correction vector

$$\underline{\delta} = \underline{b} + \lambda \underline{c} \qquad (1.5.20)$$

where $\underline{b}$ and $\underline{c}$ are the correction vectors for the Taylor method and the method of steepest descents, respectively. Initially λ is large, so that for $\underline{a}_0$ far away from $\underline{a}$ the method corresponds to the method of steepest descents. As the fitting continues, however, and $\underline{a}_i$ approaches $\underline{a}$, λ is decreased so that the method becomes more like Taylor's method. Marquardt's method achieves the best of both worlds, and fits the function quickly both far away from convergence and near convergence.

1.6 IMPLEMENTATION OF METHODS

The data files created for the study of the application of both s.v.c.f. and c.v.c.f. to charge transfer kinetic systems are shown in Table 1.4. The program used to create these files was a FORTRAN program named DIGIT, which employed the explicit finite difference method discussed in Section 1.5.1. This program requires as input the total duration of the simulation t_k, the number of iterations l, (which equals the number of data points per file), the dimensionless rate constant Λ, the standard potential E^o, the number of electrons transferred n, the initial potential E_i and the scan rate ν. For programs taken from the literature the reader is directed to the appropriate references.

Table 1.4: Definition of systems and returned fit parameters for application of s.v.c.f. to single peak charge transfer kinetic systems

Filename	Λ[a]	Pot.[b]	Height[c]	Width[b]	R^2
A	1.133×10^{-3}	-0.6614	1.85	76.0	0.9980
B	1.133×10^{-2}	-0.6023	1.85	76.0	0.9980
C	0.1133	-0.5441	1.94	73.3	0.9990
D	0.2667	-0.5289	2.08	68.5	0.9996
E	0.5667	-0.5143	2.39	59.2	0.9999
F	1.133	-0.5078	2.65	53.4	0.9999
G	5.667	-0.5019	3.01	47.1	0.9999
H	11.33	-0.5011	3.06	46.2	0.9999
I	1.133×10^{2}	-0.5004	3.12	45.4	0.9999
J	1.133×10^{3}	-0.5003	3.13	45.3	0.9999

a) Other parameters defining the systems are discussed in the text.
b) Units for potential are V, of width are mV.
c) Arbitrary units.

The dimensionless rate constants for each file are included in Table 1.4. All files are of one peak, have potential ranges from 0.0 V to -1.0 V, and assume t_k = 1.0, α = 0.5, E^o = -0.5 V, and n = 2. All files required 512 iterations, which took about 85 seconds of CPU time to complete.

DIGIT, like all programs used in this work, was run on a laboratory microcomputer with a Digital Equipment Corp. LSI-11/23 CPU. The operating system was DEC RT-11, Version IV, with a FORTRAN IV compiler. The system possessed graphics capability via a Tektronix 4006 terminal and 4662 digital plotter, and was equipped with Data Systems DSD-440 floppy disk data storage.

After creation, the artificial charge transfer kinetic files were semidifferentiated by a FORTRAN called GDSEMI which employed the G1 algorithm as given by (1.5.16). The time for the semidifferentiation of a 512 point file was about 80 seconds. The semidifferentiated files were written to disk and used as input for the curve fitting program BIMFIT, which is based on the sequential simplex algorithm, and for the program MARFIT, which is based on Marquardt's method. Each program uses as a fitting function

$$f(E) = A \operatorname{sech}^2 \{B(E-C)\} \qquad (1.6.1)$$

The variable A is called the returned peak height and is the height at the peak maximum. B is related to the peak width by peak width = 1.7627/B, where the peak width is the FWHM of the sech^2 peak.

Finally, C is called the peak potential and is the potential of the $sech^2$ peak at the peak maximum. As input, each program requires only the number of peaks in the input data file and the file itself. Each program first determines trial values of A, B and C for each peak using an iterative stripping approach (92).

After the initial guesses to the parameters have been found the two programs differ. The simplex algorithm in BIMFIT is implemented through the subroutine NELMIN as given by O'Neill (93), with corrections from Chambers and Ertel (94), Benyon (95), and Hill (96). NELMIN requires a function to evaluate the response at the vertices (which is the coefficient of determination R^2, calculated as 1 - (the error sum of squares S(a) divided by the variance of the dependent variable.)) As input NELMIN requires dependent and independent variable arrays, the number of parameters to be fit, and an array of initial guesses to the parameters. The program also requires stepping values by which to vary the parameters as the simplex is created; these were chosen to be 10 mV for the peak potential, half of the height for the peak height, and the FWHM for the peak width. The program terminates whenever the variance of the coefficients of determination among all of the vertices of the simplex was less than 1×10^{-12}. Times for fitting of single peaks were on the order of 50-80 seconds.

The subroutine CURFIT to do curve fitting using Marquardt's method was taken from Bevington (89). This is a driver subroutine; it requires other subroutines to evaluate the fitting function, to

evaluate the derivatives of the fitting function, and to do matrix inversion. As input CURFIT requires an independent and dependent variable array, the number of parameters to be fit, an array containing the values of the parameters, and the value of the coefficient λ used in (1.5.20) and not to be confused with the dimensionless homogeneous rate constant. Lambda is initially set equal to 1000. The convergence criterion for this program is that the relative change in each of the parameters be less than 0.1%. Typical times for the fitting of single peaks using MARFIT were on the order of 25-30 seconds.

The output for both programs is the final values of the peak potentials, heights and widths. Also output are the final coefficient of determination and the time in seconds needed to do the fit.

The returned values of peak potential, height and width by BIMFIT and MARFIT were nearly identical for the files considered in this work. The time required for fitting was more than twice as long for BIMFIT than for MARFIT. This decreased fitting time has also been noted for the fitting of peaks in Mossbauer spectroscopy (97) using both the simplex method and the Gauss iterative method, which is similar to Marquardt's method. However, the fitting program used throughout Chapters 2 and 3 is BIMFIT. This is because MARFIT was not available for use at the time this earlier work was done.

Synthetic semiderivative voltammograms of overlapping waves corresponding to systems with reversible and non-reversible charge transfer kinetics were also created. This was done to demonstrate the

effectiveness of s.v.c.f. in fitting systems with non-reversible charge transfer kinetics. These waves were constructed by adding $sech^2$ functions with specified peak potentials, heights and widths to the semiderivatives of the files in Table 1.4. The added $sech^2$ function was in all cases of approximately the same height as the wave to which it was added, was of 45.3 mV in width, and had a peak potential either 35, 50, or 70 mV cathodic to the peak potential of the file to which it was added.

After creation, the overlapped semiderivative was used as input to the curve fitting programs, and also to versions of BIMFIT and MARFIT called CNWSBM and CNWSMR, respectively. These programs are the same as the original except that the peak widths are not varied, but rather are entered as input parameters to the program. In this study, peak widths input to CNWSBM and CNWSMR were the returned peak widths taken from application of BIMFIT and MARFIT to the semiderivatives of the single peak charge transfer kinetic systems. As for BIMFIT and MARFIT, results from these two programs were identical, except that CNWSMR was about twice as fast as CNWSBM.

In addition to s.v.c.f., a c.v.c.f. technique based on (1.4.4) was used for the analysis of the files in Table 1.4. The program used to accomplish this is a FORTRAN program called QUASMI. This first semiintegrates the input current data, and then employs a fitting function

$$f(E_j) = \ln\left\{\frac{A-m(E_j)\ [1+\exp\ (\frac{nF}{RT}\ (E_j-C))]}{i(E_j)}\right\} \qquad (1.6.2)$$

to fit the data, where A is the limiting value of m(E) at very negative potentials (here taken as the average of the last 50 points of the semiintegral), and C is a parameter to be varied.

The correct C is from (1.4.4) $C = E^o$. The best estimate of C is achieved by varying C so that the variance in the linear least squares fit of E_j to $f(E_j)$, defined by

$$s^2 = \frac{\Sigma\ f^2(E_j)-a\ \Sigma\ f(E_j)-b\ \Sigma\ E_i f(E_j)}{NP-2} \qquad (1.6.3)$$

is a minimum. In (1.6.3), a and b are the slope and intercept of the fit, and the sums are only over certain E_j. Because the exponential term either blows up or goes to zero for E much different from E_j, the fitting function was weighted so that $f(E_j)$ was non-zero only for those values of E_j such that $0.1A < m(E_j) < 0.9A$. The process used to determine C is an interactive one, allowing the user to view plots of s^2 as a function of C. After the user chooses the range over which C is to be varied, QUASMI plots the variance and, if so desired, determines the interpolated minimum of the variance plot, which is the best estimate of C (or E^o). The program then does one final fit of E_j to $f(E_j)$, and returns the slope and intercept from this fit. From (1.4.4), the transfer coefficient is

$$\alpha = \left(\frac{RT}{nF}\right) \text{Slope} \qquad (1.6.4)$$

and the dimensionless heterogeneous rate constant is

$$\ln \Lambda = -\frac{\alpha n F E^{o}}{RT} - \frac{1}{2} \ln \left(\frac{nF}{RT}\right) - \text{Intercept} \qquad (1.6.5)$$

where $E^{o} = C$.

The data files created for the study of the s.v.c.f. and c.v.c.f. techniques as applied to the CE mechanism with reversible charge transfer are shown in Table 1.5, along with the corresponding rate constants. The program DIGIT was used to create files K through P, with a modification to enter the forward and backward homogeneous rate constants instead of the dimensionless charge transfer rate constant. The FORTRAN program NSSOL1, employing Nicholson and Shain's simulation method, was used for the creation of files Q through CC. This program was based on the use of (1.5.11). NSSOL1 required the same input as the modified version of DIGIT just described. For both programs the equilibrium constant $K = k_f/k_b$ was assumed to be 10^{-4}; other input parameters were the same as those input to DIGIT for the charge transfer systems. All files required 512 iterations, and either program required about 180 seconds of CPU time.

Files K through CC were semidifferentiated and input to BIMFIT to determine the applicability of s.v.c.f. to the CE mechanism. Perhaps more importantly, several c.v.c.f. techniques were applied to the

Table 1.5: Definition of systems and results for application of s.v.c.f. to voltammograms of the CE mechanism with a reversible charge transfer

Filename	$\lambda^{a,b}$	Pot.[b]	Height[c]	Width[b]	R^2
K	0.00100	-0.5003	2.211×10^{-4}	45.4	0.9999
L	0.0100	-0.5007	2.219×10^{-4}	46.2	0.9958
M	0.0500	-0.5023	2.284×10^{-4}	48.8	0.9338
N	0.100	-0.5042	2.409×10^{-4}	50.4	0.8457
O	0.200	-0.5075	2.639×10^{-4}	52.8	0.7315
P	0.500	-0.5159	3.351×10^{-4}	58.8	0.6316
Q	1.00	-0.5234	4.543×10^{-4}	75.7	0.6064
R	2.00	-0.5276	6.428×10^{-4}	75.5	0.6065
S	3.00	-0.5301	7.869×10^{-4}	74.6	0.6055
T	5.00	-0.5334	1.018×10^{-3}	74.8	0.6065
U	10.0	-0.5379	1.437×10^{-3}	75.3	0.6090
V	100.	-0.5530	4.389×10^{-3}	55.6	0.5687
W	1.00×10^{3}	-0.5781	1.266×10^{-2}	78.7	0.6720
X	1.00×10^{4}	-0.5913	3.875×10^{-2}	82.0	0.6964
Y	1.00×10^{6}	-0.6182	0.3044	90.6	0.8407
Z	1.00×10^{8}	-0.6203	1.340	59.2	0.9851
AA	1.00×10^{10}	-0.6196	2.067	47.1	0.9998
BB	1.00×10^{11}	-0.6195	2.156	46.0	0.9999
CC	1.00×10^{12}	-0.6195	2.185	45.6	0.9999

a) Other parameters defining the systems are discussed in the text.
b) Units of potential are V, of width are mV.
c) Arbitrary units.

analysis of these files. The first applied was intended to enhance the analysis of systems in the KP zone of behavior. A FORTRAN program KPSEMI was written to accomplish this. The program first semiintegrates the input current file. After semiintegration, a further transformation was made by means of (1.4.5), where i^* is the limiting value of the current at negative potentials, and was chosen as the average of the last 50 current points. The file f(E) was then written to disk and used as input to BIMFIT.

Another FORTRAN program, called KESEMI, was written to effect the analysis of systems in the KE zone of kinetic behavior. This program initially semiintegrates the input current file. After this, the program varies a parameter C in the fitting function

$$f(E) = m(E) + Ci(E) \qquad (1.6.6)$$

From (1.4.9), for the correct value of C, at very negative potentials f(E) is a constant. KESEMI determines a best estimate of C by varying C so as to make the absolute value of the slope returned from a linear least squares fit of f(E) to E a minimum. The last 50 points of the file are used for this purpose. After the best estimate is determined, the value of $K\lambda^{1/2}$ is determined from (1.4.11). The function f(E) is determined for the entire file using the best estimate, and the transformed file is subsequently written to disk. The transformed file is then used as input to BIMFIT.

Several data files were created to investigate the application of

c.v.c.f. to a CE mechanism coupled to a non-reversible charge transfer. A FORTRAN program NSSOL3 was used to create these files. This program was based on (1.5.15). Input to the program was the same as that of NSSOL1, with the addition of the dimensionless rate constant and transfer coefficient for the charge transfer reaction. The files created are shown in Table 1.6, along with the input Λ for each file. The forward and backward homogeneous rate constant for each file was 1.947×10^{5} s^{-1} and 1.947×10^{9} s^{-1}, respectively, which results in $K = 10^{-4}$ and $\lambda = 2.5 \times 10^{7}$ for each file. The transfer coefficient was chosen as 0.5, and the other input parameters were those used in creating files K through CC.

A c.v.c.f. technique based on (1.4.14) was used for the analysis of files DD through NN. As discussed in Section 1.4.2, for very negative potentials (1.4.14) reduces to (1.3.34). Thus, the FORTRAN program ALLSMI first uses the methods of KESEMI to determine the parameter C in (1.6.6). After the best estimate of C is found so as to make the function f(E) of (1.6.6) as flat as possible for the last 50 points, the entire file is transformed by means of (1.6.6), using the best estimate. The resultant file can than be analyzed by the methods that QUASMI uses to find E^{o}, α and Λ.

Finally, several data files were created to study the applicability of the s.v.c.f. technique to systems of the EC mechanism with a reversible charge transfer. The program used to create these files was a FORTRAN program called NSSOL2. The files created by NSSOL2 are shown in Table 1.7, along with the corresponding

Table 1.6: Definition of systems and results of application of c.v.c.f. for CE mechanism with quasi-reversible charge transfer kinetics

Filename	Λ^a	$K\lambda^{1/2}$	$E^{o\ b}$	$K\ (x10^{-4})^b$	$\lambda(x10^7)$	α^b	Λ^b
DD	1.772×10^3	0.508		No Minimum			
EE	8.862×10^2	0.508	-0.6174	1.06	2.30	0.542	479.
FF	3.545×10^2	0.508	-0.6175	1.06	2.30	0.508	313.
GG	1.772×10^2	0.509	-0.6175	1.06	2.31	0.500	177.
HH	8.862×10^1	0.508	-0.6175	1.06	2.30	0.500	91.1
II	3.545×10^1	0.508	-0.6175	1.06	2.30	0.500	36.6
JJ	1.772×10^1	0.508	-0.6175	1.06	2.30	0.500	18.4
KK	8.862	0.499	-0.6177	1.04	2.30	0.500	9.10
LL	3.545	0.498	-0.6181	1.01	2.43	0.500	3.65
MM	1.772	0.498	-0.6156	1.23	1.64	0.500	1.81
NN	8.862×10^{-1}	0.497		No Minimum			

a) Other parameters defining the files are discussed in the text.
b) Calculated by ALLSMI as discussed in the text.
c) Units are V.

Table 1.7: Results for application of s.v.c.f. to voltammograms of the EC mechanism with a reversible charge transfer

Filename	λ[a]	Potl.[b]	Height[c]	Width[b]	R^2
OO	1.00×10^{12}	-0.3819	2.20	45.4	1.000
PP	1.00×10^{9}	-0.3846	2.26	44.0	1.000
QQ	1.00×10^{6}	-0.4102	2.51	39.6	0.999
RR	1.00×10^{4}	-0.4385	2.55	39.1	0.999
SS	5.00×10^{2}	-0.4576	2.55	39.0	0.998
TT	1.00×10^{2}	-0.4679	2.55	39.0	0.998
UU	5.00×10^{1}	-0.4724	2.55	39.0	0.998
VV	5.00	-0.4868	2.52	39.7	0.999
WW	1.00	-0.4948	2.39	42.0	0.999
XX	0.100	-0.4994	2.23	44.9	1.000
YY	1.00×10^{-2}	-0.5001	2.20	45.4	1.000
ZZ	1.00×10^{-4}	-0.5002	2.20	45.5	1.000

a) Other parameters defining the files are discussed in the text.
b) Units of potential are V, of width are mV.
c) Arbitrary units.

dimensionless homogeneous rate constants. Besides the rate constants, other input parameters to NSSOL2 were the same as those input to NSSOL1. The equilibrium constant assumed for the files was $K = 10^4$. After creation, files were semidifferentiated and written to disk.

Several files of overlapped waves were also created to determine the applicability of s.v.c.f. for the fitting of waves of the EC mechanism. $Sech^2$ functions were added to the semiderivative of the file TT of Table 1.7. The height of the added function was 2.55, the FWHM was 45 mV, and the peak potentials of the functions were varied to be between 25 and 60 mV cathodic to the peak potential of the semiderivative peak. After the $sech^2$ functions were added, the files were written to disk and used as input to BIMFIT.

1.7 RESULTS AND DISCUSSION

1.7.1 Charge Transfer Kinetics

As was seen in Section 1.3.1, the s.v.c.f. technique is not strictly valid for the curve fitting of semiderivatives of non-reversible charge transfers. Nonetheless, s.v.c.f. is the only technique based on c.p.s.v. that allows one to attempt the resolution of overlapped lsv peaks. Because, as was seen, the appearance of the semiderivative of an irreversible charge transfer is very much like that of a reversible charge transfer, it was thought that, even though there would be some error in the fitting, because of the peak resolution ability it might prove useful to try to use s.v.c.f. for non-reversible charge transfers. The first discussion, then, is on

the effectiveness of the application of s.v.c.f. to the curve fitting of the non-reversible charge transfer.

The effectiveness of any curve fitting technique is judged by how well returned fit peak parameters obey relations derived from theory. For the semiderivative voltammetric curve fitting technique as applied to charge transfer kinetic systems, this first implies that the semiderivative is $sech^2$ in form, as is stated by (1.3.14) for reversible charge transfer systems, and implied by Figure 1.7 for irreversible charge transfers. The first condition of validity of s.v.c.f. for any system must be the return of a coefficient of determination, as defined before, close to 1, whenever there is no appreciable noise or distortion in the voltammogram.

The s.v.c.f. technique will be considered valid for non-reversible charge transfer systems only when, in addition to the return of R^2 close to 1, returned peak parameters agree with parameters derived from theoretical relations. This is because the coefficient of determination is not a reliable criterion on which to judge the accuracy of a peak resolution technique; oftentimes large coefficients of determination are returned from fits to peaks, while the fit parameters are in great error. Useable relations with which to judge the effectiveness of s.v.c.f. exist only for reversible and irreversible charge transfer kinetic systems. The relations that may be so used are (1.3.15) and (1.3.16) for reversible charge transfers and (1.3.21) and (1.3.22) for irreversible charge transfers. From (1.3.15) and (1.3.16) if s.v.c.f. is valid for reversible charge

transfer systems, then returned peak potentials and widths for these systems will be -0.500 V and 45.3 mV, respectively. If s.v.c.f. is to be valid for irreversible charge transfer systems, the returned peak widths for these systems will be 75.5 mV, as given by (1.3.22), and a linear least squares fit of returned peak potential vs. ln Λ for these systems will have a slope of 25.7 mV, and an intercept of -0.435 V, as given by (1.3.21).

The returned fit parameters for the application of s.v.c.f. to the simple charge transfer system are shown in Table 1.4. From the definitions of charge transfer reversibility and irreversiblity given in Section 1.2.1, files I and J are seen to be reversible while files A and perhaps B are irreversible. A linear least squares fit of returned E_p vs. ln Λ for files A and B gave a slope of 0.0257 V and an intercept of -0.4313 V. Comparisons of these values and the returned peak parameters for files A, B, I, and J with the values predicted in the preceding paragraph show close agreement between fit and theoretical parameters for both reversible and irreversible charge transfer systems. Coefficients of determination are close to 1 for the four files. Both conditions of validity are fulfilled for the application of s.v.c.f. to both reversible and irreversible charge transfer systems.

There are no simple relations with which returned peak potentials or widths can be used to judge the effectiveness of s.v.c.f. for systems with quasi-reversible charge transfer kinetics. Because the returned R^2 values get closer to 1 as Λ is increased, and because

quasi-reversible systems become more and more reversible as Λ is increased, one might expect semiderivatives of waves of these systems to become more and more $sech^2$ in shape as Λ is increased. The semiderivative voltammetric curve fitting technique is expected to better fit these semiderivatives than in the completely irreversible case.

There is another way to show that s.v.c.f. is valid for non-reversible charge transfer systems. One may overlap semiderivatives of waves for these systems with $sech^2$ functions and use s.v.c.f. to resolve the overlapped peaks. The accuracy with which parameters are returned from the fused peak waves gives an indication of the suitability of s.v.c.f. for the curve fitting of the wave for the quasi-reversible system, and incidentally gives an indication of how well peak resolution of such overlapped systems may work.

Towards this end, the accuracy of resolution is rather arbitrarily defined as

$$\text{Accuracy} = 1 - \frac{1}{NP} \sum_{i=1}^{p} \left| \frac{(\text{Returned peak parameter} - \text{True peak parameter})}{\text{True peak parameter}} \right| \qquad (1.7.1)$$

where NP is the number of peaks, and P is the number of parameters, 3 x NP. Because the peak potential is referenced to an arbitrary zero, the residual in peak potential is not divided by the true peak

potential; rather, it is divided by the true peak width, giving (perhaps) a less biased estimate of the accuracy. Failure of resolution is defined as the return of accuracy less than 0.85

A plot of accuracy vs. increasing Λ is shown in Fig. 1.8. Note that the abscissa is not to any scale , but rather reflects only an ordering of accuracy with increasing Λ. These plots of accuracy in general increase with Λ. This implies that fits of semiderivatives of waves of non-reversible charge transfer kinetic systems improve with increasing Λ. The $sech^2$ function is an even better fitting function for the semiderivative of a quasi-reversible charge transfer system than it is for an irreversible charge transfer system.

It is interesting that accuracy does not always increase monotonically with increasing Λ, and that accuracy does not always increase with increasing peak separation. This may be the result of the obtaining of a false minimum by the curve fitting programs. If the peak potential of a fit peak is changed slightly, the R^2 between experimental peak and fit peak changes greatly. If fit peak height and width are changed simultaneously so as to increase height and decrease width (or vice versa) the returned R^2 changes only slightly. In this case the small non-$sech^2$ nature of a semiderivative of a wave for a non-reversible charge transfer system could, in the right circumstances, affect returned accuracy greatly.

One way to negate this effect is to constrain the peak widths in the fitting program, using input peak widths from single peak data. This is equivalent to empirical approaches employed in the past

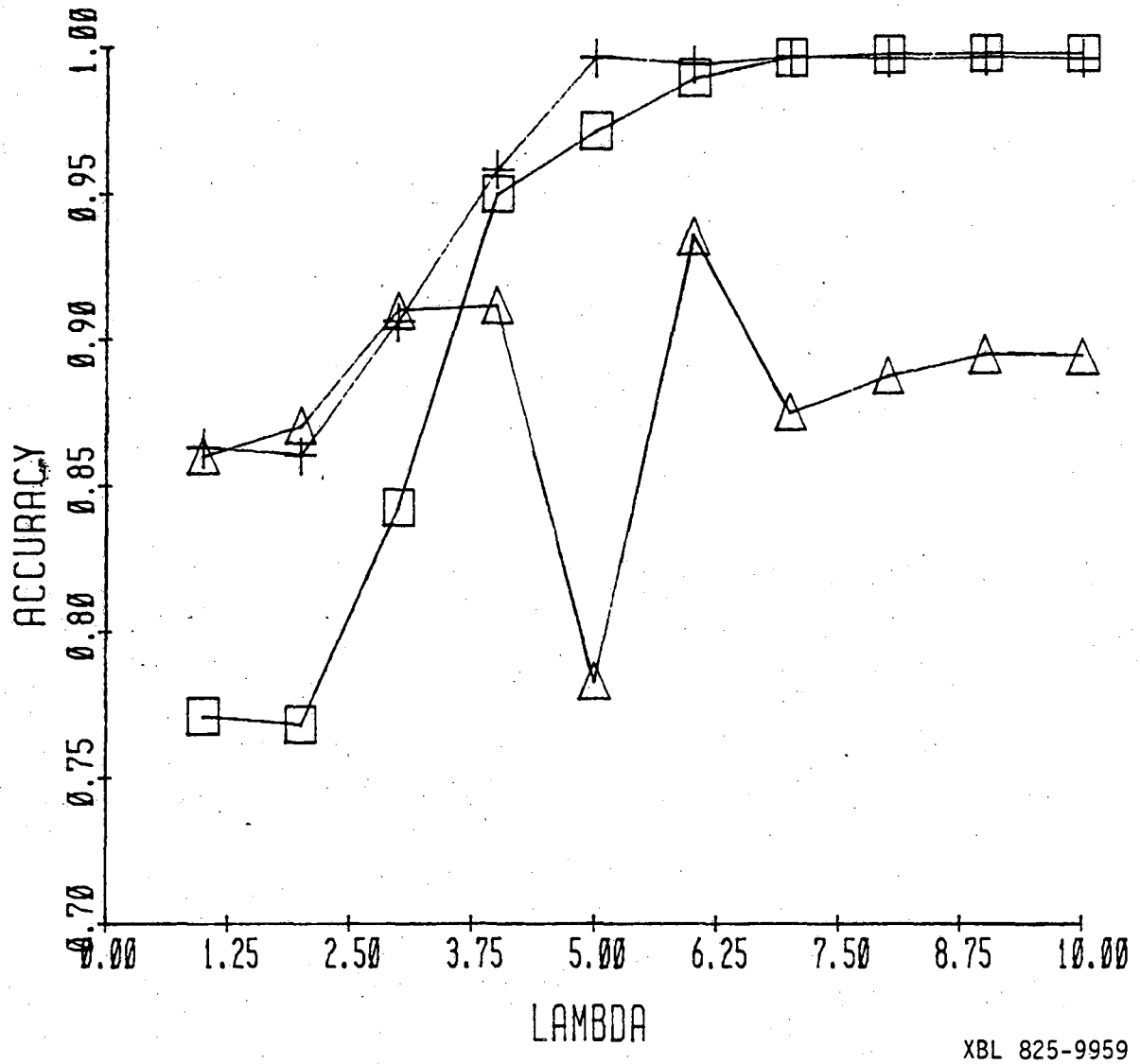

Figure 1.8: Plots of accuracy vs. increasing dimensionless heterogeneous rate constant for parameters returned from application of s.v.c.f. to overlapped waves of non-reversible charge transfer systems. The abscissa is not to scale. Triangles are accuracies for overlapped systems with peak potentials 35 mV apart, squares are accuracies for peaks 50 mV apart, and crosses are accuracies for systems 70 mV apart.

(98-100). Figure 1.9 shows a plot of accuracy vs. increasing Λ for constrained width fits. These curves always change monotonically with increasing Λ, except for some small fluctuations at accuracy very near 1. The ordering of accuracy with peak separation goes almost monotonically from most overlapped to least overlapped systems for a given Λ. This indicates that a great deal of the effect attributed to a false minimum has been eliminated. Note also that if failure is defined as the return of accuracy < 0.90 that resolution succeeds for all systems except for the totally irreversible systems at 35 mV peak separation.

C.v.c.f. can be judged in its analysis of simple charge transfer systems much more easily. If returned kinetic parameters from QUASMI are the same as the parameters used to create the system, the c.v.c.f. technique works. The results for the application of c.v.c.f. are shown in Table 1.8. The systems with 'No Minimum' are systems that did not exhibit a minimum in the plot of s^2 vs. C. These are the systems that were determined to be either reversible or irreversible; for these systems, the dependence of the $f(E_j)$ function of (1.6.2) on the exponential term disappears.

It is seen that the c.v.c.f. technique does quite a good job of returning the various electrode parameters. Returned values of C are all near the input standard potential of -0.5 V , transfer coefficients are near the input 0.5, and the returned Λ for each system is close to the input dimensionless rate constant.

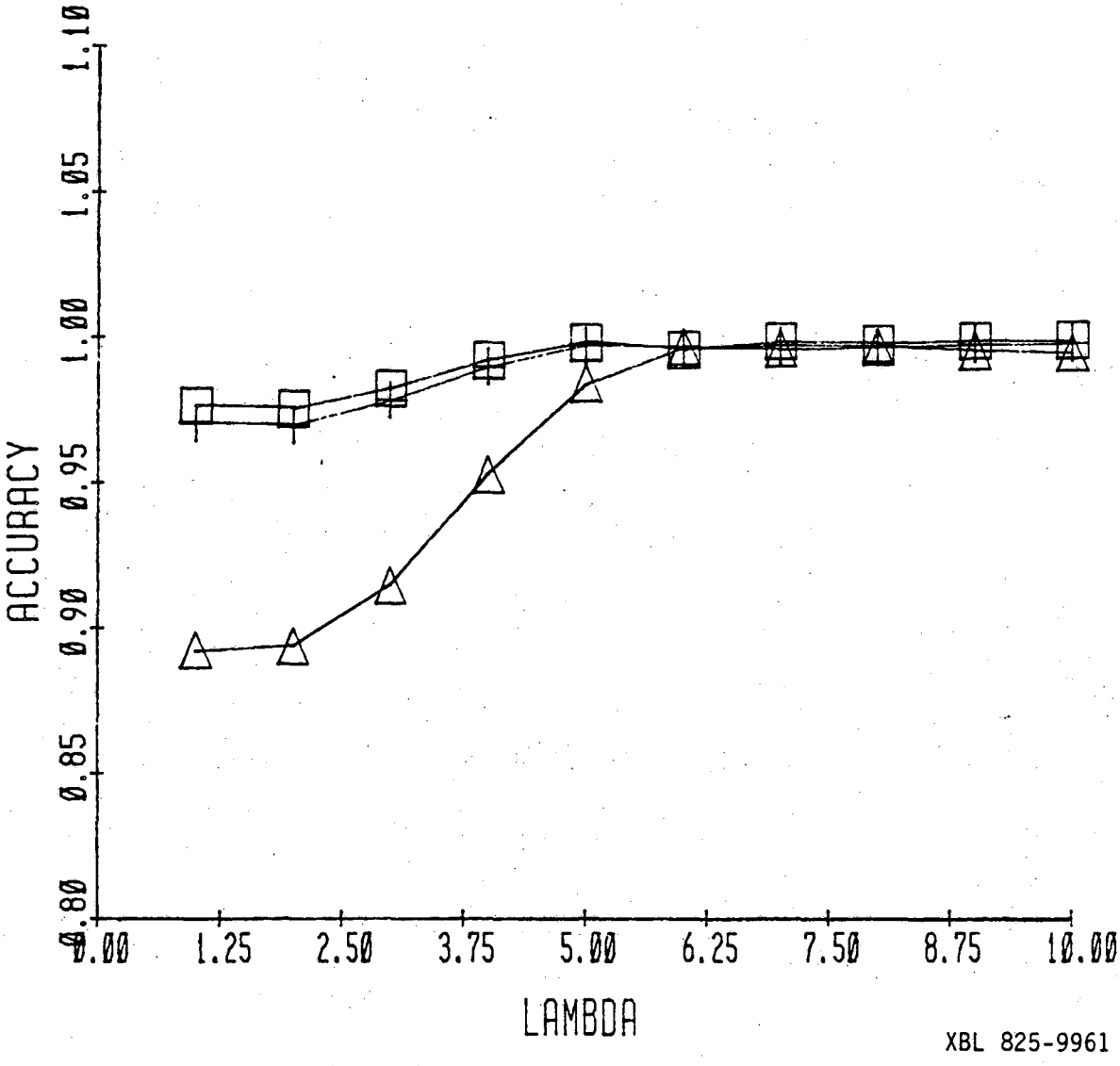

Figure 1.9: Same as Figure 1.8, except that accuracies are determined from CNWSBM fits. Input peak widths to CNWSBM are taken from BIMFIT fits to single peak data.

Table 1.8: Results of c.v.c.f. for simple charge transfer systems

Filename	Λ	Potl.[a,b]	α[b]	Λ[b]	s^2 [b]
A	1.133×10^{-3}		No Minimum		
B	1.133×10^{-2}		No Minimum		
C	0.1133	-0.4992	0.504	0.110	1.84×10^{-6}
D	0.2267	-0.4995	0.504	0.224	2.73×10^{-6}
E	0.5667	-0.4995	0.504	0.564	7.71×10^{-6}
F	1.133	-0.4995	0.505	1.131	2.16×10^{-6}
G	5.667	-0.4994	0.524	5.36	4.76×10^{-4}
H	11.33	-0.4993	0.563	9.38	1.60×10^{-3}
I	1.133×10^{2}		No Minimum		
J	1.133×10^{3}		No Minimum		

a) Units of potential are V.
b) Calculated by QUASMI as discussed in text.

The plots of s^2 vs. C for the individual systems lead to some speculation about the usefulness of this technique as applied to real data. Figure 1.10 shows the variance plots for, from bottom to top, systems C, E, G, and H. The plot for system C is very flat; for systems like C, that are on the verge of either reversibility or irreversibility, it is quite possible that in the presence of noise or distortion that a false minimum might be obtained. Indeed, the variances shown in Figure 1.10 for all systems are quite small. It might be that with noisy real data that the increase in s^2 due to noise might overwhelm the small variances QUASMI uses to determine the best estimate of C. In general, though, in doing kinetic investigations noise is not a difficulty, because samples are run under carefully controlled conditions, and signals are large.

1.7.2 CE Mechanism

The effectiveness of semiderivative voltammetric curve fitting for systems with non-reversible homogeneous kinetics is judged in the same way as is s.v.c.f. for systems with non-reversible charge transfer kinetics. The methods are valid for only those systems where returned fit parameters are close to those predicted from theory and returned R^2 values are close to 1.

Relations that may be used for the evaluation of s.v.c.f. for the CE mechanism with a reversible charge transfer are (1.3.15), (1.3.32) and (1.3.16). From (1.3.15), a pure diffusion system has a semiderivative with a peak potential equal to the reversible half-wave

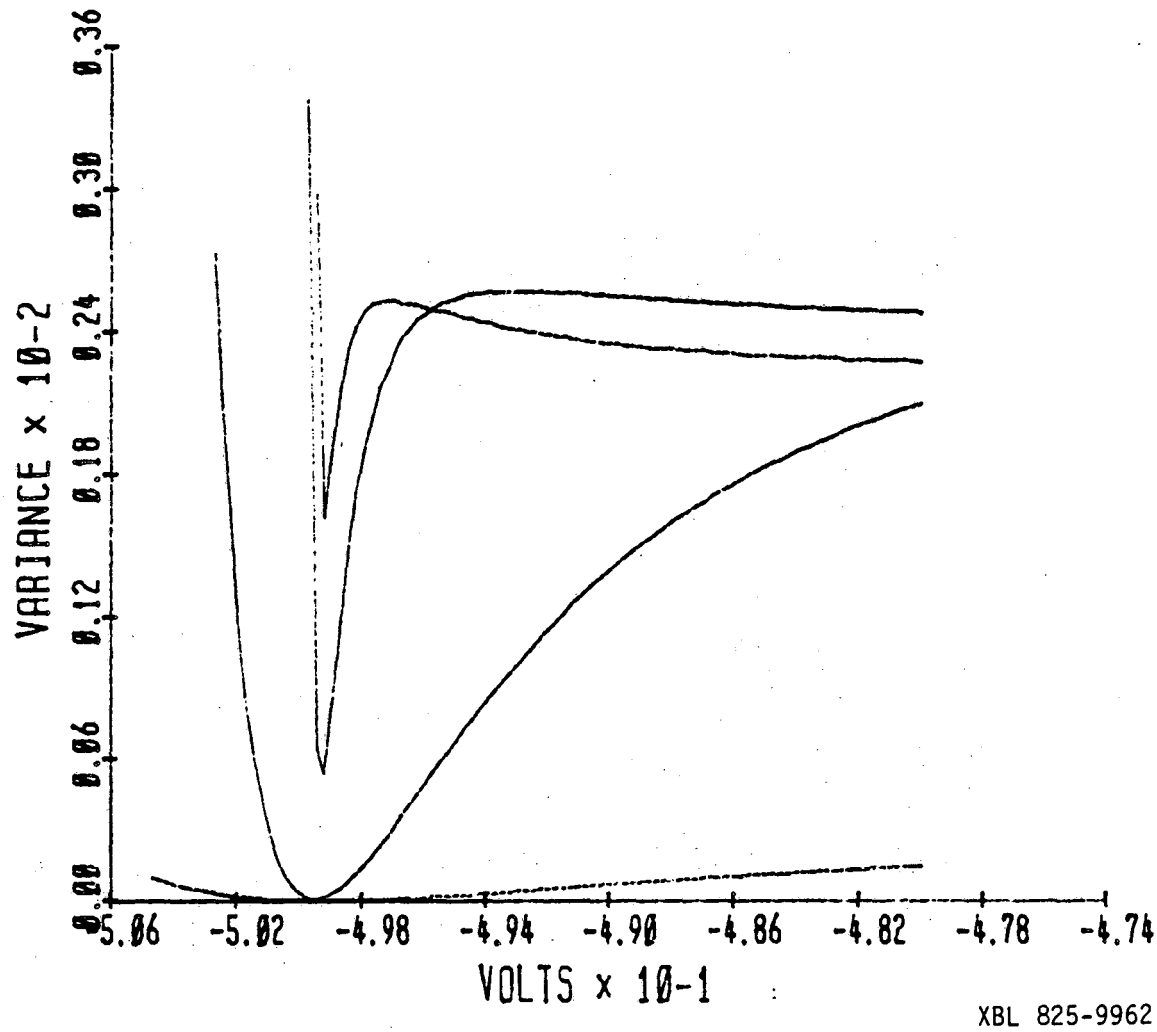

Figure 1.10: Variance of the linear least squares fit of E_j vs. the function $f(E_j)$ of (1.5.2) as a function of C. From bottom to top are the variances for files C, E, G, and H.

potential, which for all systems studied is -0.5000 V. For an equilibrium constant of 10^{-4}, from (1.3.32) the peak potential of the semiderivative of a modified diffusion system should be -0.618 V. Peak widths of semiderivatives of systems with either form of reversible behavior should be 45.3 mV. For s.v.c.f. to be considered valid in either the pure diffusion or modified diffusion zone of kinetic behavior, returned peak parameters must be close to these.

Table 1.5 gives returned peak parameters and R^2 for the application of s.v.c.f. the CE mechanism with a reversible charge transfer. From Section 1.2.2, systems K and L should exhibit pure diffusion behavior and systems AA, BB, and CC should exhibit modified diffusion behavior. Returned peak parameters for these systems, and for system Z also, show both good agreement with theoretical parameters and R^2 close to 1. The limits of validity of the s.v.c.f. technique as applied to this mechanism can be said to extend to the boundaries of the pure and modified diffusion zones as defined in Section 1.2.2.

The returned R^2 values for the application of s.v.c.f. to systems of the CE mechanism with behavior that is not classically reversible suggest that s.v.c.f. is not valid for the curve fitting of waves for these systems. One relation applicable for testing the validity of s.v.c.f. for these systems is a relation for peak height given by Nicholson and Shain (38)

$$\frac{1}{i_k} = \frac{1.02}{i_d} + \frac{0.471}{i_d K}\frac{1}{\sqrt{\lambda}} \qquad (1.7.2)$$

where i_k is the peak height of an l.s.v. wave for a system with preceding homogeneous kinetics, and i_d is the peak height of an l.s.v. wave in the limit of large λ for the same equilibrium constant and is called the diffusion current.

Linear least squares fits of $1/i_k$ vs. $1/\sqrt{\lambda}$ were made for i_k taken as the interpolated peak height of the systems of Table 1.5, and for i_k taken as the returned peak height from the application of s.v.c.f. to the same homogeneous kinetic system. Slopes and intercepts are related to i_d and K through (1.7.2). Table 1.9 shows the actual i_d (taken as 0.4463 from Nicholson and Shain) and K, and the i_d and K calculated from slopes and intercepts of the linear least squares fits. Calculated i_d and K for both fits agree well with the actual i_d and K, although the results found from heights returned by s.v.c.f. are a little low in both cases. Thus, although the R^2 values are poor, the error in the returned peak height is small.

Figure 1.11 shows the semiderivative of system S and the reconstructed sech^2 fit to that system. For the first part of the wave, including the peak, the sech^2 function fits fairly well; it is only at more negative potentials, where the homogeneous kinetics have more of an effect, that the greater portion of the misfit occurs. Even though returned peak heights are in error only by a small amount, the s.v.c.f. technique is not a valid approach for the CE mechanism

Table 1.9: Actual and determined diffusion currents and equilibrium constants for the CE mechanism

	Actual values	Interpolated values[a]	S.v.c.f. values[b]
i_d	0.443	0.446	0.432
K	1.00×10^{-4}	1.01×10^{-4}	0.757×10^{-4}

a) Values are determined from linear least squares fits of $1/\sqrt{\lambda}$ to $1/i_k$, where i_k is the peak height of the l.s.v. wave determined from parabolic interpolation.

b) Values are determined from linear least squares fits of $1/\sqrt{\lambda}$ to $1/i_k$, where i_k is the returned peak height from s.v.c.f.

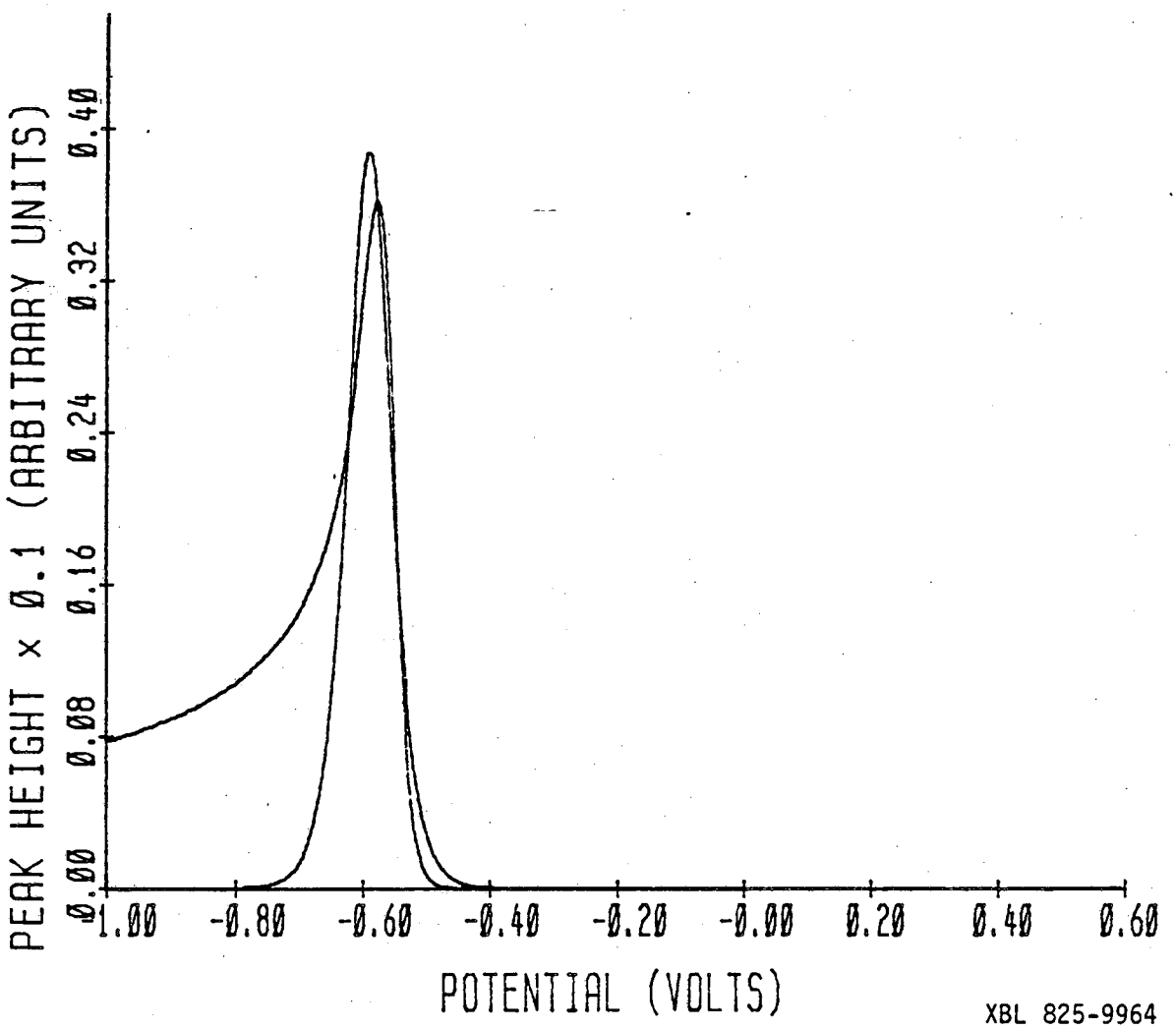

Figure 1.11: Semiderivative and fit $sech^2$ function for file S.

not in a diffusion controlled limiting case.

The results for the application of c.v.c.f. to systems not in the diffusion controlled zones of behavior are more rewarding. The first application of c.v.c.f. to be considered is the application of (1.4.5), which should be valid when applied to systems in the pure kinetic case of limiting behavior. From Section 1.2.2, the systems of Table 1.5 that exhibit this type of behavior should be systems P through X.

For c.v.c.f. to be a valid technique returned parameters from the application should match those parameters used in creating the systems. More specifically, returned peak heights should be close to one; returned peak widths, from (1.4.7), should be close to 22.6 mV; and returned peak widths should be related to the input dimensionless homogeneous rate constant through (1.4.6). In addition, (1.4.5) requires that the coefficient of determination for the fit be close to one.

Table 1.10 shows returned values of the parameters from the application of this c.v.c.f. technique to some of the systems of Table 1.5. Figure 1.12 shows the result of the application of (1.4.5) to system S, and the $sech^2$ fit to this transformed system. The returned values of K in this table were calculated by means of (1.4.6) with the assumption of E^o = - 0.5 V. For all systems, except the extreme systems P and X, coefficients of determination are near one, calculated λ values are near the input λ, peak heights are one, and peak widths are close to 22.6 mV. This c.v.c.f. technique exhibits

Table 1.10: Returned peak parameters for the application of the pure kinetic c.v.c.f. technique to waves of the CE mechanism

Filename[a]	Potl.[b]	Calc. λ	Height	Width[b]	R^2
N	-0.5341		0.986	73.5	0.9396
O	-0.4707		0.0062	3.7	0.0001
P	-0.5107	0.0680	1.003	13.1	0.9935
Q	-0.5279	0.991	1.001	22.5	0.9999
R	-0.5323	1.97	1.001	22.5	0.9999
S	-0.5349	2.95	1.000	22.5	0.9999
T	-0.5382	4.93	1.000	22.4	0.9999
U	-0.5426	9.79	1.000	22.4	0.9999
V	-0.5571	93.7	1.001	22.1	0.9999
W	-0.5710	817.	1.003	21.1	0.9996
X	-0.5833	5550.	1.006	18.8	0.9956
Y	-0.5963		1.239	5.1	0.0846

a) As defined in Table 1.5.
b) Units of potential are V, of width are mV.

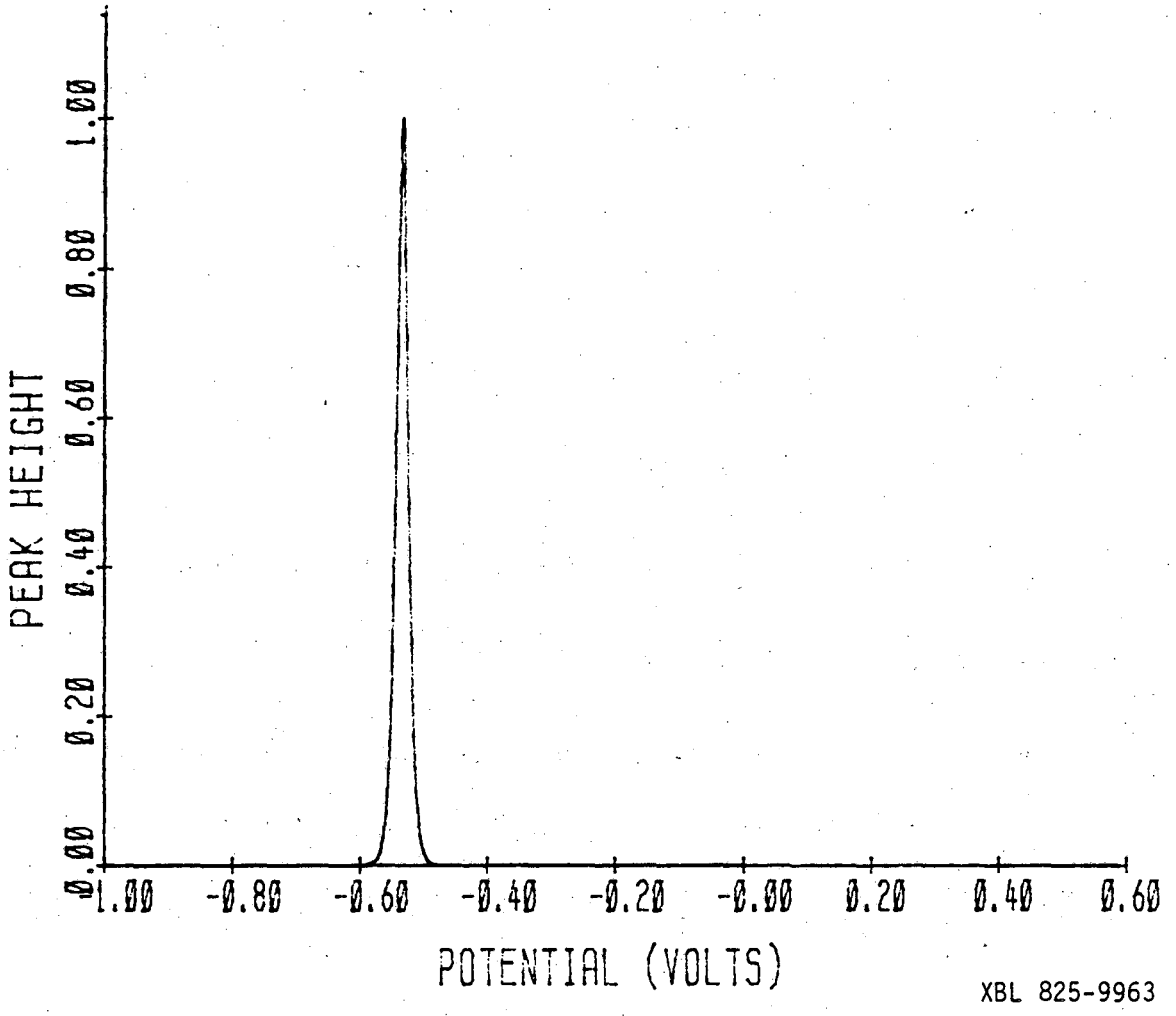

Figure 1.12: Function created by the application of (1.4.5) to file S, and the sech^2 fit to this function.

all the criteria of validity for those systems for which the technique should be valid.

C.v.c.f. also works well when applied to systems in the KE zone of limiting behavior. For these systems the c.v.c.f. equation used is (1.4.8). If this technique is valid one should be able to obtain the correct value of $K\lambda^{1/2}$ for the particular system without any other information. If in addition E^o is known, then through (1.3.32) one should be able to determine the equilibrium constant, and thus λ, for the system. This value must match the input equilibrium constant, which for all systems is 1.00×10^{-4}. Peak heights again should be close to one, and peak widths close to 22.6 mV.

Table 1.11 shows the results of the sequential application of KESEMI and BIMFIT to some of the systems of Table 1.5. Systems from Table 1.5 that should be in the KE zone are systems Y, Z, and AA. To augment these systems, three other systems; X1, Y1, and Z1 were created in the same way as those of Table 1.5 except with input dimensionless homogeneous rate constants of 1.00×10^5, 1.00×10^7, and 1.00×10^9, respectively. Shown in Table 1.11 along with the returned peak parameters from BIMFIT are the returned $K\lambda^{1/2}$ from the application of KESEMI, the equilibrium constant K calculated by means of (1.3.32) with the assumption of $E^o = -0.5$ V, and the λ derived from $K\lambda^{1/2}$ and K. The results for systems X1 through AA exhibit all the criteria of validity necessary to say that c.v.c.f. is also valid when applied to systems in the KE limiting case of behavior.

Table 1.11: Application of c.v.c.f. to systems in the KE zone of the CE mechanism with reversible charge transfer

Filename[a]	Potl.[b]	Height	Width[b]	R^2	$K\lambda^{1/2}$	$K\ (\times 10^{-4})$	λ
X	-0.6106	1.13	10.9	0.2132	0.0101	1.81	
X1	-0.6145	1.02	17.8	0.9305	0.0322	1.34	5.79×10^4
Y	-0.6183	1.00	22.7	0.9999	0.101	0.995	1.03×10^6
Y1	-0.6184	1.00	22.7	0.9999	0.315	0.988	1.02×10^7
Z	-0.6185	1.00	22.6	0.9999	0.983	0.980	1.01×10^8
Z1	-0.6185	1.00	22.7	0.9999	3.09	0.980	9.94×10^8
AA	-0.6187	1.00	22.9	0.9999	12.2	0.967	1.59×10^{10}

a) As defined in Table 1.5 and text.
b) Units of potential are V, of width are mV.

There is one more application of c.v.c.f. to review: that is the application of (1.4.10) and (1.4.11) to systems of the CE mechanism coupled with a quasi-reversible charge transfer. The results of this application are shown in Table 1.6. All of the input physical parameters for the systems can be determined directly from the application of (1.4.10) and (1.4.11) to the systems, so that there is no need (as with QUASMI) to output a transformed f(E) system to fit with BIMFIT. For the systems of Table 1.6, the input $K = 10^{-4}$, and the input λ was 2.5×10^{7}, so that $K\lambda^{1/2}$ for all systems was 0.5. The input Λ for each system is also shown.

The results of Table 1.6 show very good agreement with the input parameters. It is to be remembered that nothing was assumed in the procurement of all of the returned parameters; every parameter was obtained by means of c.p.s.v. theory. This example shows the potential power of the c.v.c.f. technique, especially when applied to systems not in limiting cases of kinetic behavior.

1.7.3 EC Mechanism

Last to be considered is the application of s.v.c.f. to the EC mechanism with a reversible charge transfer. The results of this application are shown in Table 1.7. The systems vary over the entire range of kinetic limiting behavior, from the DO behavior of OO to the DE behavior of ZZ. It is seen that returned coefficients of determination for the sech^2 fits to semiderivatives of the systems are close to one not only for the diffusion controlled systems, but are

close to one even for the pure kinetic systems of SS, TT, and UU. For these latter three systems peak heights are about 10% higher than for the diffusion controlled cases, which matches the results of lsv theory. The peak widths for these three systems are only slightly smaller than those of the diffusion controlled systems. The semiderivative of system TT is shown in Figure 1.13, along with the $sech^2$ fit to this system. The fit is seen to be a good approximation to the semiderivative. Because of these results, and because results for the KO and KE zones are even better than those of the KP zone, s.v.c.f. is seen to be effective in the fitting of systems of the EC mechanism.

Other evidence supporting this view comes from Figure 1.14. This figure shows the returned accuracy, calculated via (1.7.1), for fits to systems composed of a $sech^2$ function overlapped with the semiderivative of file TT. The abscissa of the plot shows the difference in peak potentials between semiderivative and $sech^2$ function. The accuracy is large, even down to small peak separations. This implies that s.v.c.f. would be effective in the resolution of lsv waves of the EC mechanism.

1.8 CONCLUSIONS

The s.v.c.f. method has been shown to be valid not only in the fitting of 'reversible' linear sweep voltammograms (i.e., those with diffusion controlled homogeneous kinetics and reversible charge transfers) but also in the curve fitting of other systems. The

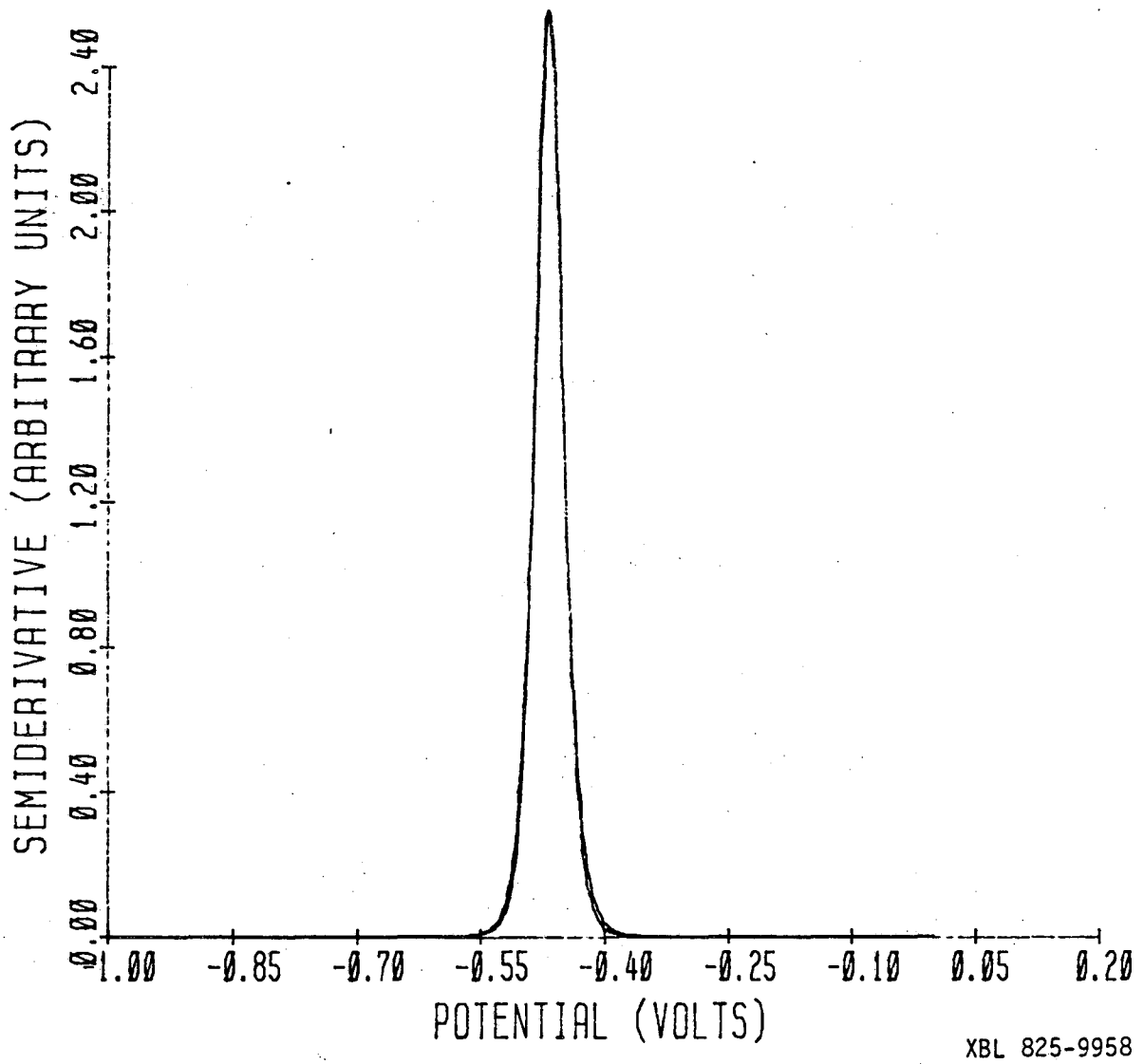

Figure 1.13: Semiderivative of file TT, and the $sech^2$ fit to this semiderivative.

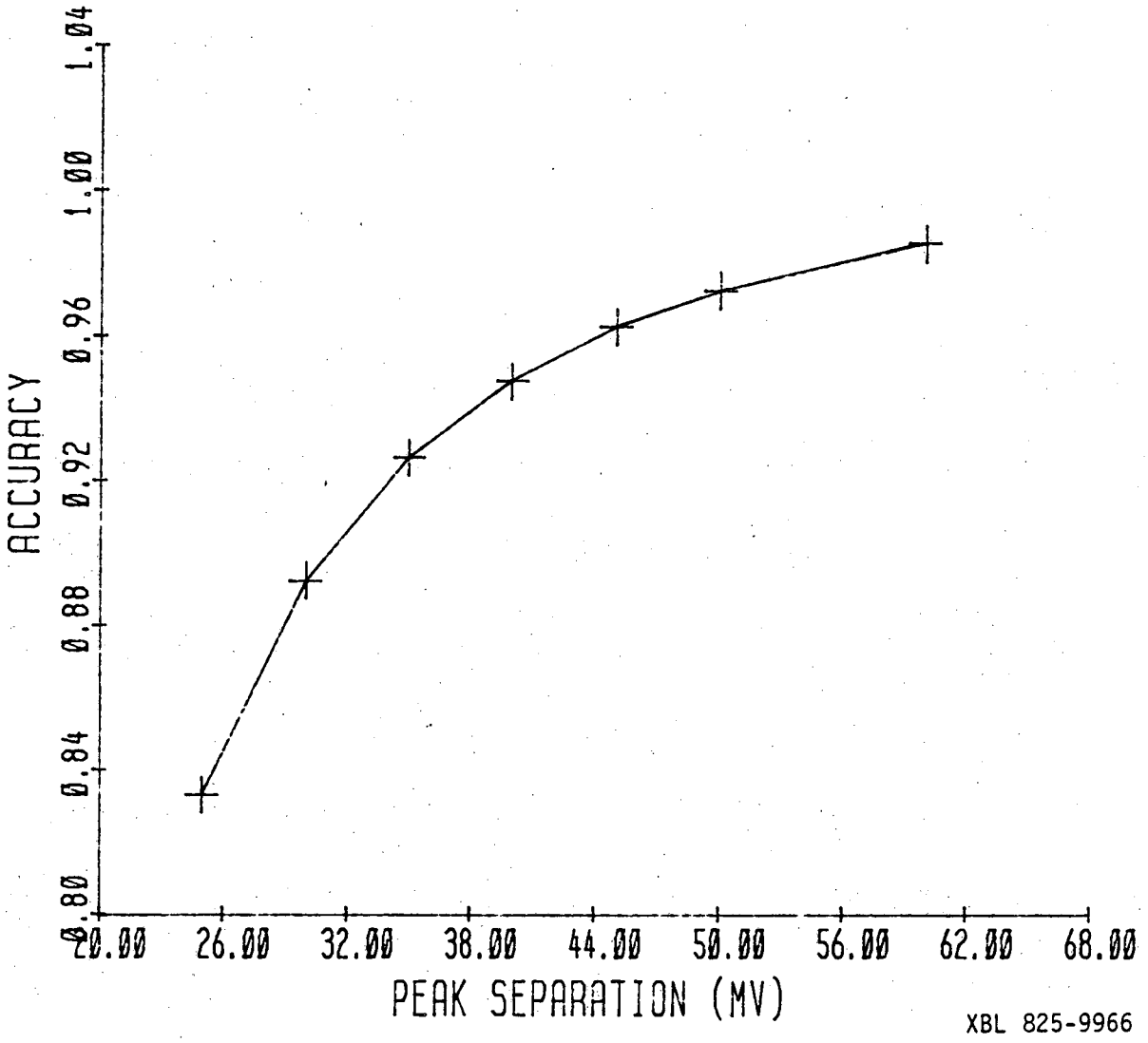

Figure 1.14: Plot of accuracy vs. peak separation for parameters returned from $sech^2$ fits to the semiderivative of file TT overlapped with a $sech^2$ function.

s.v.c.f. technique works well in fitting $sech^2$ functions to semiderivatives of voltammograms of systems with simple, non-reversible charge transfer kinetics, or in fitting semiderivatives of voltammograms of systems with succeeding homogeneous kinetics coupled with a reversible charge transfer, but does not work well for systems with preceding homogeneous kinetics not in diffusion controlled limiting cases. For the classically reversible system, and for the non-reversible charge transfer and waves of the EC mechanisms, it appears possible to use s.v.c.f. as a tool for the accurate resolution of overlapping voltammetric waves. Enhanced resolution is provided by the use of a curve fitting program like CNWSBM that uses peak parameters from single peak data as input.

Several c.v.c.f. techniques have also been shown to be useful when applied to artificial lsv data. To the extent that these artificial data reflect the behavior of real electrochemical systems, the c.v.c.f. techniques are a valuable tool for the return of both charge transfer and homogeneous kinetic information. The great advantage of the c.v.c.f. techniques is that they allow the analysis of complex electrochemical systems that until the introduction of this technique were not amenable to analysis. This is an advantage because these more complex electrochemical systems contain more information than the simpler limiting cases of systems used for analysis previously, and thus allow the return of more information from the same amount of data.

References

1) G. Barker and A.W. Gardner, Z. Anal. Chem. 173, 79 (1960)

2) E.P. Parry and R.A. Osteryoung, Anal. Chem. 37, 1634 (1964)

3) J.G. Osteryoung and R.A. Osteryoung, Amer. Lab. 4, 8 (1972)

4) J.B. Flato, Anal. Chem. 44(11), 75A (1972)

5) G.C. Barker, Congress on Analytical Chemistry in Industry, St. Andrews, June 1957

6) L. Ramaley and M.S. Krause, Jr., Anal. Chem. 41, 1362 (1969)

7) M.S. Krause, Jr. and L. Ramaley, Anal. Chem. 41, 1365 (1969)

8) D.E. Smith, Electroanal. Chem. 1, 1 (1966)

9) D.E. Smith, Crit. Rev. Anal. Chem. 2, 247 (1971)

10) F.E. Woodard, W.S. Woodward and C.N. Reilly, Anal. Chem. 53, 1251A (1981)

11) R.A. Annino, Adv. Chromatogr. 15, 33 (1977)

12) D.E. Smith, Anal. Chem. 48, 221A, 517A (1976)

13) G.M. Hieftje, Anal. Chem. 44, 69A (1972)

14) H.J. Skov and L. Kryger, Anal. Chim. Acta 122, 179 (1980)

15) M. Bos, Anal. Chim. Acta 122, 193 (1980)

16) J.S. Mattson, H.B. Mark, and H.C. MacDonald, "Computers in Chemistry and Instrumentation," vol. 2, "Electrochemistry," Marcel Dekker, New York, 1972

17) L. Kryger, Anal. Chim. Acta 133, 591 (1981)

18) S.P. Perone, Anal. Chem. 43, 1288 (1971)

19) Q.V. Thomas, L. Kryger and S.P. Perone, Anal. Chem. 48, 761 (1976)

20) L. Kryger and D. Jagner, Anal. Chim. Acta 78, 251 (1975)

21) J. Mortensen, E. Ouziel, H.J. Skov and L. Kryger, Anal. Chim. Acta 112, 297 (1979)

22) L. Kryger, D. Jagner and H.J. Skov, Anal. Chim. Acta 78, 241 (1975)

23) L. Kryger and D. Jagner, Anal. Chim. Acta 78, 251 (1975)

24) T. Anfallt and M. Strandberg, Anal. Chim. Acta 103, 379 (1978)

25) P. Delahay, "New Instrumental Techniques in Electrochemistry," Interscience, New York, 1954

26) J. Heyrovsky and J. Kuta, "Principles of Polarography," Academic Press, New York, 1966

27) H. Schmidt and M. Von Stackelberg, "Modern Polarographic Methods," Academic Press, New York, 1963

28) L. Meites, "Polarographic Techniques," 2nd ed., Interscience, New York, 1965

29) A.J. Bard and L. Faulkner, "Electrochemical Methods," Wiley and Sons, New York, 1980

30) L.A. Matheson and N. Nichols, Trans. Electrochem. Soc. 73, 193 (1938)

31) J.E.B. Randles, Trans. Faraday Soc. 44, 327 (1948)

32) A. Sevcik, Collect. Czech. Chem. Commun. 13, 349 (1948)

33) P. Delahay, J. Am. Chem. Soc. 75, 1190 (1953)

34) W.J. Albery, "Electrode Kinetics," Clarendon, Oxford, 1975

35) Z. Galus, "Fundamentals of Electrochemical Analysis," Wiley, London, 1976

36) K.J. Vetter, "Electrochemical Kinetics," Academic Press, New York, 1967

37) H. Matsuda and Y. Ayabe, Z. Electrochem. 59, 494 (1955)

38) R.S. Nicholson and I. Shain, Anal. Chem. 36, 706 (1964)

39) J.M. Saveant and E. Vianello, Electrochem. Acta 8, 905 (1963)

40) Ibid., 12, 629 (1967)

41) J.J. Lingane, Chem. Rev. 29, 1 (1941)

42) L. Nadjo and J.M. Saveant, J. Electroanal. Chem. 48, 113 (1973)

43) M. Grenness and K.B. Oldham, Anal. Chem. 44, 121 (1972)

44) J.C. Imbeaux and J.M. Saveant, J. Electroanal. Chem. 44, 169 (1973)

45) P.E. Whitson, H.W. Van den Born and D.H. Evans, Anal. Chem. 45, 1298 (1973)

46) K.B. Oldham and J. Spanier, J. Electroanal. Chem. 26, 331 (1970)

47) C.P. Andrieux, L. Nadjo and J.M. Saveant, J. Electroanal. Chem. 26, 147 (1970)

48) K.B. Oldham, Anal. Chem. 44, 196 (1972)

49) J.H. Carney and H.C. Miller, Anal. Chem. 45, 2175 (1973)

50) H.W. Van den Born and D.H. Evans, Anal. Chem. 46, 643 (1974)

51) R.S. Rodgers, Anal. Chem. 47, 281 (1975)

52) K.B. Oldham, Anal. Chem. 45, 39 (1973)

53) M. Goto and D. Ishii, J. Electroanal. Chem. 61, 361 (1975)

54) P. Dalrymple-Alford, M. Goto and K.B. Oldham, J. Electroanal. Chem. 85, 1 (1977)

55) M. Goto, K. Ikenoya and D. Ishii, Anal. Chem. 51, 110 (1979)

56) M. Goto, K. Ikenoya, M. Kajihara, and D. Ishii, Anal. Chim. Acta 101, 131 (1978)

57) K.B. Oldham and G.D. Zoski, Anal. Chem. 52, 2116 (1980)

58) M. Goto and D. Ishii, J. Electroanal. Chem. 102, 49 (1979)

59) F. Ammar and J.M. Saveant, J. Electroanal. Chem. 47, 215 (1973)

60) L. Nadjo, J.M. Saveant and D. Tessier, J. Electroanal. Chem. 52, 403 (1974)

61) J.M. Saveant and D. Tessier, J. Electroanal. Chem. 61, 251 (1975)

62) Ibid., 65, 57 (1975)

63) C. Amatore, L. Nadjo and J.M. Saveant, J. Electroanal. Chem. 90, 321 (1978)

64) L. Nadjo and J.M. Saveant, J. Electroanal. Chem. 91, 189 (1978)

65) M. Goto and K.B. Oldham, Anal. Chem. 48, 1671 (1976)

66) J. Toman, R.M. Corn and S.D. Brown, Anal. Chim. Acta 123, 187 (1980)

67) R.S. Nicholson, Anal. Chem. 38, 1406 (1966)

68) C.P. Andriex, L. Nadjo and J.M. Saveant, J. Electroanal. Chem. 26, 147 (1970)

69) L. Nadjo and J.M. Saveant, J. Electroanal. Chem. 30, 41 (1971)

70) S.W. Feldberg, J. Phys. Chem. 75, 2377 (1971)

71) L. Nadjo and J.M. Saveant, Electrochem. Acta 16, 887 (1971)

72) M.K. Hanafey, R.L. Scott, T.H. Ridgeway and C.N. Reilly, Anal. Chem. 50, 116 (1978)

73) S.W. Feldberg, Electroanal. Chem. 3, 199 (1969)

74) S.W. Feldberg, "Computers in Chemistry and Instrumentation," Chap. 7 in vol. 2, "Electrochemistry," J.S. Mattson, H.B. Mark, Jr. and H.C. MacDonald, Jr., eds., Marcel Dekker, New York, 1972

75) A.J. Bard and L. Faulkner, "Electrochemical Methods," John Wiley and Sons, New York, 1980

76) T.M. Apostol, "Mathematical Analysis," 2nd ed., Addison Wesley, Reading, Mass., 1974

77) F. Whiting and P.W. Carr, J. Electroanal. Chem. 81, 1 (1977)

78) B. Speiser and A. Rieker, J. Electroanal. Chem. 102, 1 (1979)

79) B. Speiser, J. Electroanal. Chem. 110, 69 (1980)

80) B. Carnahan, H.A. Luther and J.O. Wilkes, "Applied Numerical Methods," John Wiley and Sons, New York, 1969

81) A. Huber, Monatsh. Math. Phys. 47, 240 (1939)

82) R.S. Nicholson and M.C. Olmstead, Chap. 5 in "Electrochemistry," J.S. Mattison, H.B. Mark and H.C. MacDonald, eds., Marcel Dekker, New York, 1972

83) T. Brown, private communication

84) K.B. Oldham and J. Spanier, "Fractional Calculus," Academic Press, New York, 1974

85) T.A. Brubaker, R. Tracy and C.L. Pomernacki, Anal. Chem. 50, 1017A (1978)

86) T.A. Brubaker and K.R. O'Keefe, Anal. Chem. 51, 1385A (1979)

87) L. Meites, CRC Crit. Rev. Anal. Chem. 8, 1 (1979)

88) N.R. Draper and H. Smith, "Applied Regression Analysis," John Wiley and Sons, New York, 1966

89) P.R. Bevington, "Data Reduction and Error Analysis for the Physical Sciences," McGraw-Hill, New York, 1969

90) S.N. Deming and S.L. Morgan, Anal. Chem. 45, 278A (1973)

91) S.N. Deming and L.R. Parker, Jr., CRC Crit. Rev. Anal. Chem. 7, 187 (1978)

92) P.J. Statham, X-Ray Spectrom. 5, 16 (1976)

93) R. O'Neill, Appl. Statistics 13, 338 (1971)

94) J.M. Chambers and J.E. Ertel, Appl. Statistics 23, 250 (1974)

95) P.R. Benyon, Appl. Statistics 25, 97 (1976)

96) I.D. Hill, Appl. Statistics 27, 380 (1978)

97) S.K. Silber, R.A. Dean and R.A. Geanangel, Computer Chem. 4, 123 (1980)

98) S.P. Perone and W.F. Gutknecht, Anal. Chem. 42, 906 (1970)

99) S.P. Perone and L.B. Sybrandt, Anal. Chem. 43, 382 (1971)

100) P.A. Boudreau and S.P. Perone, Anal. Chem. 51, 811 (1979)

CHAPTER 2

SEMIDERIVATIVE VOLTAMMETRIC CURVE FITTING IN LINEAR SWEEP VOLTAMMETRY AND ANODIC STRIPPING VOLTAMMETRY

2.1 INTRODUCTION

In the first chapter of this work convolutive voltametric curve fitting techniques were shown to be valid in the fitting of simulated linear sweep voltammograms. It is known from long experience that scientific techniques developed from the assumption of simple systems like those of the simulated voltammograms often fail to describe complex real systems. The work of Chapter 1 ignores, for example, the possibility that complex homogeneous kinetic mechanisms or adsorption onto the electrode surface might distort a voltammogram. For the most commonly used electrode, the hanging mercury drop electrode, diffusion will actually be spherical, and not linear; this will affect the shape of the wave. Other effects, such as large residual current, or even simple noise, could cause the c.v.c.f. techniques to fail. Any of these effects, and others not mentioned, could alter the shape of the voltammogram sufficiently so that the application of s.v.c.f. would give wildly erroneous results.

Before c.v.c.f. may be exploited for the inherent advantages of curve fitting techniques, the question of how useful c.v.c.f. is for the analysis of real electrochemical data must be answered. The answer will be determined for one of the c.v.c.f. techniques, semiderivative voltammetric curve fitting. This chapter will discuss the usefulness of s.v.c.f. for the curve fitting of real linear sweep voltammetric data. In addition, it will be shown that s.v.c.f. is applicable to some electrochemical systems when anodic stripping voltammetry is used. The usefulness of s.v.c.f. in the analysis of

asv data will also be determined. The effects of perturbing influences such as sphericity effects, residual current, finite plating time in asv and non-reversible homogeneous kinetics will also be discussed. Finally, results for the application of s.v.c.f. to linear sweep voltammograms will be compared with results from untransformed voltammograms to gain insight into the possible benefits of s.v.c.f.

2.2 ANODIC STRIPPING VOLTAMMETRY

Anodic stripping voltammetry is an old technique; Zbinden (1) was the first to publish work on the use of electrolytic stripping to determine copper dissolved in solution. The advantage of stripping voltammetry is the great increase in sensitivity which derives from the concentration of metal into or onto an electrode before the stripping. This preconcentration often extends limits of detection for electrochemical methods by three or four orders of magnitude.

There have been several long review articles and books published on stripping voltammetry in the last fifteen years. Some of the most useful and comprehensive have been those written by Barendrecht (2), Vydra et al. (3) and Brainina (4). Other reviews exist on more specific topics in stripping voltammetry. In this work the stripping technique used is anodic stripping voltammetry at a hanging mercury drop electrode.

In its most general form, analysis via anodic stripping voltammetry occurs in three steps. (See Figure 2.1). Initially the

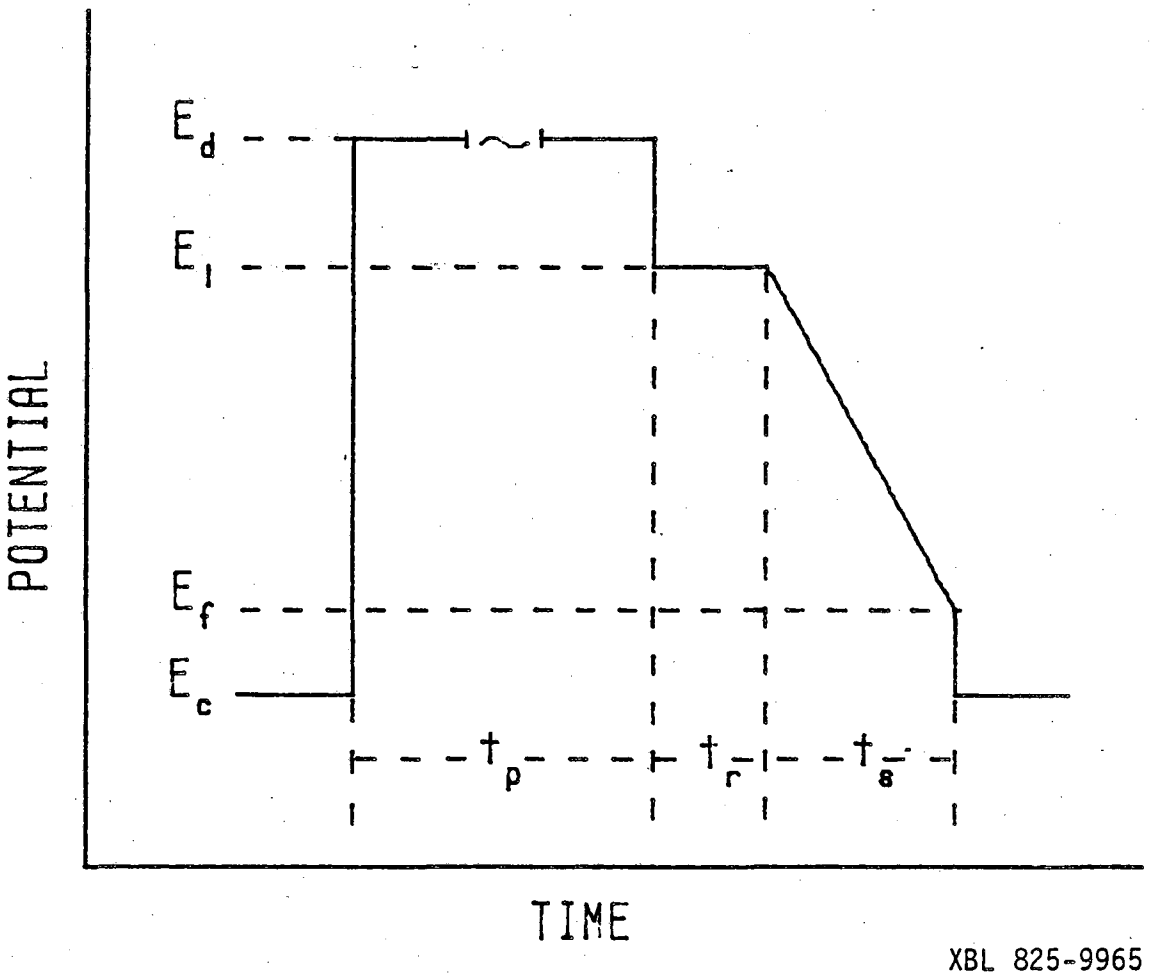

Figure 2.1: Potential vs. time function for anodic stripping voltammetry.

potential at the working electrode is held at some potential positive enough so that essentially no metal species is reduced. The potential is then made negative enough so that the metal ions of analytic interest are electrodeposited into the drop in the form of an amalgam; this is called the electrodeposition step. The choice of the electrodeposition potential E_d is made so that the potential is several hundred millivolts more negative than the $E_{1/2}$ of the species of interest that is most easily oxidized. Species with $E_{1/2}$ more negative than E_d are not plated into the electrode, and thus are not seen in the following stripping step. This selectivity is an attractive feature of asv for purposes of quantitative analysis.

The solution is usually stirred during the deposition period to increase the flux of electroactive species to the working electrode, thereby increasing both the amount of metal plated and the current during the stripping step. The current evolved by the plating reaches a limiting value described by the following semiempirical relation (2)

$$i_\ell = 4\pi r_o nFD_{ox} C^*_{ox} + knr_o^2 D_{ox}^{2/3} C^*_{ox} u^{1/2} \qquad (2.2.1)$$

where u = rate of stirring in rpm, r_o is the radius of the drop, and k is a constant particular to a specific cell geometry. If the duration of the deposition period is τ seconds, the molar amalgam concentration of Red at the end of the period is (2)

$$C^*_{red,Hg} = \frac{3i_\ell \tau}{4\pi r_o nF} \qquad (2.2.2)$$

so that $C^*_{red,Hg}$ is seen to be directly proportional to C^*_{ox}. The amalgam concentration increases with the duration, so that the longer the plating time the better the sensitivity. Unfortunately, if a HMDE is used, at very long plating times appreciable amounts of Red begin to diffuse into the Hg capillary, so that (2.2.2) no longer holds. The maximum period for a linear response of $C^*_{red,Hg}$ to C^*_{ox} is about 30 minutes, while more usual plating times are around 10-20 minutes.

After the electrodeposition step comes a rest period of several seconds. At the beginning of this period the potential of the working electrode is changed to E_i, the initial potential for the stripping process, and the stirring of the solution is stopped. The potential is changed to E_i at this time so that capacitive current resultant from the potential step will die away before the stripping step. The stirring of the solution is stopped so that mass transport occurs only by diffusion, and so that the concentration profile of Red within the Hg drop may become homogeneous. It was shown by Shain and Lewison (5) that for long plating times the concentration becomes nearly homogeneous after about 20 seconds. Typical durations for the rest period are from 20-30 seconds.

The last step is the stripping process itself. During this step all the various waveforms that can be applied to an electrode during analyses without plating may be applied to the electrode with

preconcentrated metal amalgam. In this work a linearly varying potential ramp was applied to the electrode. If the radius of the electrode is large enough, and the concentration profile within the drop at the end of the rest period is homogeneous, then during the stripping step mass transport occurs by linear, semi-infinite diffusion (6). This means that the relations developed in Chap. 1 for c.v.c.f. applied to lsv will be expected to apply to asv also, for the particular mechanism of the system considered.

2.3 RESTATEMENT OF THEORY FOR S.V.C.F.

The full treatment of the theory of s.v.c.f. for electrochemical systems for which it has been proved valid is given in Chapter 1. In short, for a reversible charge transfer, or for very rapid preceding or following first order reactions coupled with a reversible charge transfer, the semiderivative is given by

$$e(E) = \frac{nFm^*}{4RT} \operatorname{sech}^2 \left\{ \frac{nF}{2RT} (E-E_p) \right\} \qquad (2.3.1)$$

where

$$m^* = nFAC_i^* \sqrt{D_{ox}\nu} \qquad (2.3.2)$$

and $C_i^* = C_{ox}^*$ for lsv, and $C_i^* = C_{red,Hg}^*$ for asv. The potential at the maximum of the semiderivative peak E_p is

$$E_p = E^r_{1/2} \tag{2.3.3}$$

for a simple, reversible charge transfer, and is

$$E_p = E^r_{1/2} + \frac{RT}{nF} \ln \left(\frac{K}{K+1}\right) \tag{2.3.4}$$

for a reversible charge transfer coupled with rapid preceding or following first order homogeneous kinetics. The width at half the peak maximum is, assuming T = 25°C,

$$FWHM = \frac{90.6}{n} \text{ mV} \tag{2.3.5}$$

and the height of the peak H is

$$H = \frac{nFm^*}{4RT} = \frac{(nF)^2 A\, C_i^* \sqrt{D_{ox}\nu}}{4RT} \tag{2.3.6}$$

so that the height is seen to be linearly proportional to n^2, A, C_i^*, and $\nu^{1/2}$.

In this work linear sweep voltammetry is used to accomplish the reduction of a metal to a mercury amalgam from a solution containing metal complexed by complexing ligands. The mechanism for this is, for the formation of only one complex in solution, that of the CE mechanism of (1.2.10)

$$ML_p \underset{k_b}{\overset{k_f}{\rightleftharpoons}} M^{n+}$$

$$M^{n+} + ne^- = M(Hg) \qquad (2.3.7)$$

if the concentration of the complexing ligand is assumed to be much greater than that of the metal. If this is the case, then the reaction is pseudo-first order, and the rate constants of (2.3.7) are functions of the ligand concentration.

Often several complexes exist in solution simultaneously. If the dissociation kinetics are very rapid for every complex the results of (2.3.1) through (2.3.6) still obtain, with the peak potential now given by (7)

$$E_p = E^r_{1/2} - \frac{RT}{nF} \ln \sum_{i=0}^{N} \beta_i C_L^i \qquad (2.3.8)$$

where the sum is over the N complexes in solution, and the β_i are the stability constants for the complexation reactions, defined by

$$\beta_i = \frac{[ML_i]}{[M^+] [L^{b-}]^i} \qquad (2.3.9)$$

If only one complex is formed, the behavior of systems that are not classically reversible should be that seen in Chapter 1; s.v.c.f.

will not fit semiderivatives of these systems well at all. It is expected that similar behavior would result for a system of several complexes.

Anodic stripping voltammetry is used in this work to strip metal from a mercury amalgam into a solution containing a great excess of complexing ligands. This means that the homogeneous kinetic mechanism for asv is not the CE mechanism of (2.3.7), but rather is the pseudo-first order EC mechanism of (1.2.17)

$$M(Hg) = M^{n+} + ne^- \qquad (2.3.10)$$

$$M^{n+} \underset{k_b}{\overset{k_f}{\rightleftharpoons}} ML_p$$

where, again, the charge transfer reaction is assumed to be reversible. Again, if only one complex is formed, and if the homogeneous kinetics are very rapid, the pertinent relations are those of (2.3.1) through (2.3.6), with the peak potential given by (2.3.8). If the homogeneous kinetics are not classically reversible, it is still expected that s.v.c.f. will work well (See Section 1.7.3). Peaks should be about 10% larger and 10% narrower than in the classically reversible case.

If several complexes exist simultaneously, and all of the dissociation equilibria are very fast, the s.v.c.f. relations should be those of the CE mechanism with several complexes and fast kinetics.

One might expect that if some of the equilibria are not rapid, the shape of the resultant voltammogram would be like that of the kinetically controlled EC mechanism for one complex. It is possible that the s.v.c.f. technique would still serve to fit the asv data.

2.4 EXPERIMENTAL

2.4.1 Cell and Electrodes

The working electrode for all experiments in this work was a Metrohm hanging mercury drop electrode (HMDE). This electrode consists of two main parts: a micrometer-plunger assembly that is seated on top of a piece of capillary tubing with a small reservoir on top. When the micrometer head is turned the plunger is forced into the reservoir, extruding a reproducible volume of mercury out of the end of the length of capillary tubing. The surface tension of the mercury causes it to assume the shape of a sphere.

Most of the difficulties that developed during the course of an experiment were directly traceable to some problem with the HMDE. Very often the end of the capillary tubing would get dirty and cause the drop to fall off. This could usually be alleviated by cleaning the capillary for fifteen minutes in boiling HNO_3, and then coating the capillary with a 5% solution of $(CH_3)_2SiCl_2$ in CCl_4. After such a treatment the HMDE would usually behave well for several months, when the process would have to be repeated.

The reference electrode was a homemade Ag/AgCl electrode. This electrode was used instead of the more common saturated calomel electrode (SCE) because many of the solutions under investigation contained large amounts of ClO_4^-. Because $KClO_4$ is only marginally soluble, over a period of time the Vycor frit separating the KCl filling solution in the SCE from the solution containing ClO_4^- would become clogged. This resulted in an undefined potential at the working electrode. By using a Ag wire coated with AgCl, and a $NaCl/NaClO_4$ filling solution as a reference electrode, problems with clogging were avoided. This electrode was measured to be at a stable potential +44 mV vs. SCE at T = 20.^oC. The counter electrode was a heavy gauge Pt wire.

The cell, cell holder and purge tube were all Princeton Applied Research (PAR) equipment. The geometry of the cell was such that the reference electrode was placed as close as possible to the working electrode, so as to minimize uncompensated solution resistance. The cell was thermostatted by placement in a water bath that was a Pyrex dish 19.1 cm in diameter by 9.8 cm tall. Inside the dish was a coil of copper tubing through which ran water from a larger heat bath. The larger heat bath was simply a wastebasket lined with plastic. The bath was heated and stirred by a Haake Model E12 circulator, and the water surface was covered with the polystyrene 'foamies', normally used in packing, to prevent heat loss to the atmosphere. Water was pumped from the wastebasket by the circulator through a short length of Tygon tubing to the copper coil, and back.

For asv an 8 x 1.5 mm Teflon coated magnetic stirring bar was included inside the cell. The stirrer was a Corning PC-351 Hot Plate/Stirrer. This was powered by an extension cord, in the middle of which was an International Rectifier D1202 Solid State Relay. This relay, when a potential of 0.0 V is input to it, is open, allowing no current to flow through the extension cord. When a voltage of 5.0 V or more is input to the relay it closes, allowing current to pass. The relay was interfaced to the microcomputer via a digital to analog converter for precise control of stirring.

2.4.2 Potentiostat and Linear Ramp Generator

The potentiostat used in all experiments was a PAR 173 potentiostat. This is a three electrode potentiostat, and can be used as either a synthetic or analytic tool. The potentiostat is designed to be run in either a controlled current or controlled potential mode. For all experiments in this work the potentiostat was run in the controlled potential mode. The potentiostat on its own does not have the capability of applying other than a constant potential to the working electrode; it does, however, have two inputs through which any potential function may be applied. The potential between reference and working electrode was output directly from the mainframe of the potentiostat. The current passing through the cell is output via a separate plug in module. The module used in this work was the PAR 179 Digital Coulometer.

There are two major disadvantages to the use of this

potentiostat. Firstly, because the 173 is intended to serve as a synthetic instrument, it has to be able to push a lot of current through a solution. This results in a lot of noise; compared to some other potentiostats, the 173 is quite noisy. The noise is primarily 60 Hz 'pickup' noise, and harmonics of 60 Hz. Currents much smaller than about 100 nA are obscured by the noise in this instrument. Secondly, the sensitivity of the 179 current follower is graded only in orders of magnitude. This causes problems when one is forced to change scales because of an increase in signal. When the sensitivity is reduced by an order of magnitude, the signal is indeed reduced by an order of magnitude, but the noise, unfortunately, is not. What is at the higher sensitivity a scan with large signal and little noise becomes at the lower sensitivity a small signal with relatively more noise.

A PAR 175 linear scan generator is used to apply a potential function to the potentiostat. This is a very useful instrument because it is quite adaptable to computer interfacing. Initial and final potentials are set on this generator (values ranging from ±10 V can be chosen for either) as well as the scan rate, which can be chosen to be from 1 mV to 10000 V/s. The unit is equipped with two TTL triggers, one of which can be used to start a scan, and one of which can be used to end a scan by resetting the unit to the initial parameters. By means of these two triggers, and the settings dialed into the PAR 175, the computer is able to control the entire experiment.

2.4.3 Computer

There were two different micro-computers used in these experiments. The microcomputer used to acquire data was a Digital Equipment Corp. (DEC) MINC 11-2/B microcomputer system. The MINC is a package instrument intended for use in laboratory experimentation. The MINC is controlled by an LSI-11/2 CPU with 32K memory of 16 bit words, (28K of which are available for user programming), and has an DEC RX02 dual drive, double density floppy disk drive for data storage purposes. The terminal for this MINC was a VT105 terminal, which is capable of simultaneously plotting two 512 point arrays.

The largest advantage of the MINC is the ease with which the computer may be interfaced. This is because peripheral devices exist as modules for such things as a real time clock, analog to digital converter and others. These simply plug into slots provided for them in an expanded backplane. Most of the wiring for the interfacing of these units is already done, so that only a very meager knowledge of electronics is needed to complete a laboratory microcomputer system.

The unfortunate feature of the MINC is that these peripherals are not very powerful. The analog to digital converter, for example, has a minimum sampling time of about 69 μs per point for 12-bit resolution. This is exceedingly slow, and hampers the use of the electrochemical apparatus in doing experiments at very fast scan rates.

The devices in use with these experiments include a real time

clock that is programmable to 5 different counting frequencies. This kept the time for the events that occurred during the course of an experiment. A digital to analog converter (D/A) with 12-bit resolution, 4 outputs, user selectable voltages ranges was used to provide offset voltages in asv and to trigger the PAR 175. An analog to digital converter (A/D) with 12 differential and 16 single ended inputs, 12-bit resolution, and range from -5 to +5 V, was used to sample both current and potential data from the potentiostat.

A more powerful microcomputer is used for data manipulation and analysis. The CPU is a DEC LSI-11/23 with floating point chip accessory. This CPU is about twice as fast as the LSI-11/2, has the capability of doing floating point operations directly, and, besides the 32K of core memory, has the capability of addressing an extra 100K of "virtual" memory. The processor was mounted in a Netcom Products, Inc. bin, and for data storage was equipped with a Data Systems DSD440 dual drive, double density floppy disk drive. The terminal was also a DEC VT105; for more sophisticated graphics, a Tektronix 4006-1 terminal and a Tektronix 4662 digital plotter were available, both driven via a DLV11-J serial I/O board. For hardcopy of programs, data files, etc., a DEC LA120 printer was interfaced via a DLV11-J, and finally, for text processing an IBM Selectric typewriter was interfaced via a DLV11 board, and an Escon Products, Inc. interface. Both computers used the DEC RT-11 operating system, both versions 3B and 4.

2.4.4 Computer Programs

A great variety of computer programs were written to perform data acquisition and analysis. Two programs, GDSEMI and BIMFIT, were discussed in Section 1.5. Other programs to do experimental control and data acquisition, and to do data analysis, are described here.

2.4.4.1 Voltammetry Programs

The lsv and asv programs to do voltammetric control and data sampling were called ROB4 and JEFF3, respectively. Each program consists of a FORTRAN driver program, and various FORTRAN and MACRO (DEC assembly language) subroutines to perform individual functions. The programs are large, and extensive overlaying of subroutines is necessary to be able to fit the program into the 28K words of user memory. This is feasible because the different subroutines do not depend on one another and therefore do not have to be resident in memory simultaneously. The logical procedure for both programs is depicted in a flow chart in Figure 2.2.

Each program begins with a statement as to what connections must be made for the program to operate correctly. The lsv program ROB4 requires connections from the electrometer monitor on the PAR 173 and the current output on the PAR 179 to analog to digital converters. These allow monitoring the potential and current, respectively, as a function of time, which is kept by the real time clock. ROB4 also requires a connection from a digital-to-analog converter to both the external trigger and frame reset inputs on the PAR 175 linear scan

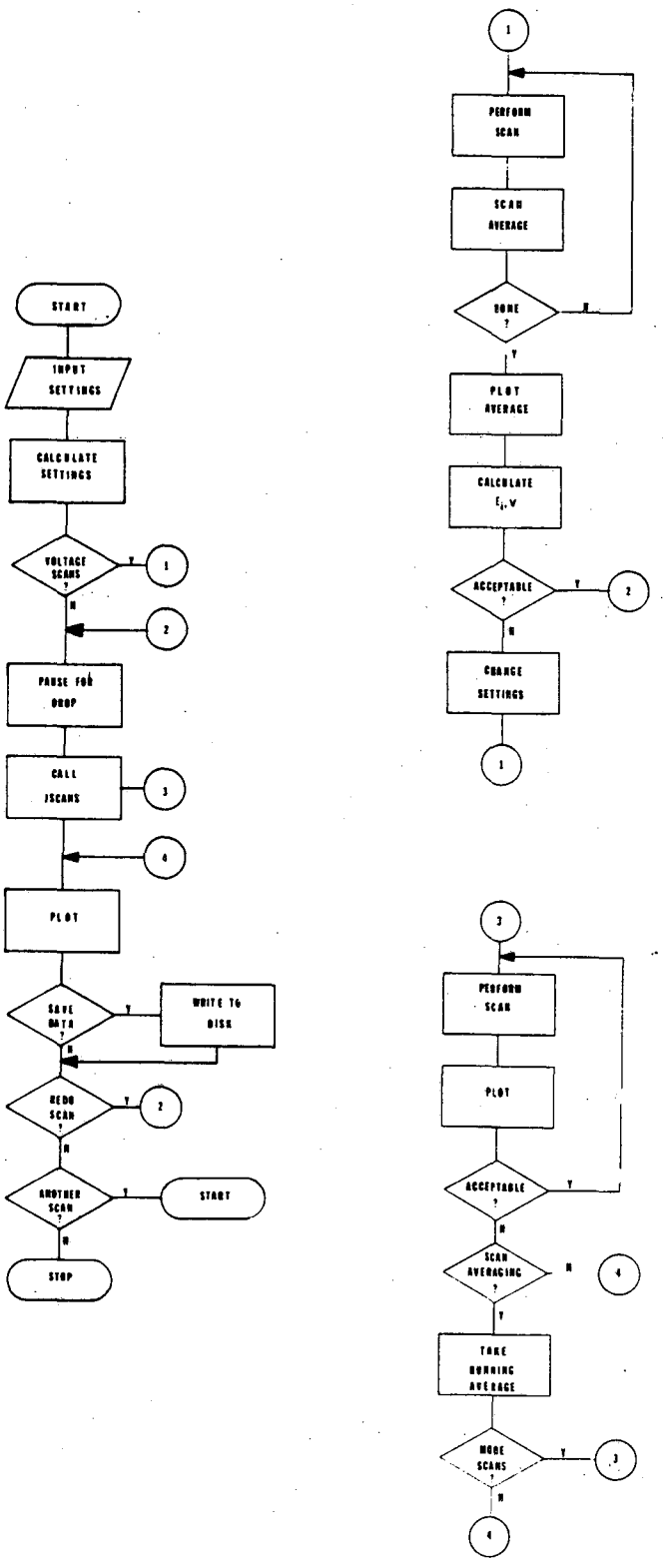

Figure 2.2: Flow diagram for voltammetry programs.

generator. A positive going voltage to the external trigger starts the generation of the linear ramp, and a negative going voltage to the frame reset sets all conditions back to the initial conditions. The asv program JEFF3 in addition requires leads from DACs to both the relay controlled stirrer, and to one of the voltage inputs on the PAR 173. The latter connection provides the voltage offset for plating and cleaning.

For both programs, the first step after the machine connections and settings are made is the entering of parameters for the scan. The computer checks these parameters to see whether they are compatible with hardware capabilities, and calculates from them the corresponding integer numbers that are written to the various device addresses.

After all parameters have been input, the program executes the experiment. The MACRO subroutine JSCANS actually performed experimental control and data acquisition. Because assembly language routines are much more efficient than routines written in higher level languages, assembly language subroutines run much faster. Thus, it is essential to use assembly language subroutines to perform real time experimental control and data acquisition functions. A good introduction to MACRO programming for the LSI-11/2 is given in Cooper's book (8). The programming for the particular hardware this system implements was done with the assistance of the DEC 'Microcomputer Processor Handbook' (9) and 'Microcomputer Interfaces Handbook' (10).

The first step in the actual experiment is the calibration of the potential file. If calibration of the potential is desired, four scans are taken by sending a positive trigger to the PAR 175, and the potential between the working and reference elctrodes is monitored as a function of time. A running average of the potential is performed after each individual scan is taken. After the final average is determined, a linear least squares fit of the potential to the clock time gives the real initial potential and scan rate. If these are acceptable, then the potential file for subsequent voltammograms run at that scan rate is constructed from them. If E_i and ν are not acceptable, the machine settings are changed, and another four potential scans are taken.

After an acceptable E_i and ν are found, and the potential file created, the current scans are taken. Prior to the actual scan the program pauses to allow a new drop to be extruded from the HMDE. For both programs, the subroutine JSCANS then performs the actual scan. In ROB3, this involves only the monitoring of the current produced by a linear potential sweep. JEFF3 has in addition the cleaning, plating and rest steps to control. The potential at the working electrode is held at the cleaning potential for 10 seconds while stirring is initiated. The potential is then changed to the plating potential. Six seconds before the end of the plating period the stirring is discontinued. At the end of the period, the potential is changed to the rest potential, and is held at this potential for 15 seconds. The scan is taken at the end of the rest period.

Both ROB4 and JEFF3 have the capability for signal averaging. This is done by taking a running average after each acceptable voltammogram. After the voltammetric data are taken they are plotted on the VT105. If the observed voltammogram is acceptable and no scan averaging is required, the current and potential files are written to disk. If the voltammogram is not acceptable or more scans are required for signal averaging purposes, another scan is taken.

2.4.4.2 Fourier Filtering

Most noise in electrochemical data is high frequency noise; most electrochemical signals are of relatively low frequency. This is the rationale for Fourier transform based filtering, which has been discussed in many places (11, 12 among others). A detailed discussion of the Fourier transform is given in Chapter 4. The filtering program used in this work is called BAJSM. A Fourier transform subroutine given by Mertz (13) was used to the forward and backward discrete Fourier transform (DFT). Before transformation, the voltammogram was rotated as per Hayes et al. (11) so as to avoid aliasing effects. A step function filter was used to keep the first 19 points on either side of the DC offset, and apply a linearly decreasing ramp to the next four. All other frequencies were set equal to zero. The back transform was then taken, and the resultant filtered voltammogram was scaled back to the original.

2.4.4.3 Background Subtraction

Much of the current seen in a voltammogram comes from non-faradaic sources, and is usually called residual current. Most of residual current, if a solution has been deoxygenated, comes from the charging of the so called 'double layer' in solution, and for this reason is called capacitive current. That this component can be quite significant is seen from typical capacities of solutions at mercury electrodes, which generally are in the range of 10 to 50 Coulombs/cm^2 (14). For a hanging mercury drop electrode with a surface area of 4 mm^2, an electrochemical scan with a scan rate of 1.0 V/s evolves a capacitive current of 1 μA, about the same current evolved by a faradaic reaction at a concentration of 10^{-5} M.

Much of the work done in electrochemistry since 1960 has been aimed at lessening the effect of capacitive current. Most of the work done employs pulse methods. These rely on the fact that after a potential step, the capacitive current decays as exp(-t/RC), where RC is the time constant of the electrochemical cell, and t is the time elapsed since the potential step, while the faradaic current decays as $t^{-1/2}$, more slowly. By waiting for a period after the potential step the ratio of i_f/i_c increases, although the total current itself decreases. Through this mechanism the use of pulse techniques is widely accepted to increase sensitivity in voltammetry by about an order of magnitude. Unfortunately, however, large scan rates are not possible using pulse methods.

A method that has been less frequently used is the differential method. In this method the residual current alone is measured by

simultaneously scanning two solutions, one with depolarizer and one without, so that upon subtraction of one current from the other all that is left is the current due to the depolarizer. For obvious reasons this technique would be difficult to extend to the analysis of complex solutions; however, there are quite a few occasions in which a procedure similar to the differential method may be adopted. In asv, for example, Kryger and Jagner (15) and Brown and Kowalski (16) developed a technique where, after stripping, the electrode is cleaned, and a second scan occurs without plating. This second scan is almost wholly residual current, and upon subtraction of the second scan from the first, only faradaic current is left.

The method used in this work is similar to the differential method; in all of the solutions considered, a background scan of electrolyte without depolarizer was first taken and stored on disk. Depolarizer is added to the electrolyte in small amounts with an Eppendorf pipette, and a voltammogram taken. After data are taken and filtered, the background voltammogram is subtracted point by point from the sample voltammogram using the program BBACK.

2.4.4.4 Semidifferentiation and Curve Fitting

The final steps in the data analysis procedure are semidifferentiation and the application of a sech curve fitting program. These are accomplished by the programs GDSEMI and BIMFIT, which are described in Section 1.6. Typical times for convergence of BIMFIT for the files discussed in Section 2.5 were from 100-200

seconds. Times were considerably longer for some other files, especially the noisy files of Section 2.5.4.

2.4.5 Solutions

The composition of all the solutions used in this work is outlined in Table 2.1. There were two different kinds of experiments performed. For series A through E, voltammograms were taken after each of a series of standard additions to a background electrolyte in order to observe the effects of concentration on s.v.c.f. The background electrolyte for the lsv standard additions series A through C was a solution of 0.58 M HCl. This background electrolyte was chosen because all the metals considered in this study were known to be reversible or near reversible in this electrolyte. The HCl background was made by the dilution of Mallinckrodt A.R. HCl with laboratory deionized water. This deionized water was used in making dilutions for all the solutions studies by lsv.

The individual series A, B, and C differed by which of the three metals Pb^{2+}, Cd^{2+} or In^{3+} were added to the electrolyte. Stock solutions of Cd^{2+} and Pb^{2+} were made by the dissolution of AR Cd and Pb metal in a minimum amount of HNO_3, followed by dilution. The In^{3+} stock was made by dissolving Alfa Products 99.95% In_2O_3 in a small amount of hot $HClO_4$, followed by dilution. The Pb^{2+}, Cd^{2+} and In^{3+} stock solutions were then standardized by EDTA titrations (17) to concentrations of 1.96×10^{-2}M, 2.09×10^{-2}M and 2.02×10^{-2}M, respectively. The concentrations of metal for the individual

Table 2.1 Composition of solutions used in this work

L.s.v. standard addition series

All solutions include 25 ml of 0.58 M HCl background electrolyte with

Series

A: 6-20 µl additions of Pb^{2+}_{2+} stock solution
B: 5-20 µl additions of Cd^{2+}_{3+} stock solution
C: 5-20 µl additions of In^{3+} stock solution

L.s.v. stock solution concentrations:
$[Pb^{2+}] = 1.96 \times 10^{-2}$ M $[Cd^{2+}] = 2.09 \times 10^{-2}$ M $[In^{3+}] = 2.02 \times 10^{-2}$ M

A.s.v. standard addition series

All solutions include 25 ml of 0.58 M purified HCl background electrolyte with:

Series

D: 5-20 µl additions of Tl^{+}_{3+} stock solution
E: 6-20 µl additions of In^{3+} stock solution

A.s.v. stock solution concentrations:
$[Tl^{+}] = 8.84 \times 10^{-5}$ M $[In^{3+}] = 2.02 \times 10^{-4}$ M

L.s.v. single solutions:

All solutions diluted with laboratory deionized water.

F: $[Cd^{2+}] = 4.2 \times 10^{-5}$ M, [HCl] = 0.23 M, $[HClO_4]$ = 0.69 M
G: $[In^{3+}] = 4.0 \times 10^{-5}$ M, [HCl] = 0.23 M, $[HClO_4]$ = 0.69 M
H: $[Cd(NO_3)_2] = 2.0 \times 10^{-3}$ M, $[NaClO_4]$ = 1.01 M, pH = 5.0

A.s.v. single solutions:

Made with quartz distilled water.

I: $[Pb(NO_3)_2] = 4.2 \times 10^{-7}$ M, [NaCl] = 0.56 M, $[NaClO_4]$ = 0.50 M

additions in each standard addition series are shown in Table 2.2. The metal stock solutions were stored in tightly closed linear polyethylene bottles.

The standard addition series D and E examined by asv were also based on a background electrolyte of 0.58 M HCl. Because of the great sensitivity of asv special care must be taken to use ultra-pure reagents, especially for those reagents that are present in large concentrations. The HCl background was prepared from 6 M HCl that had been purified by the sub-boiling distillation method of Mattison (18). This reagent was stored in pre-leached Teflon bottles to avoid contamination from the container walls. The water used to dilute the HCl, and used in the dilution of solutions for all asv experiments, was taken from a pre-leached all vitreous silica quartz still. No metal contaminants were seen in a solution of this water and a purified $NaClO_4$ reagent when asv with a thin film mercury electrode and a plating time of ten minutes was performed.

The In^{3+} and Cd^{2+} metal stock solutions for the asv standard addition series were made fresh daily by a 1:100 dilution of the stock solutions used in lsv. A Tl stock solution was created by the dissolution of AR $TlNO_3$ directly in deionized water, and standardized gravimetrically via a CrO_4^- precipitation method taken from Vogel (19). The concentration of metal for each individual addition in each series is shown in Table 2.3.

In addition to the several series just described, four single solutions were made to investigate the effects of perturbing

Table 2.2: Results for application of s.v.c.f. to FT filtered, background subtracted, linear sweep voltammograms

Filename	Conc.[a]	Potl.[b]	Height[b]	Width[b]	R^2
A1	1.57	-0.4864	8.20	45.2	0.944
A2	3.14	-0.4864	16.5	46.4	0.991
A3	4.72	-0.4855	24.2	45.3	0.988
A4	6.29	-0.4864	33.0	43.8	0.996
A5	7.86	-0.4863	40.6	45.3	0.998
A6	9.42	-0.4859	47.9	44.1	0.997
B1	1.67	-0.6894	7.45	42.6	0.854
B2	3.34	-0.6885	13.9	47.6	0.966
B3	5.01	-0.6885	21.6	46.0	0.980
B4	6.68	-0.6878	30.1	45.2	0.988
B5	8.36	-0.6879	35.8	47.1	0.994
C1	1.62	-0.6521	11.0	36.9	0.953
C2	3.24	-0.6522	21.9	34.7	0.972
C3	4.85	-0.6516	30.2	36.8	0.986
C4	6.47	-0.6516	41.0	37.0	0.993
C5	8.09	-0.6512	52.5	36.7	0.992

a) Units for concentration are 10^{-5} M.
b) Units for potential are V, for height are $\mu A/V^{1/2}$, and for width are mV.

Table 2.3: Results for application of s.v.c.f. to FT filtered, background subtracted, anodic stripping voltammograms

Filename	Conc.[a]	Potl.[b]	Height[b]	Width[b]	R^2
D1	0.707	-0.5440	1.14	98.4	0.969
D2	1.41	-0.5443	1.99	92.5	0.989
D3	2.12	-0.5440	2.71	94.6	0.993
D4	2.83	-0.5437	3.48	92.0	0.994
D5	3.54	-0.5438	4.28	94.4	0.996
E1	1.62	-0.6487	8.30	27.2	0.941
E2	3.24	-0.6489	19.4	29.8	0.987
E3	4.85	-0.6491	30.9	28.7	0.992
E4	6.47	-0.6488	40.4	29.1	0.995
E5	8.09	-0.6488	53.3	28.7	0.996
E6	9.71	-0.6487	64.7	28.8	0.997

a) Units for concentration are 10^{-7} M.
b) Units for potential are V, for height are $\mu A/V^{1/2}$, and for width are mV.

influences on s.v.c.f. Two solutions, F and G, were created to study the effects of varying scan rates on s.v.c.f. The background electrolyte for both solutions was made by diluting Mallinckrodt AR HCl and $HClO_4$ to concentrations of 0.23 M and 0.69 M, respectively. The final solutions were made by adding 50 µl of Cd^{2+} and In^{3+} stock solutions into 25 ml of the electrolyte.

A solution was made to examine the effect of electrode drop size on the s.v.c.f. technique. Solution H was made by dissolving AR $Cd(NO_3)_2$ and G.F. Smith Co. AR $NaClO_4$ to concentrations of 2.0×10^{-5} M and 1.01 M, respectively, and then adjusting the pH of the solution to 5.0 to prevent hydrolysis of the Cd^{2+}.

A final solution, solution I, was made to investigate the effects of asv plating time on s.v.c.f. The background electrolyte for this solution was made from the dilution of purified NaCl and $NaClO_4$ with quartz-distilled water. These purified electrolytes were made by the electrolytic purification of AR NaCl and $NaClO_4$ over a mercury pool cathode that was held at a potential of -1.5 V vs. SCE. Electrolysis was done under an Ar atmosphere for about a week. These purified reagents were then stored in pre-leached Teflon bottles. The solution I was made by adding 50 µl of 2.1×10^{-5} M AR $Pb(NO_3)_2$ to 25 ml of the background electrolyte, which was standardized at $[Cl^-]$ = 0.56 M and $[ClO_4^-]$ = 0.50 M. The final solution was adjusted to a pH of 3.9 by additions of Ventron ultra-pure $HClO_4$.

2.4.6 Procedure

For the lsv standard addition series A, B, and C, 25 ml of the background electrolyte was first pipetted into a clean, dry cell, and bubbled for 5-10 minutes with Ar to remove oxygen. A mercury drop was then extruded by rotating the micrometer head of the HMDE 0.50 revolutions, which creates a drop of 0.57 mm radius. The program ROB4 was then used to run the experiment and take data. After a voltammogram was taken of the background electrolyte and written to disk, five or six 20 ml standard additions of metal stock solution were made, after each of which a voltammogram was taken and written to disk. A typical linear sweep voltammogram before data analysis is shown in Figure 2.3. For series A-C all scans were taken from an initial potential of -0.2 V. vs. the Ag/AgCl electrode to a final potential of -0.9 V at a scan rate of 1.00 V/s. For all lsv experiments the sensitivity setting on the PAR 179 coulometer was 10 μA/full scale. A new drop was extruded for each lsv or asv scan.

The procedure for the voltammograms taken of solutions F, G, and H were quite similar. For the scan rate investigation done on solutions F and G the procedure was the same, except that no standard additions were made. Instead, a series of voltammograms were taken of each solution at different scan rates, where The scan rates used are shown in Table 2.4.

For the drop size investigation done on Solution H, different drop sizes were achieved by rotating the HMDE micrometer head from 0.05 rev. to 0.50 rev. in increments of 0.05 rev. The weight of mercury extruded for 10 revolutions of the micrometer head was

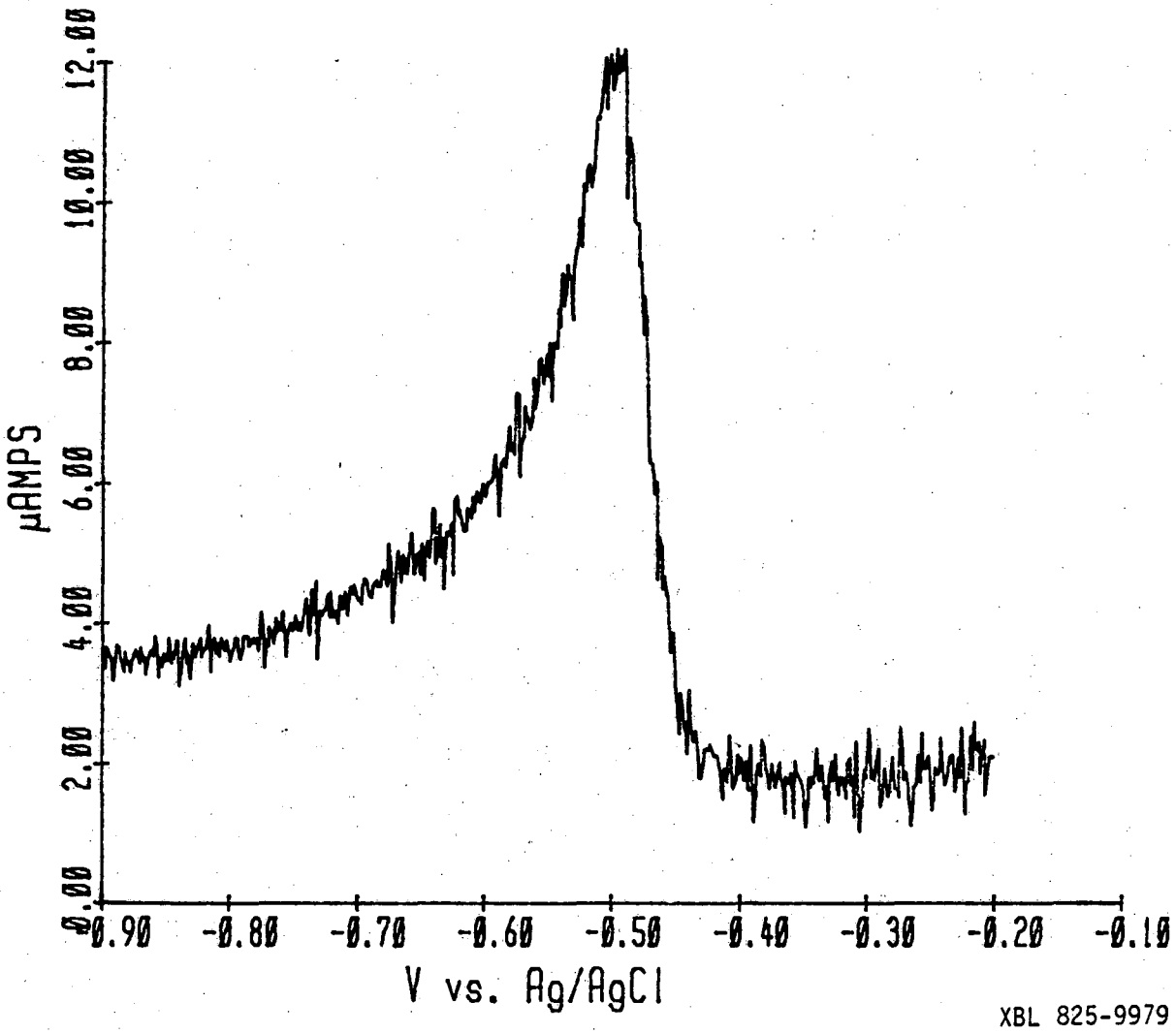

Figure 2.3: Raw lsv data of file A6.

Table 2.4: Dependence of fit peak parameters on scan rate for l.s.v. single peak data

	Solution	Scan Rate (V/s)							
		0.1017	0.2031	0.5077	0.9895	1.983	4.950	10.03	20.09
Peak potential, in V	F	-.6764	-.6761	-.6756	-.6754	-.6755	-.6752	-.6780	-.6750
	G	-.6396	-.6400	-.6410	-.6413	-.6431	-.6417	-.6448	-.6444
Peak Height, in $\mu A/V^{1/2}$	F	5.67	8.10	13.17	17.55	24.10	40.0	55.5	78.0
	G	17.3	22.1	29.2	33.8	27.2	20.9	16.0	11.8
Peak Width, in mV	F	44.7	46.1	44.0	45.4	44.3	44.0	41.3	46.0
	G	37.6	39.4	42.8	47.6	54.4	60.7	69.5	70.6
$H/\nu^{1/2}$, in $\mu A \cdot s^{1/2}/V$	F	17.78	17.97	17.48	17.64	17.11	17.98	17.53	17.40
	G	54.2	49.0	41.0	34.0	27.2	20.9	16.0	11.8
R^2	F	0.994	0.996	0.985	0.993	0.983	0.987	0.972	0.993
	G	0.969	0.974	0.972	0.971	0.960	0.952	0.951	0.909
$E_p - E_{p/2}$, in mV	F	28.7	28.7	28.0	28.9	27.9	28.7	28.4	29.4
	G	23.7	23.3	26.2	27.3	33.1	34.1	43.2	43.3

determined to be 0.211 g at 24°C. The density of mercury at 24°C is 1.354×10^{-2} g/μl (20), so that this weight corresponds to a volume of 15.6 μl of Hg. Thus 1.56 μl of Hg is extruded per revolution of the micrometer head. The radius of the drop can be determined from

$$r_o = \left\{ \frac{3(1.56)}{4\pi} \text{ rev.} \right\}^{1/3} \qquad (2.4.1)$$

The radii are shown along with the revolutions of the micrometer head in Table 2.5. The initial potential for the voltammograms taken in this experiment was -0.4 V vs. the Ag/AgCl electrode, the final potential was -0.9 V, and the scan rate 1.0 V/s.

The stripping voltammograms for series D and E of Table 2.1 were taken in much the same way as the voltammograms of series A, B, and C, except that the program JEFF3 was used instead of ROB4. For D and E, the plating potential was -1.0 V vs. Ag/AgCl and the plating time was 600 s. The rest potential was -0.9 V, the scan rate 1.00 V/s, and the final potential -0.2 V. The potential used to clean the electrode both before and after experiments was -0.235 V.

For the anodic stripping voltammograms taken for the plating time investigation done on Solution I, the rest potential was -0.8 V vs. Ag/AgCl, and the final potential was -0.1 V. The plating times used for this study are shown in Table 2.6. All stripping voltammograms were taken at a sensitivity of 1 μA/full scale, and a drop size of 0.50 rev.

Table 2.5: Results for drop size studies[a]

Filename	Radius	Surface Area	Potl.	Height	Width	R^2
H1	0.265	0.882	-0.6263	25.5	47.0	0.9994
H2	0.334	1.40	-0.6262	35.4	47.1	0.9993
H3	0.382	1.83	-0.6259	45.2	46.8	0.9996
H4	0.421	2.23	-0.6261	53.8	46.8	0.9996
H5	0.453	2.58	-0.6257	66.4	46.6	0.9996
H6	0.482	2.92	-0.6259	69.1	46.8	0.9998
H7	0.507	3.23	-0.6259	75.2	46.6	0.9997
H8	0.530	3.53	-0.6262	81.7	46.9	0.9996
H9	0.551	3.82	-0.6262	88.1	46.7	0.9996
H10	0.571	4.10	-0.6261	95.1	46.9	0.9997

a) Units for radius are mm, for surface area are mm^2, for other parameters are those of Table 2.2.

Table 2.6: Results for asv plating time studies[a]

Filename	Time	Potl.	Height	Width
I1	100.	-0.4544	2.05	46.0
I2	150.	-0.4543	2.99	45.4
I3	300.	-0.4545	6.55	44.0
I4	450.	-0.4546	9.63	44.7
I5	600.	-0.4548	13.25	45.1

a) Units for time are seconds, all others are those of Table 2.3.

After all data were taken and written to disk, the data analysis procedure began. The full data analysis procedure was fourfold; first, Fourier transform filtering, followed by point by point background subtraction, followed by semidifferentiation, and lastly the curve fitting of a sech function. The last two steps are, of course, the s.v.c.f. technique as outlined in Chapter 1. The effect of the application of the three data analysis programs BAJSM, BBACK and GDSEMI is to change the raw lsv data file of Figure 2.3 to that of Figure 2.4. To determine the effects of perturbing influences on the s.v.c.f. techniques, some of the steps of the data treatment were skipped; this will be discussed in the appropriate section.

2.5 RESULTS

2.5.1 Classically Reversible Lsv Systems

The effectiveness of the s.v.c.f. technique in its application to real data is determined in much the same way as is the effectiveness of s.v.c.f. applied to the artificial data of Chapter 1. From the results of Chapter 1, returned coefficients of determination should be close to 1, at least in the limit of a large signal to noise (S/N) ratio. Returned peak potentials should be close to reported $E_{1/2}$ values, as predicted by (2.3.3); similarly, peak widths should be close to the predicted peak widths of (2.3.5). From (2.3.6) reported peak heights should be linearly proportional to C^*_{ox}, $\nu^{1/2}$, and A.

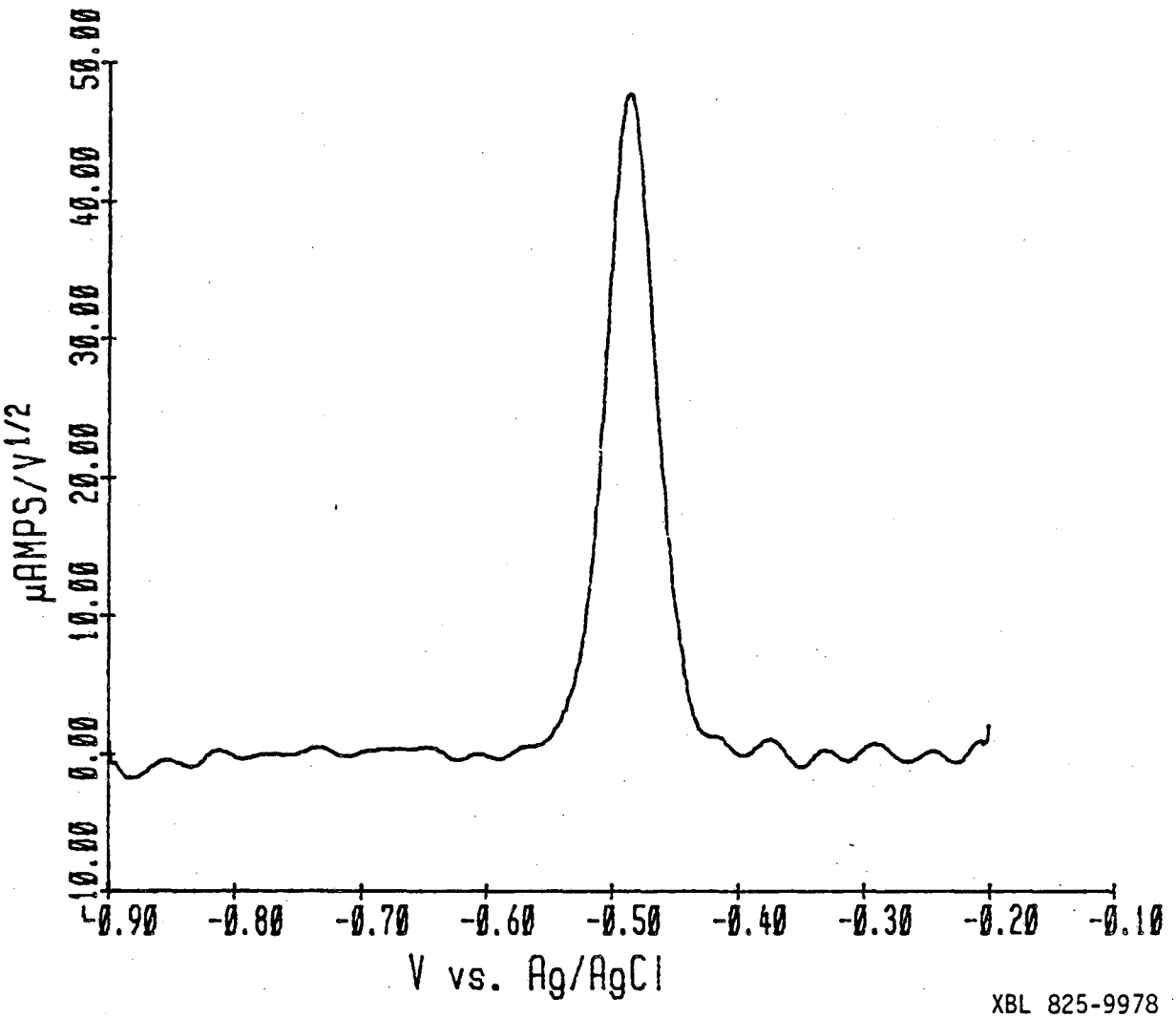

Figure 2.4: FT filtered, background subtracted semiderivative of file A6.

Table 2.2 shows results for the application of s.v.c.f. to the FT filtered, background subtracted voltammograms of series A and B. The averages and standard deviations of the peak potential and width for the series of Table 2.2 are shown in Table 2.7, along with the slopes, intercepts and regression coefficients for linear least squares fits of concentration to returned peak height for these series. The average peak potentials and widths are repeated in Table 2.8, which also shows $E_{1/2}$ and peak width values taken from the polarographic literature (21), and $E^r_{1/2}$ and peak width values taken from the filtered, background subtracted but not semidifferentiated voltammograms of series A and B.

The peak width values are indicative of the reversibility of the reaction. For the polarographic data, the Tomes (22) criterion

$$E_{3/4} - E_{1/4} = \frac{56.4}{n} \text{ mV} \qquad (2.5.1)$$

can be used to determine reversibility, while for the unsemidifferentiated voltammetric data of this work (1.2.6) can be used. The $E^r_{1/2}$ values found for this work are corrected to be vs. the SCE, and (1.2.4) was used to determine $E^r_{1/2}$ from the unsemidifferentiated voltammetric data.

Application of the Tomes criterion to the previous polarographic data of Table 2.8 indicate that the Cd^{2+} and Pb^{2+} systems should be classically reversible two electron charge transfers. This is confirmed for the systems studied in this work by the application of

Table 2.7: Average peak parameters and results of straight line fits of concentration to peak height for data of Tables 2.2 and 2.3

Series	Potl.[b]	Width[b]	Slope	Intercept	r^2
A[c]	-0.4862 ± 0.0004	45.0 ± 0.9	5.09	0.42	0.999
B[c]	-0.6884 ± 0.0006	45.7 ± 2.0	4.36	-0.08	0.998
C[c]	-0.6517 ± 0.0004	36.4 ± 1.0	6.31	0.67	0.999
D[d,e]	-0.5440 ± 0.0002	93.4 ± 1.3	1.10	0.394	0.999
E[d,e]	-0.6488 ± 0.0002	29.0 ± 0.4	6.95	-3.17	0.999

a) Slope, intercept and r^2 are from the linear least squares fit of concentration to peak height in each series.
b) Units for potential are V vs. the Ag/AgCl electrode, for width are mV.
c) Units for slope and intercept are $\mu A/[V^{1/2} \times 10^{-5} M]$ and $\mu A/V^{1/2}$.
d) Units for slope and intercept are $\mu A/[V^{1/2} \times 10^{-7} M]$ and $\mu A/V^{1/2}$.
e) Averages and straight line fits do not include first point in series.

Table 2.8: Average half-wave potentials and peak widths

Element	Other works[a]		This work			
	$E_{1/2}$ [b]	$E_p-E_{p/2}$ [b]	$E_{1/2}$ [c]	$E_p-E_{p/2}$	E_p	FWHM
Pb	-0.435	28.	-0.441	27.8	-0.442	45.0
Cd	-0.642	28.	-0.644	28.6	-0.644	45.7
In (lsv)	-0.597	19.	-0.608	22.1	-0.608	36.4
Tl	-0.475	58.	-0.501	57.3	-0.500	93.4
In (asv)	-0.597	19.	-0.605	19.1	-0.605	29.0

a) Units for $E_{1/2}$ are V, for widths are mV. $E_{1/2}$ is reported vs. the saturated calomel electrode.
b) Values are from Ref. 10. Supporting electrolyte is 1F HCl, except for In, which is 1F KCl.
c) Calculated from (1.2.4).

(1.2.6) to the $E_p-E_{p/2}$ values for the filtered, background subtracted voltammogram. These are very close to the 28.2 mV expected for a reversible two electron charge transfer.

For these reversible charge transfer systems Table 2.2 shows that returned R^2 values from the application of s.v.c.f. are near one and increase with increasing concentration, i.e. with increasing S/N. Table 2.8 shows that average peak potentials from s.v.c.f. are close to both polarographic $E_{1/2}$ values and to $E^r_{1/2}$ values calculated from the unsemidifferentiated data. Returned peak widths are close to the expected 45.3 mV calculated from (2.3.5); in fact, they are within one standard deviation of 45.3 mV. Returned parameters show good agreement with values expected from (2.3.1), (2.3.3), and (2.3.5) for these classically reversible systems.

Table 2.7 shows that regression coefficients are near one and intercepts near zero for fits of peak height to concentration for series A and B. These data imply that the peak height is linearly proportional to C^*_{ox}.

Table 2.4 shows the results of an investigation on the effects of scan rate on solution F of Table 2.1. The $E_p-E_{p/2}$ for the voltammograms taken at the different scan rates are all near the classically reversible value of 28.2 mV, indicating that the system is reversible over the entire range of scan rates. Returned peak widths for solution F are all close to 45.3 mV, providing further confirmation of the validity of (2.3.5). The $H/\nu^{1/2}$ values are the ratios of semiderivative peak heights to the square root of the scan

rate. This remains essentially constant over the range of scan rates, at a value of about 17.6. This implies that for reversible files, the peak height of the semiderivative is proportional to the square root of the scan rate.

Solution H of Table 2.1, like in composition to solution F, is expected also to be reversible. Table 2.5 shows the results of the drop size investigation on solution H. The returned peak widths all near 45 mV indicate that the charge transfer reaction is reversible. A linear least squares fit of returned peak height to surface area for the ten drop sizes has a regression coefficient of 0.998. This satisfies the last of the criteria necessary to say that s.v.c.f. is valid when applied to real, classically reversible lsv systems.

2.5.2 Kinetically Controlled Lsv Systems

Tables 2.2, 2.7 and 2.8 also show results for the application of s.v.c.f. to filtered, background subtracted files of series C, which is In^{3+} in a solution of 0.58 M HCl. Previous polarographic data for In^{3+} in 1F KCl (Ref. 23, and Table 2.8) indicate that this three electron charge transfer reaction is not quite classically reversible. The $E_p-E_{p/2}$ from the unsemidifferentiated voltammogram is also larger than the 18.8 mV expected for a classically reversible three electron charge transfer, further implying a slightly non-reversible system.

Even though the series C is not classically reversible, the returned results show that s.v.c.f. works well for this particular system. Returned R^2 values are close to 1, and returned peak

potentials are close to those of previous works. Returned peak widths are broadened as compared to the 30.2 mV peak width expected for a three electron charge transfer, indicating the non-reversible nature. The straight line fit of concentration to peak height has a large regression coefficient and small intercept, indicating good linearity in spite of the non-reversibility. The slope is larger than the slopes for the Cd^{2+} or Pb^{2+} straight line fits, but not by as much as would be expected from (2.3.6) for a three electron charge transfer, probably because of the non-reversibility.

Table 2.4 shows the results of the effects of scan rate on Solution I. This system is expected to be less classically reversible than the system of series C because of the decreased Cl^- concentration and increased ClO_4^- concentration, in which In^{3+} is known to be irreversible (3). The E_p-$E_{p/2}$ values bear this out; even for the lowest scan rate the E_p-$E_{p/2}$ value is larger than the E_p-$E_{p/2}$ for series C. The E_p-$E_{p/2}$ values increase with scan rate, indicating that the system is becoming less and less reversible, and more and more affected by the homogeneous kinetics. A plot of the semiderivative for the highest scan rate shows that the semiderivative is skewed toward negative potentials. This is indicative of a kinetic zone of behavior of the CE mechanism. (See Chapter 1, and especially Figure 1.11.)

The results of Table 2.4 imply that the s.v.c.f. technique becomes increasingly worse in fitting lsv systems that are controlled more and more by the homogeneous kinetics. As scan rates increase,

decreasing the dimensionless homogeneous rate constant λ (defined by (1.2.11)), R^2 values degrade, indicating a worsening of fit. Peak widths increase steadily to a maximum of about 70 mV and peak potentials decrease steadily. The $H/\nu^{1/2}$ values decrease steadily, indicating that semiderivative peak height does not increase as $\nu^{1/2}$. In fact, for $\nu > 0.9895$ V/s the peak heights are seen to actually decrease. While s.v.c.f. is effective in the analysis of slightly non-reversible peaks, it is not generally effective for the fitting of voltammograms in kinetically controlled zones of behavior of the CE mechanism.

2.5.3 Sphericity Effects

The data of Table 2.5 should also show the effects of the sphericity of the drop on the s.v.c.f. technique. The current for a diffusion controlled system is given by (24)

$$i(t) = i(t)_{planar} + \frac{nFA\, D_{ox} C^*_{ox}}{r_o}\, \phi(t) \qquad (2.5.2)$$

where ϕ is the tabulated spherical correction factor of Nicholson and Shain (25), and r_o is the radius of the HMDE. The spherical correction term becomes large at small r_o; it also becomes large at small scan rate ν, since the planar term goes as $\nu^{1/2}$. The semiintegral of a voltammogram where spherical terms are significant has a gradually sloping limiting plateau (26). This implies that the semiderivative will be a $sech^2$ function slightly broadened and skewed

toward cathodic potentials. Table 2.5 shows that the results for the two smallest drop sizes do show a slight shift to cathodic potentials, and a slight peak broadening, but the sphericity effect is not really large enough to be significant at this scan rate.

2.5.4 Effect of Electrochemical Noise

All of the c.v.c.f. equations were derived with the assumption that the only source of current was that of a charge transfer reaction of the appropriate kinetic mechanism. If there is current due to any other source it will cause some error in the returned results.

One source of error that is always present to some extent is simple noise. In the course of the data processing done to obtain the results of Table 2.2, Fourier transform based filtering was used to eliminate high frequency noise prior to the application of s.v.c.f. Since it is a least squares based curve fitting technique, in the right circumstances s.v.c.f. should succeed in fitting a very noisy voltammogram. It is interesting to see whether or not s.v.c.f. can enhance the S/N ratio of very noisy electrochemical data.

Table 2.9 shows returned peak parameters for series A, B, and C. In the data processing done to achieve these results voltammograms were not FT filtered, but were background subtracted, prior to s.v.c.f. When compared to Table 2.2, the results of Table 2.9 show that for the data encountered in this work s.v.c.f. is not effective in returning correct parameters from noisy linear sweep voltammograms.

Table 2.9: Results of s.v.c.f. for background subtracted voltammograms of Table 2.2[a]

Filename	Potl.	Height	Width	R^2
A1	-0.6325	30.1	0.5	0.008
A2	-0.6670	29.4	0.4	0.001
A3	-0.4871	31.5	23.8	0.330
A4	-0.4869	39.3	28.9	0.397
A5	-0.4866	44.3	36.4	0.497
A6	-0.4860	56.3	34.0	0.583
B1	-0.7340	10.1	0.5	0.001
B2	-0.6907	17.9	18.0	0.090
B3	-0.6901	28.0	24.1	0.232
B4	-0.6892	37.6	25.8	0.324
B5	-0.6886	39.5	37.5	0.539
C1	-0.6464	14.1	10.7	0.098
C2	-0.6516	27.7	16.1	0.160
C3	-0.6510	37.9	22.2	0.329
C4	-0.6516	45.3	27.3	0.503
C5	-0.6507	55.1	33.1	0.681

a) Units of all parameters are those of Table 2.2.

There are several reasons why in this case s.v.c.f. does not enhance the S/N ratio. Least squares curve fitting techniques are successful in fitting data in which noise is independent and uncorrelated, as is the case for random errors. A frequency plane analysis of the data shows that for this system noise is not random, but is rather periodic. Figure 2.5 shows the power spectrum of the voltammogram A6. This spectrum has spikes in it at high frequencies; this is indicative of some kind of periodic noise, and in fact the period of the noise can be shown to be at multiples of 60 Hz. The noise is probably 'pick-up' noise, which is induced from unshielded or badly shielded a.c. power lines. Periodic noise is not independent and uncorrelated, so that the basic assumptions underlying the application of least squares fitting techniques do not hold true. The noise in all of the data of this work is predominantly pick-up noise, so that the s.v.c.f. technique cannot be used to enhance S/N ratio.

Even if noise is random, s.v.c.f. may not help in improving the S/N ratio. This is because the process of semidifferentiation, like any differentiation technique, accentuates high frequency components of a voltammogram. The power spectrum of the unfiltered, background subtracted semiderivative of A6 is shown in Figure 2.6. The high frequency spikes in this figure are relatively larger than in Figure 2.5. The semidifferentiated voltammogram is relatively noisier than the original voltammogram, and this serves to offset any gain in S/N ratio achieved through curve fitting. Since random noise also is a high frequency component of the voltammogram, this lack of gain in S/N is true even if the noise is random.

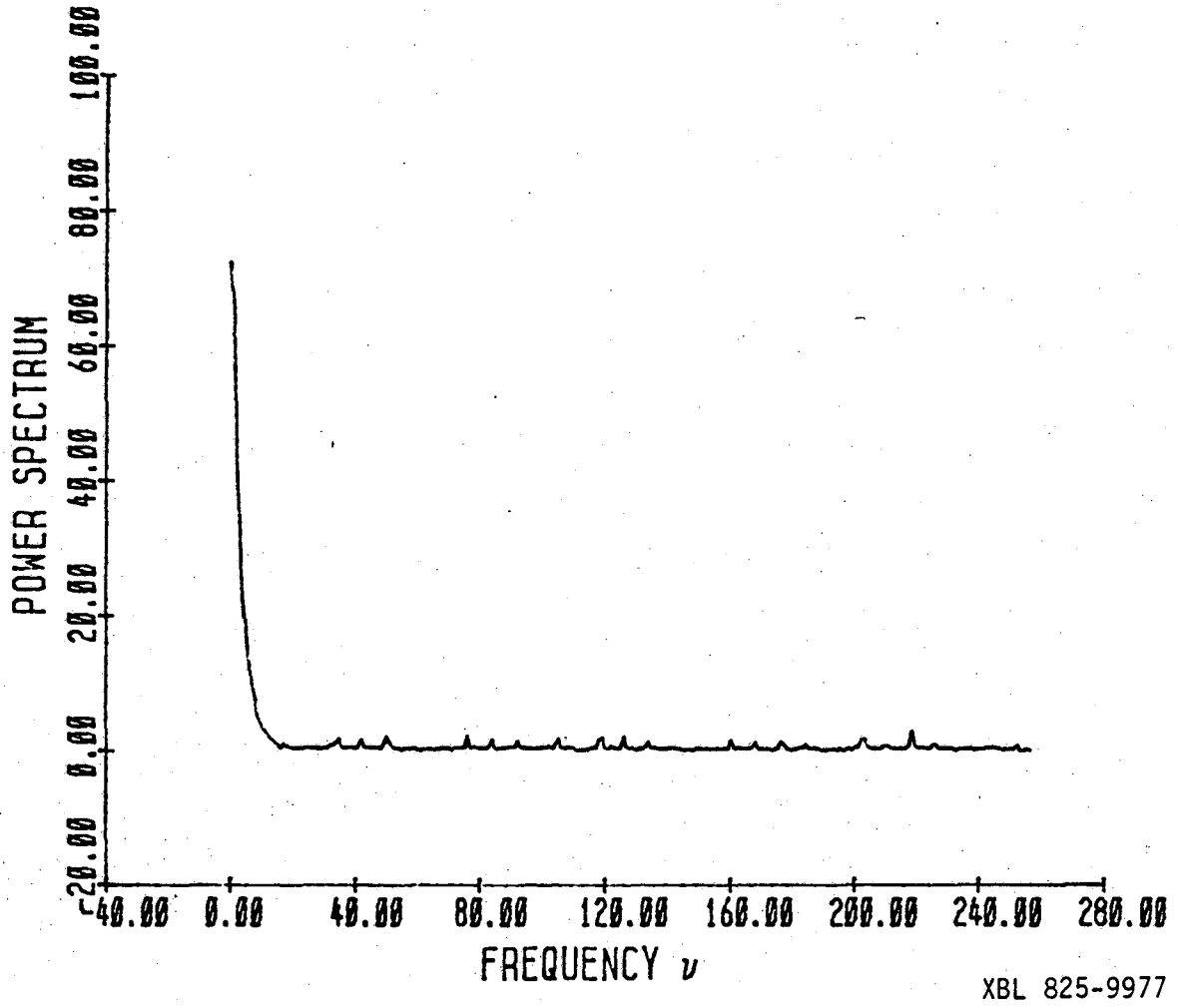

Figure 2.5: Power spectrum of raw lsv data of file A6.

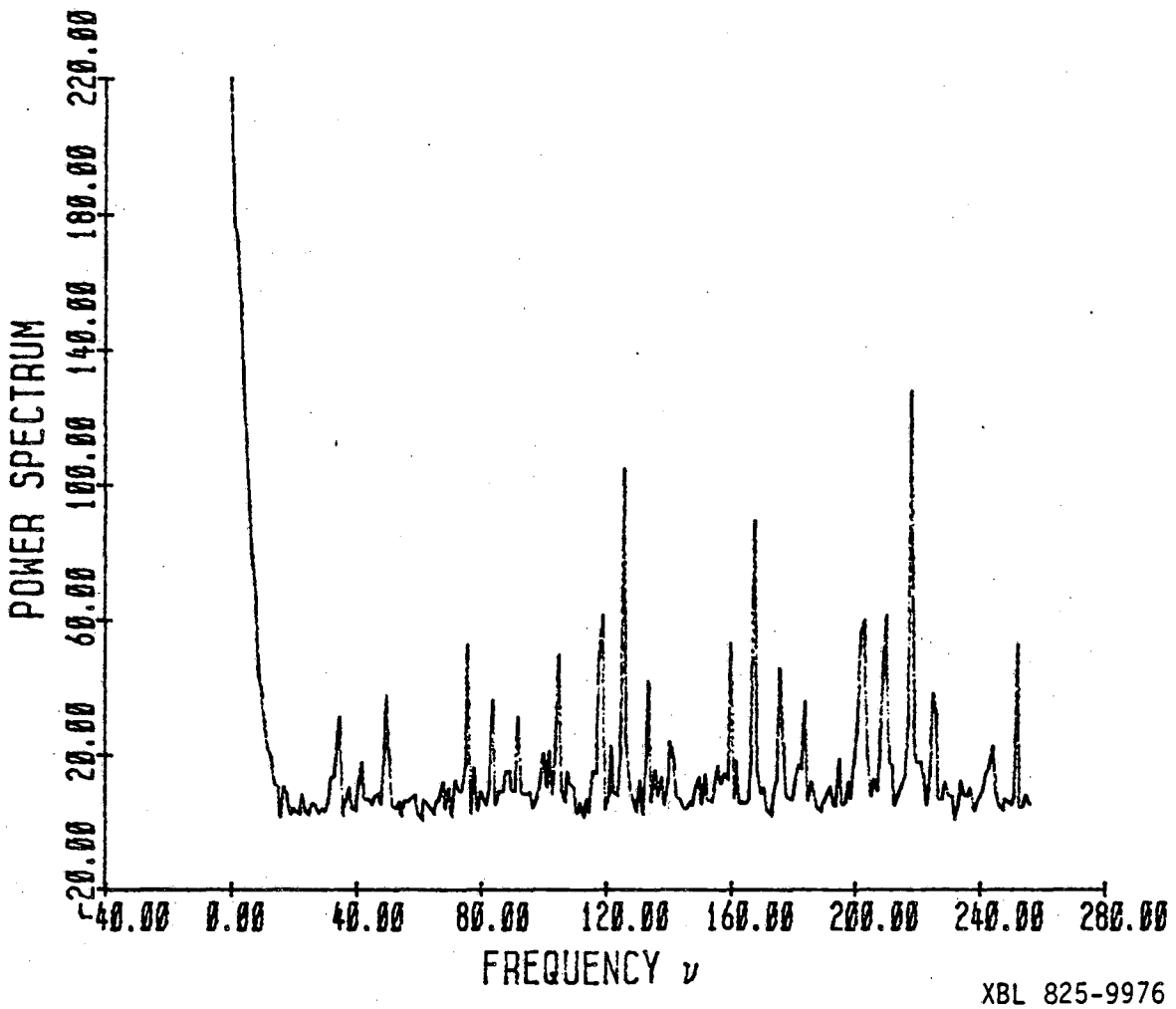

Figure 2.6: Power spectrum of unfiltered, background subtracted semiderivative of file A6.

Because, however, the FT filtering technique works very well in the elimination of noise from most electrochemical data, the problem of noise is really not a serious one for the application of s.v.c.f. If the time of an electrochemical experiment is much shorter than usual, as is the case for very fast scan rates, the frequency components of the signal are moved into the higher frequency part of the power spectrum, making impossible the separation of noise and signal frequency components upon which FT filtering is based. In this instance s.v.c.f. will probably not be applicable.

2.5.5 Effect of Background Current

Another source of current is the so-called background, or residual, current. Table 2.10 shows the results for the application of s.v.c.f. to voltammograms of series A, B, and C that were filtered but not background subtracted. The results for this application more nearly match the results of Table 2.2, being worse than those of Table 2.2 for the systems with smaller metal concentrations.

The peak potentials are shifted only very slightly cathodically, while peak widths for the most part increase slightly. Peak heights, especially for small concentrations, are increased greatly over the results of Table 2.2. This would make results of quantitative analysis of systems using s.v.c.f. in error at low concentrations. This is unfortunate, because in performing qualitative analysis on real systems it is usually very difficult to correct for background current, and might make s.v.c.f. unsuitable for qualitative analysis

Table 2.10: Results of s.v.c.f. for FT filtered voltammograms of Table 2.2[a]

Filename	Potl.	Height	Width	R^2
A1	-0.4857	10.8	53.8	0.336
A2	-0.4859	18.9	51.1	0.604
A3	-0.4852	26.4	49.8	0.734
A4	-0.4859	34.5	49.0	0.821
A5	-0.4859	42.3	49.0	0.878
A6	-0.4856	49.7	47.3	0.895
B1	-0.6878	7.40	44.7	0.147
B2	-0.6876	14.1	47.3	0.390
B3	-0.6880	21.4	46.9	0.613
B4	-0.6874	29.9	46.1	0.754
B5	-0.6875	35.8	47.3	0.818
C1	-0.6518	11.0	39.2	0.262
C2	-0.6521	21.7	36.6	0.551
C3	-0.6514	30.0	38.0	0.719
C4	-0.6514	40.7	38.2	0.827
C5	-0.6510	52.1	37.8	0.881

a) Units of all parameters are those of Table 2.2.

in lsv at low concentrations.

At first glance it might be thought that the situation is worse in asv, where background current is relatively larger than in lsv. In asv, however, one has the methods of Kryger, Jagner and Skov (15) and Brown and Kowalski (16) with which one might correct for the background current.

2.5.6 Classically Reversible Asv Systems

Table 2.3 shows the results for the application of s.v.c.f. to the filtered, background subtracted anodic stripping voltammograms of series D. Results from previous studies (See Table 2.8) indicate that for a similar electrolyte the Tl^+ charge transfer is actually slightly non-reversible, but the E_p-$E_{p/2}$ values determined in this work are very close to the reversible 56.5 mV, and so the system is considered classically reversible.

Just as for the classically reversible lsv systems the coefficient of determination for each of the fits in series D is close to one, and increases with concentration. The returned peak potential is fairly close to the polarographic $E_{1/2}$, and agrees exactly with the $E^r_{1/2}$ calculated directly for the voltammogram. The linear fit of concentration to peak height has a regression coefficient close to one, showing that C^*_{ox} is linear with peak height, as predicted from (2.2.1), (2.2.2) and (2.3.6). The intercept, although still small, is relatively larger in comparison with the slope than are the intercepts for the lsv series. The cause of this is not clear, at present, but

the possibility of contamination is always significant at the concentration levels used in asv. A fit of concentration to peak height for the unsemidifferentiated sripping voltammograms has a similarly large intercept. This supports the hypothesis that the large intecept is not due to the s.v.c.f. technique.

The idea of contamination is further hinted at by the anomaly of the large average peak widths. The theoretical peak width for a one electron charge transfer is 90.6 mV. The broader peak width cannot be ascribed to non-reversibility; as seen in Chapter 1, the non-reversible EC mehcanism results in narrower semiderivative peaks, not broader peaks. The answer lies in a look at the semiderivative (Figure 2.7). on either side of the foot of the peak are what appear to be small peaks at -0.69 V, -0.65 V and -0.46 V. These are potentials at which Cd^{2+}, In^{3+} and Pb^{2+} peaks are expected; the peaks can be assumed to be contaminants of these three species. The effect is to broaden the peak; when two or three peaks are assumed and fit, the peak width narrows to near reversible width. The problem with contamination in this case is exacerbated because the Tl^{+} is a one-electron transfer, and the others are multi-electron transfers.

2.5.7 Kinetically Controlled Asv Systems

Tables 2.3, 2.7 and 2.8 also show results for the application of s.v.c.f. to the anodic stripping voltammograms of series E. The systems of series E are basically the same as those of series C, so that one would expect the behavior of the system to be not quite

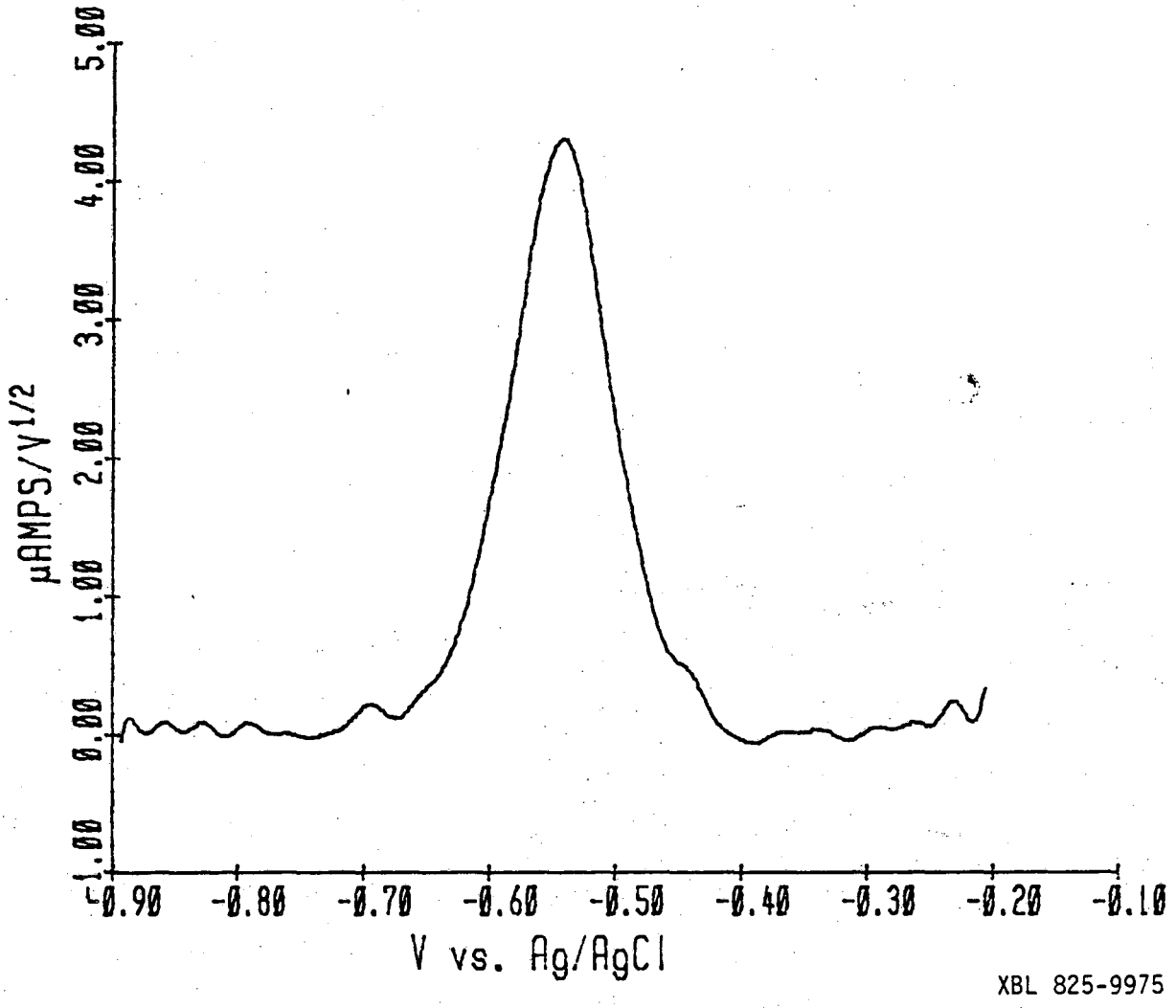

Figure 2.7: FT filtered, background subtracted semiderivative of file D5.

classically reversible. In contrast to the lsv system of Section 2.5.2, however, because this is an EC mechanism, semiderivative peaks should be slightly narrower than the 30.2 mV expected for a three electron charge transfer. It is expected that even if the system is kinetically controlled that s.v.c.f. might still work well.

The results of the tables confirm the expectations. Returned peak potentials are close both to literature $E_{1/2}$ values and the E_p values found for series C. Least squares fits of concentration to peak height show a linear dependence between these two variables. Peak widths are only slightly narrower than the reversible 30.2 mV, indicating that (as was seen in Section 2.5.2) the system is only slightly non-reversible. S.v.c.f. appears to be valid in the fitting of non-reversible asv systems.

2.5.8 Effect of Plating Time in Asv

Table 2.6 shows the effects of plating time in asv on the results of s.v.c.f. The solution this investigation was done on was Solution I; the times shown in Table 2.6 are the plating times in seconds. From (2.2.2) and (2.3.6), a plot of H vs. plating time τ should be linear, going through the origin. A linear least squares fit gives a large regression coefficient of 0.9986, indicating good linearity. The intercept of -0.27 is an indication of the error involved in the asv background subtraction, again probably due to contamination.

The large R^2 values and peak widths near the reversible peak width of 45.3 mV imply that the amalgam concentration is homogeneous

at the end of the rest period, because diffusion is apparently semi-infinite. A non-semi-infinite, non-homogeneous system should have narrowed, cathodically shifted peaks, because the concentration of amalgam is less towards the center of the drop. This phenomenon causes the narrow peaks observed in asv with thin film mercury electrodes (27).

2.6 CONCLUSIONS

In this chapter semiderivative voltammetric curve fitting has been shown to be effective in the curve fitting of real linear sweep and anodic stripping voltammograms. For systems that are composed of metal complexed by ligands, in the limit of large ligand concentration the c.p.s.v. theory works for the pseudo-first order association and dissociation reactions. For lsv and asv systems that are classically reversible, returned parameters from application of s.v.c.f. agree well with parameters found in the literature and with expected results from s.v.c.f.

S.v.c.f. has also been shown to be effective in fitting some systems that are not classically reversible, both lsv and asv. Results from the use of s.v.c.f. for these systems reflect the results of Chapter 1, in particular the peak broadening and narrowing effects noted for the lsv and asv systems, which indicate that perhaps the artificial data of Chapter 1 in the kinetically controlled realms do mirror the behavior of real data. Other factors, such as sphericity effects, drop size effects, and effects of finite plating

time in asv, apparently have no effect on the use of s.v.c.f. for usual drop sizes, plating times and scan rates.

There are some perturbing effects, however, that can make s.v.c.f. ineffective in fitting electrochemical data. In lsv, it was shown that s.v.c.f., except for only slightly non-reversible systems, is ineffective in the curve fitting of kinetically controlled systems. The addition of a large amount of high frequency noise, whether periodic or random, will play havoc with results, which implies that noisy voltammograms must be filtered before application of s.v.c.f. Residual currents also distort the shape of a semiderivative, especially at low concentrations. This means that results for quantitative analysis using s.v.c.f. could be in great error unless the background is compensated. This would be very difficult to do in lsv for real samples; however, in asv, the methods of Kryger et al. (15) and Brown and Kowalski (16) make possible elimination of background.

The advantages of the s.v.c.f. technique derive from the fact that it is a curve fitting technique. As stated in Chapter 1, curve fitting can lead to signal to noise enhancement and resolution enhancement. Although the s.v.c.f. technique does not lead to significant increases in S/N enhancement, s.v.c.f. does have much to offer in the way of enhancement of resolution of overlapping lsv and asv waves. This is discussed in the next chapter.

References

1) C. Zbinden, Bull. Soc. Chim. Biol. 13, 35 (1931)

2) E. Barendrecht, Electroanal. Chem. 2, 53 (1967)

3) F. Vydra, K. Stulik and E. Julakova, "Electrochemical Stripping Analysis," Wiley, New York, 1976

4) Kh. Z. Brainina, "Stripping Voltammetry in Chemical Analysis," Wiley, New York, 1974

5) I. Shain and J. Lewison, Anal. Chem. 33, 187 (1961)

6) W.H. Reinmuth, Anal. Chem. 33, 85 (1961)

7) J.J. Toman, R.M. Corn and S.D. Brown, Anal. Chim. Acta 123, 187 (1980)

8) J.W. Cooper, "The Minicomputer in the Laboratory," Wiley and Sons, New York, 1977

9) Digital Equipment Corp., "Microcomputer Processor Handbook," 1980

10) Digital Equipment Corp., "Microcomputer Interfaces Handbook," 1980

11) J.W. Hayes, D.E. Glover, D.E. Smith and M.W. Overton, Anal. Chem. 45, 227 (1973)

12) G. Horlick, Anal. Chem. 44, 943 (1972)

13) L. Mertz, Appl. Optics 10, 386 (1971)

14) J.S. Newman, "Electrochemical Systems," Prentice-Hall, Englewood Cliffs, N.J., 1972

15) L. Kryger, D. Jagner and H.J. Skov, Anal. Chim. Acta 78, 241 (1975)

16) S.D. Brown and B.R. Kowalski, Anal. Chim. Acta 107, 13 (1979)

17) G. Schwarzenbach and H. Flaschka, "Complexometric Titrations," Metheun, London, 1969

18) J.M. Mattison, Anal. Chem. 44, 1715 (1972)

19) A.I. Vogel, "Textbook of Macro and Semimacro Qualitative Inorganic Analysis," 4^{th} ed., Longman, New York, 1976

20) " CRC Handbook of Chemistry and Physics," 56^{th} ed., R.C. Weast, ed., CRC Press, Cleveland, Ohio, 1975

21) L. Meites, "Polarographic Techniques," 2^{nd} ed., John Wiley and Sons, New York, 1965

22) J. Tomes, Collect. Czech. Chem. Commun. 9, 12 (1937)

23) J.J. Lingane, J. Am. Chem. Soc. 61, 2099 (1939)

24) W.H. Reinmuth, J. Am. Chem. Soc. 79, 6358 (1957)

25) R.S. Nicholson and I. Shain, Anal. Chem. 36, 706 (1964)

26) J.C. Imbeaux and J.M. Saveant, J. Electroanal. Chem. 44, 169 (1973)

27) T.M. Florence, J. Electroanal. Chem. 27, 273 (1970)

CHAPTER 3

PEAK RESOLUTION IN LINEAR SWEEP VOLTAMMETRY AND ANODIC STRIPPING VOLTAMMETRY USING SEMIDERIVATIVE VOLTAMMETRIC CURVE FITTING

3.1 INTRODUCTION

A principal difficulty in the use of dynamic electrochemistry as a quantitative analytical technique is the problem of resolution of overlapping waves. This is of particular importance in linear sweep voltammetry (lsv) and anodic stripping voltammetry (asv) at a stationary mercury electrode because of the very broad, asymmetric nature of the peaks. Another difficulty is that the current-potential relationship is not describable by an analytic function. These problems are particularly unfortunate since lsv instrumentation is easy to use and is relatively inexpensive.

There have been two general approaches to electrochemical peak resolution, a "hardware" approach and a "software" approach. The hardware approach is typified by the methods of Martin and Shain (1) and Bond and Grabaric (2). In both methods a sample is run along with a blank solution containing a suitable background electrolyte and one of the overlapped components. The concentration of this component is varied in the blank until, upon subtraction of the blank voltammogram from the sample voltammogram (whether by analog or digital means), no trace of the overlapped component is left. Besides being very time intensive, the making of a suitable blank may not even be feasible for cases in which the supporting electrolyte is complex.

The software approach, that of resolution after data taking, is perhaps more promising. Annino (3) divides software resolution techniques into two types: frequency domain and time domain (curve fitting). Peak resolution in the frequency domain can be accomplished

by the method of Kirmse and Westerburg (4). In this method the Fourier transform of an overlapped spectrum is divided by the transform of a single component, resulting in a sharpened spectrum. This is the method used by Grabaric, O'Halloran and Smith (5) in their paper on the resolution enhancement of a.c. polarographic peaks.

In electrochemistry Binkley and Dessey (6) have recently done work on the least-squares fitting of FT transformed square-wave voltammograms. In this procedure the transform of the overlapped peak is fit with the transforms of single peak data in a least squares manner by varying what would be the peak height in the time domain. This procedure is advantageous in two ways. The fit is reduced in complexity by the reduction of points in going to the frequency domain, and fits may be done on both real and imaginary parts of the transform in order to obtain an averaged, improved fit. The procedure does rely on utilization of empirical single peak parameters, however.

Another approach to the problem of resolution is a more sophisticated mathematical approach employing the Kalman filter, as demonstrated by Brown and Brown (7). The Kalman filter makes possible the linear parameter estimation of data by eliminating the necessity for the manipulation of large matrices in the solution of the problem. This method also requires as input single peak data, however.

Curve fitting of electrochemical data has been hampered by the lack of analytic current-potential functions. Some work has been done in this area, principally by Perone and co-workers (8-10). Boudreau and Perone (10) describe the application of an empirical peak shape

function (the sum of skewed gaussian and cauchy functions) in the use of curve fitting for the resolution of square wave voltammetric peaks. This function requires five parameters per peak and in addition requires that three "shape" parameters be found from single peak data. The other two parameters are determined from a least squares minimization procedure. Overlapped peaks with separations as small as 30 mV are resolved.

In Chapters 1 and 2 a method, called semiderivative voltammetric curve fitting, was developed to enable the curve fitting of semiderivatives of voltammetric data. It was shown that the $sech^2$ fitting function was a good approximation to semiderivatives of linear sweep and anodic stripping voltammograms in many cases. This provides a powerful tool for the resolution of overlapped voltammetric waves, because for the first time voltammetric data can be fit with a peak shape function derived from theory.

As discovered in Chapter 2, however, in many cases perturbing influences may make s.v.c.f. ineffective in resolving peaks. Residual current might distort the voltammetric wave, and it is to be expected that non-classically reversible kinetics for the CE mechanism might make s.v.c.f. ineffectual in resolving some lsv peaks.

This work will use s.v.c.f. to return peak parameters from lsv and asv systems that have overlapped waves. Initially a computer study will be done to determine the theoretical limits of resolution for this technique. Then the accuracy of resolution for overlapped peaks of the systems of Chapter 2 will be discussed. The effects on

the accuracy of resolution of non-classically reversible homogeneous kinetics for both lsv and asv systems, and of residual current for lsv systems, will be determined. In addition, single peak parameters will be used in fitting multiple overlapped peaks, with an eye to improving the accuracy of resolution.

3.2 THEORY

The theory for the application of convolutive potential sweep voltammetry to overlapping lsv waves of classically reversible systems was developed by Ammar and Saveant (11). The theory states that the semiintegral of the sum of two lsv waves (for reversible systems) is the sum of the semiintegrals of the individual waves. This was shown to be true for p-dinitrobenzene in acetonitrile (11). Since the semiderivative is the derivative of the semiintegral, and derivatization is a linear operation, the semiderivative of the sum of two lsv waves is the sum of the semiderivatives of the individual waves. Therefore the theory for the semiderivative of overlapped lsv waves is that of the individual semiderivatives, and is outlined in Section 2.3.

The theory for overlapping waves of non-classically systems is also that of Section 2.3. The effectiveness of s.v.c.f. in resolving overlapped semiderivative peaks should depend on its ability to fit single peak systems. S.v.c.f. will probably fail in resolving lsv waves for systems that are kinetically controlled, as s.v.c.f. does not fit these waves well. It will probably be more successful in resolving overlapping asv waves for kinetically controlled systems.

3.3 EXPERIMENTAL

The experimental set-up for these experiments is outlined in Section 2.4. All of the hardware and software used in this chapter is the same as that of the last.

The composition of the solutions studied in this work is outlined in Table 3.1. With the exception of series M, Table 3.1 lists series of solutions upon which standard addition analyses were done in exactly the same manner as in Chapter 2. The background electrolytes and stock solutions used in the construction of these solutions are those of Chapter 2, and the manner of the construction of the solutions was the same, with one difference. After a voltammogram of the supporting electrolyte alone is taken, (for use in later background subtraction), but before the series of standard addition voltammograms is taken, a single, large addition of a different metal is made. Other details about the voltammograms are exactly those of the series of standard addition runs in Chapter 2 for both lsv and asv.

One standard addition series, series M, was made up with a supporting electrolyte equivalent to those of solutions F and G of the second Chapter. This was done to determine the accuracy of resolution for the application of s.v.c.f. to kinetically controlled lsv systems. A large addition of Cd^{2+} stock solution was initially made to the background electrolyte, and subsequent additions were made of In^{3+}. After each addition a voltammogram was taken at a scan rate of 1.983 V/s. Other parameters for the voltammograms were also those of

Table 3.1. Composition of solutions used in this work

L.s.v. systems

Series

I: 100 µl of Pb^{2+} stock solution and 5-20 µl additions of Cd^{2+} stock solution to 25 ml of 0.58 M HCl.

J: 100 µl of Cd^{2+} stock solution and 5-20 µl additions of In^{3+} stock solution to 25 ml of 0.58 M HCl.

K: 100 µl of In^{3+} stock solution and 5-20 µl additions of Cd^{2+} stock solution to 25 ml of 0.58 M HCl.

L: 100 µl of both Pb^{2+} and In^{3+} stock solution and 5-20 µl additions of Cd^{2+} stock solution to 25 ml of 0.58 M HCl.

M: 50 µl of Cd^{2+} stock solution and 5-20 µl additions of In^{3+} stock solution to 25 ml of 0.23 M HCl, 0.69 M $HClO_4$.

L.s.v. stock solution concentrations:
$[Pb^{2+}] = 1.96 \times 10^{-2}$ M $[Cd^{2+}] = 2.09 \times 10^{-2}$ M $[In^{3+}] = 2.02 \times 10^{-2}$ M

A.s.v. systems

Series

N: 50 µl of Cd^{2+} stock solution and 5-20 µl additions of Tl^{+} stock solution to 25 ml of purified HCl.

O: 50 µl of In^{3+} stock solution and 5-20 µl additions of Tl^{+} stock solution to 25 ml of purified HCl.

P: 20 µl of both In^{3+} and Cd^{2+} stock solution and 5-20 µl additions of Tl^{+} stock solution to 25 ml of purified HCl.

A.s.v. stock solution concentrations:
$[Tl^{+}] = 8.84 \times 10^{-5}$ M $[In^{3+}] = 2.02 \times 10^{-4}$ M $[Cd^{2+}] = 2.09 \times 10^{-4}$ M

the standard addition series of Chapter 2.

After all data were taken, the analysis routine outlined in Chapter 2 was performed on these data. The programs BAJSM, BBACK and GDSEMI were used, in that order, to perform noise filtering, background subtraction, and semidifferentiation. These three programs transformed a voltammogram like that of Figure 3.1 into the form of Figure 3.2. The resultant semiderivative was used as input to BIMFIT, which returned a peak potential, height, and width for each of the peaks specified. The resolved components of the semiderivative of Figure 3.2 are shown in Figure 3.3.

In addition to BIMFIT, constrained width fits of series I, J, K and L were done using CNWSBM. The input peak width for each peak was taken as the average peak width for the corresponding single peak standard addition series of Chapter 2. These are given in Table 2.7.

3.4 RESULTS

3.4.1 Synthetic Fused Peak Systems

The first step in the study of the use of s.v.c.f. for the resolution of overlapping voltammograms was to determine the limits of resolution of the least squares fitting program BIMFIT. The limits of resolution were determined by applying BIMFIT to the resolution of artificial overlapped hyperbolic secant squared data. The artificial data were created by the FORTRAN program MAKEIT. Input to MAKEIT consisted of a peak potential C_i, height A_i and width B_i for each of

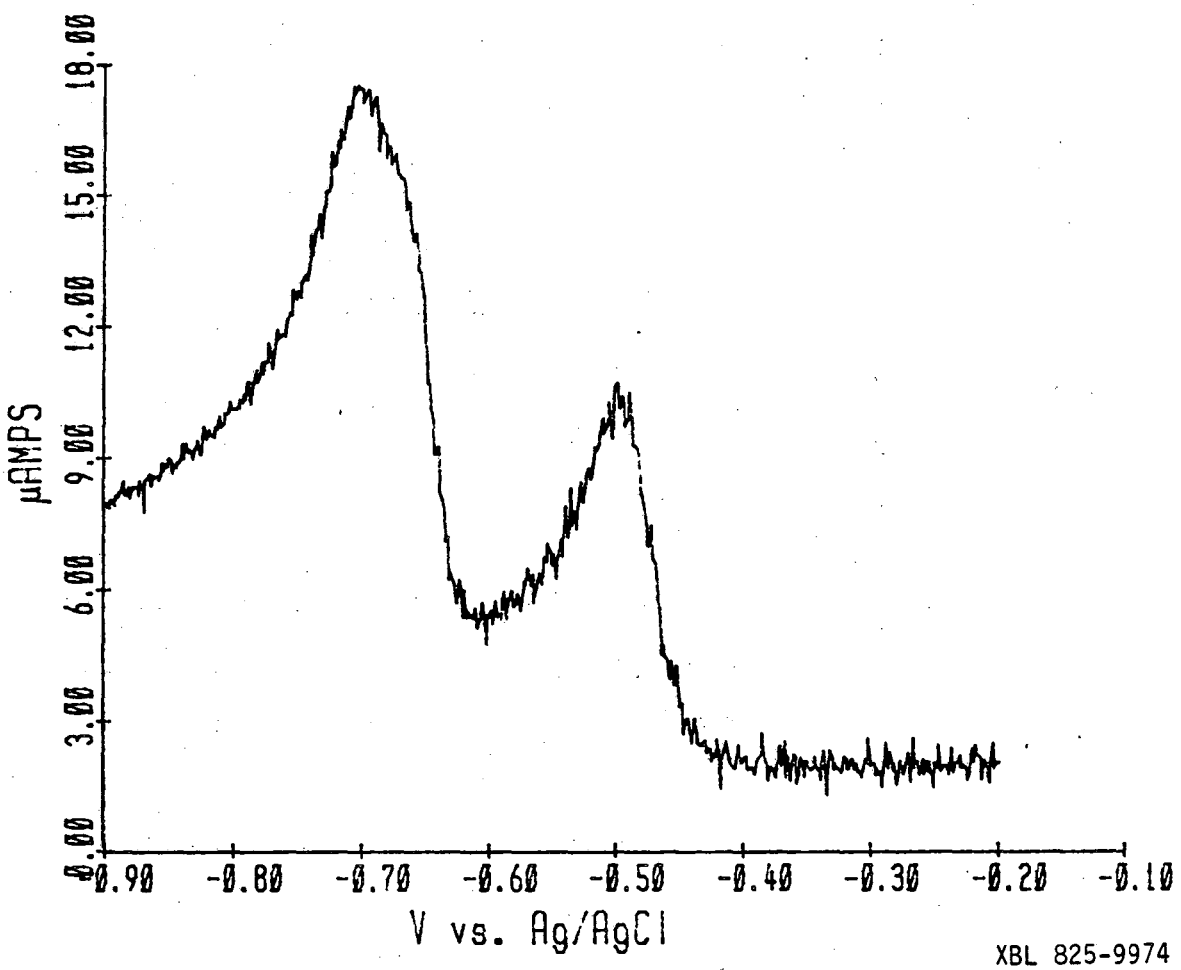

Figure 3.1: Raw lsv data of file L5, with waves due to Pb^{2+}, In^{3+}, and Cd^{2+}.

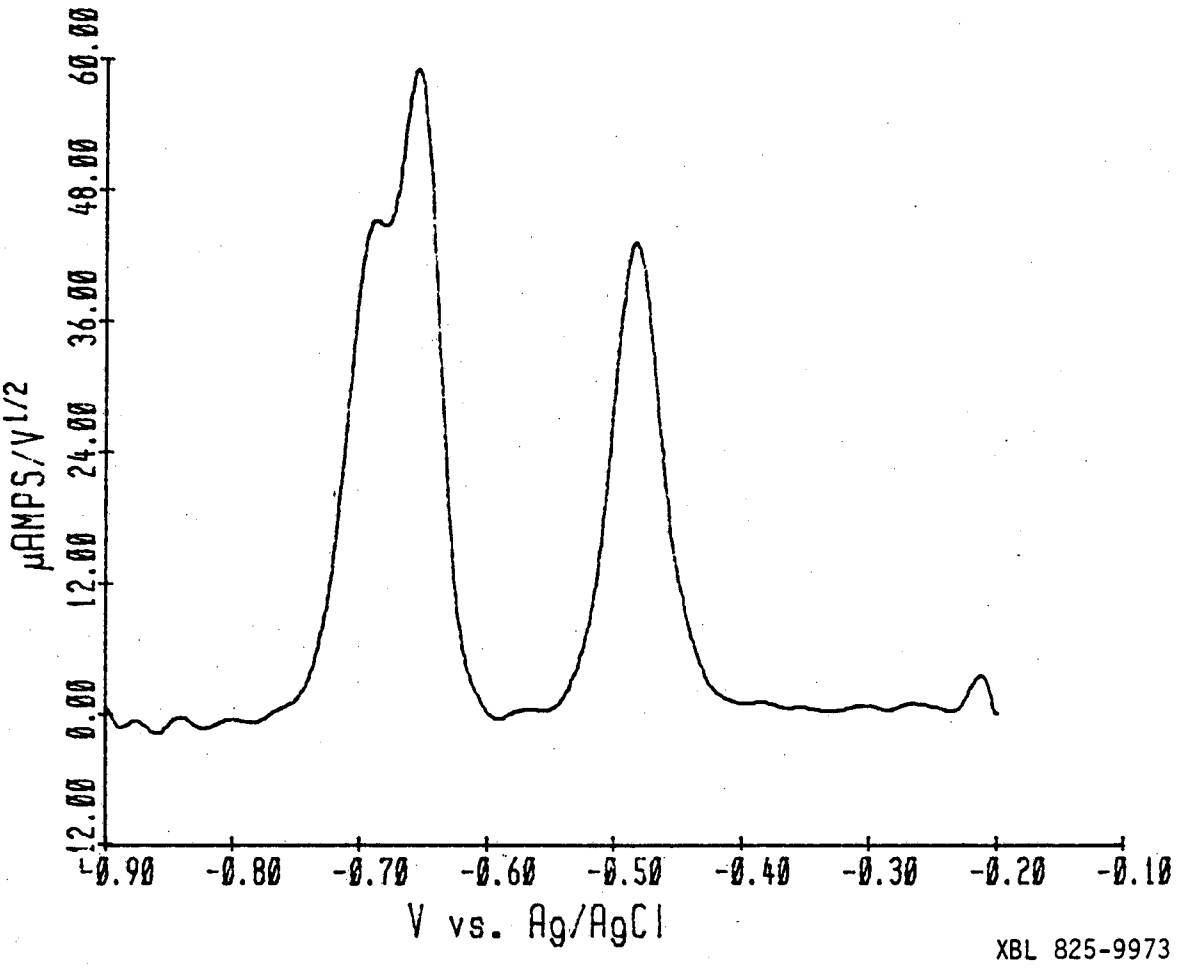

Figure 3.2: FT filtered, background subtracted semiderivative of file L5.

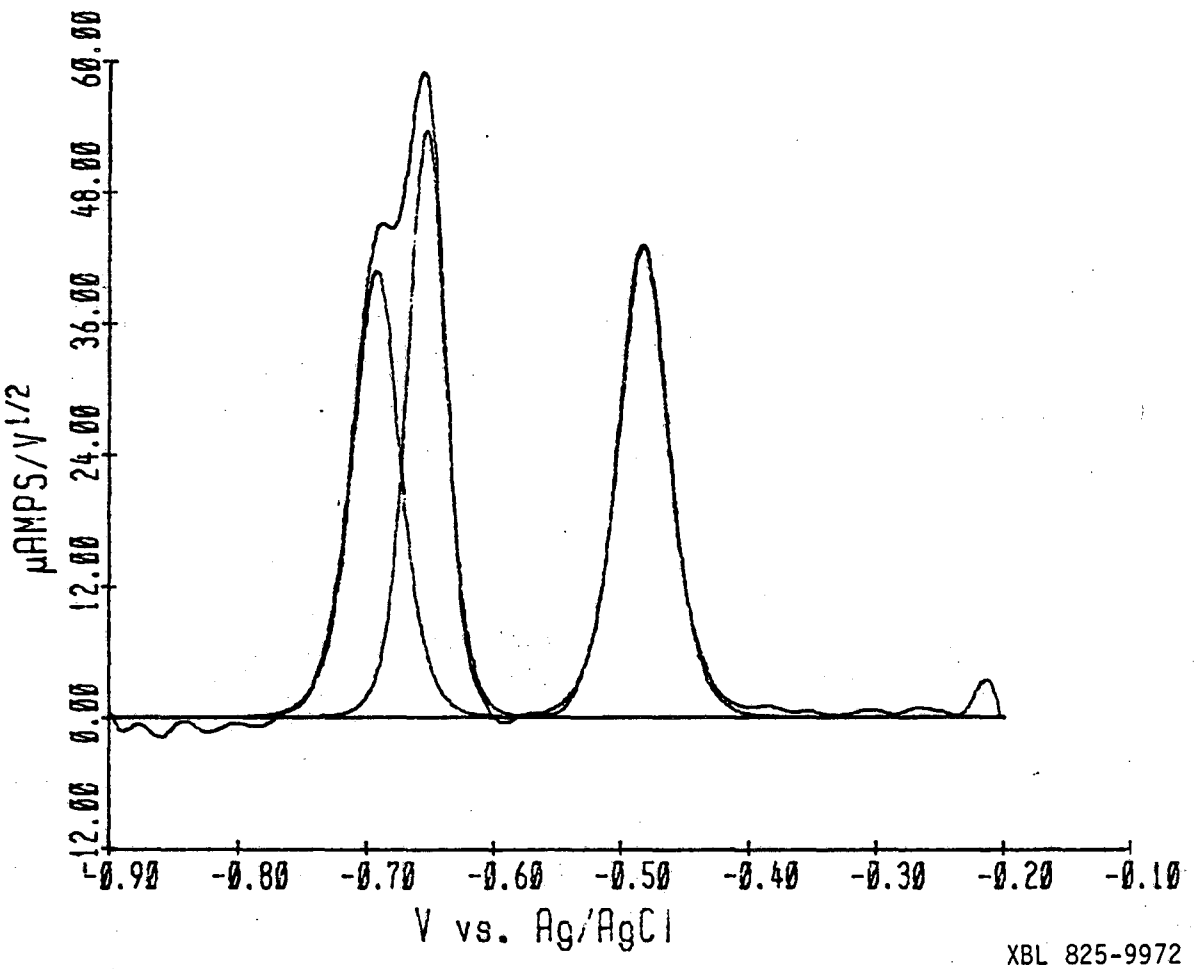

Figure 3.3: Semiderivative peak of Figure 3.2, and the fit components to the semiderivative.

two peaks; the output is given by

$$f(E) = \sum_{i=1}^{2} A_i \, \mathrm{sech}^2\{ (1.763/B_i)(E-C_i)\} \qquad (3.4.1)$$

if B_i, the peak width, is in volts.

The fitting program BIMFIT was used to return values of peak potential, height and width for this artificial sech^2 data. The parameter most sensitive to the separation in peak potential $\Delta E = |E_1-E_2|$ was the returned peak height. For this reason, an error of 10% or greater was chosen, rather arbitrarily, to constitute failure of resolution.

The effects of peak overlap are first considered for two peaks of equal height and full width at half maximum. Each sech^2 peak has a height of one, and a half-width of 40 mV, which is intermediate to the half-width expected for a classically reversible two electron charge transfer (45 mV) and a reversible three electron charge transfer (30 mV). Several files were created with peak separations ranging from 50 mV to 10 mV. It was found that resolution failed for peak separations of between 10 and 15 mV. If two peaks of equal height and unequal half-width (100 mV and 40 mV) overlap one another, resolution fails at approximately the same peak separation, between 10 and 15 mV.

The resolving power of the curve fitting program BIMFIT was also determined for peaks of equal half-width (40 mV), and heights with a ratio of 10:1. Again, several files with peak separations of between

50 to 10 mV were created. Failure of resolution was defined as the return of the height of the smaller peak with an error of 10% or greater. Judged by this definition, resolution failed at peak separations of 20 mV.

BIMFIT is seen to be powerful enough to separate $sech^2$ peaks, of about the half-width of the semiderivative of a classically reversible charge transfer system, down to peak separations of 10-20 mV. Since the half-wave potentials of real systems are almost never that close to one another, BIMFIT should be powerful enough to resolve any two semiderivatives that are $sech^2$ in shape. If the s.v.c.f. method fails to resolve two peaks, it will be because the shape of the semiderivative (due to kinetics, residual current, etc.) is not $sech^2$ in shape.

As a point of interest, the coefficient of determination R^2 obtained from the fits to the artificial sech data for which resolution failed was as close to one as it was for the data for which resolution succeeded. This illustrates the danger of relying upon R^2 as a measure of the resolving power of a fitting method.

3.4.2 Nearly Classically Reversible Lsv Systems

The success of the s.v.c.f. technique in resolving the individual components of a voltammogram containing overlapped peaks can be evaluated using several criteria. As in Chapters 1 and 2, the coefficient of determination R^2 should be near one for all fits, and should get closer to one as signal increases. Returned peak

potentials and peak widths must remain constant for all additions. Since the systems, if it is assumed that added metals do not interact, are the same as the single peak systems of Chapter 2, returned peak potentials and widths should match the averaged peak potentials and widths of Table 2.8. Since standard additions are made of one component only, the returned peak heights for the components not added must remain constant as additions are made. Lastly, linear least squares fits of returned peak height to the concentration of the added components for a given series should have a regression coefficient r^2 close to one, intercepts near zero, and slopes that are close to those of the single peak systems of Chapter 2.

Table 3.2 shows the average and standard deviation of the peak potential and width for each component of the series I, J, K, and L. Also shown are the average and standard deviation for the height of the component(s) not added in each series, and the slope, intercept, and regression coefficient r^2 for the linear least squares fit of peak height to concentration for the added component of each series. At the bottom of the table, for comparison purposes, are the same parameters for the single peak systems of Chapter 2.

The results in Table 3.2 show that, for all of the lsv series considered, even the ones with the non-reversible In^{3+}, the s.v.c.f. technique is successful in resolving the components of the system. Coefficients of determination are all near one, and increase with increasing concentration of the added component. Standard deviations for the peak potentials are small, being (for the most part) between

Table 3.2 Averages and standard deviations of returned peak parameters and results of straight line fits of peak height to concentration for nearly classically reversible lsv data [a,b,c]

	Cd			In			Pb					
Series	Potl.	Height	Width	Potl.	Height	Width	Potl.	Height	Width	Slope	Intercept	r^2
I	-.6902± 0.0004		47.1± 1.3				-.4815± 0.0003	38.9± 0.4	43.8± 0.6	4.50	-0.9	0.998
J	-.6912± 0.0014	40.5± 1.3	48.7± 1.3	-.6513± 0.0012		31.6± 1.2				5.83	2.3	0.999
K	-.6878± 0.0034		52.2± 3.3	-.6518± 0.0007	34.6± 1.3	32.3± 0.7				4.21	5.4	0.999
L	-.6859± 0.0018		49.6± 1.7	-.6489± 0.0002	49.0± 0.7	33.1± 0.2	-.4801± 0.0002	40.1± 0.5	45.2± 0.7	4.22	6.3	0.999
A							-.4862± 0.0004		45.0± 0.9	5.09	0.4	0.999
B	-.6884± 0.0006		45.7± 2.0							4.36	-0.1	0.998
C				-.6517± 0.0004		36.4± 1.0				6.31	0.7	0.999

a) Slope, intercept and r^2 result from the least squares straight line fit of peak height to the concentration of added species in each series.
b) Units for slope and intercept are $\mu A/[V^{1/2} \times 1.0 \times 10^{-5} M]$ and $\mu A/V^{1/2}$, respectively.
c) Units for potential are V vs. the Ag/AgCl electrode, for height are $\mu A/V^{1/2}$, for width are mV.

one and two mV for the added component in each series, and less than one mV for components not added. Average peak potentials for each component are close to the average peak potential for the component found in the single peak scans.

The standard deviation for the Pb peak, in the series with Pb^{2+}, is small, and the average width is close both to that of the single peak series and the theoretical 45.3 mV expected for a two electron charge transfer. Peak widths for the Cd and In peaks do not show as small a standard deviation or as good an agreement with single peak averages, especially for the three series J, K and L in which Cd^{2+} and In^{3+} are present simultaneously. The Cd peaks in particular show a large standard deviation in width, while the In peak widths are smaller, and the Cd widths broader, than the single peak averages.

There are two possible explanations for this effect. Firstly, the Cd and In peaks are much closer together (40 mV separation, peak to peak) than are the In and Pb peaks; in fact, as seen in Figure 3.2, the Pb semiderivative peak (farthest to right) is completely resolved from the others. However, the results of Section 3.4.1 imply that BIMFIT should be able to resolve these two peaks if the semiderivatives are $sech^2$ in shape. A better explanation is that the In system, as was seen in Chapter 2, is slightly non-reversible. This means that the semiderivative of the In lsv wave is not exactly $sech^2$ in shape. What is probably happening is that some of the In semiderivative is attributed to the Cd semiderivative in the $sech^2$ curve fitting step.

The peak heights for the component not added in each series remain fairly constant, as reflected by the small standard deviations in the peak height. The regression coefficients for the linear least squares fits of peak height to concentration of the added component are all near one, indicating a linear relation between concentration and peak height. The slopes are near the slopes for the single peak systems. The intercepts for series with both Cd and In are very large and positive, however. This would be the result if some of the In peak peak were attributed to the Cd peak. It is worth noting that the intercept for the Cd-Pd system, series I, is very near zero.

All in all, the results for the application of s.v.c.f. to these series of lsv waves do meet the criteria for success in the resolution of overlapping lsv waves. Lsv waves with a separation in peak potentials as small as 40 mV can be resolved, without the assumption of any single peak parameters.

3.4.3 Effect of Constraining Width

In section 3.4.2, it was noted that results for Cd and In peak widths and peak heights appeared to be slightly in error whenever these two components were present simultaneously. It was hypothesized that some of the In peak was being taken as part of the Cd peak. One way to eliminate part of the error is to use a constrained width program; i.e., fit only peak potentials and heights, while entering the peak width as input and not varying this last parameter. This was done for the files of series I, J, K and L, using the FORTRAN program CNWSBM, described in Section 1.5. Peak widths input to CNWSBM were

the average peak widths for the single peak series, taken from Table 2.8.

The averages, standard deviations, slopes, intercepts, etc. for the different series are shown in Table 3.3. Comparing these results with the results of Table 3.2, it is seen that returned peak potentials and heights remain almost unchanged for Pb, as would be expected. Returned peak potentials for In and Cd show much smaller standard deviations, indicating less error in the fit, although peak potentials are shifted slightly to more negative potentials. Standard deviations of the peak height for the component not added are smaller. For the J series, the returned height of the Cd peak is smaller than in Table 3.2, while for the K and L series, the peak height of the In peak is larger than in Table 3.2, indicating that what BIMFIT saw as part of the Cd semiderivative peak, CNWSBM sees, more correctly, as part of the In peak. The constrained width program does appear to avert part of the error retrned by BIMFIT. The returned parameters for the straight line fit show this also; slopes are closer to the single peak values, and intercepts much closer to zero. For systems with some non-reversibility, constraining the peak width can lead to significant increases in accuracy in the returned parameters.

3.4.4 Kinetically Controlled Lsv Systems

As seen in Section 2.5.2, s.v.c.f. fails in fitting the semiderivative of a metal-ligand lsv system whenever the system is kinetically controlled. It is to be expected, then, that s.v.c.f. will not be able to resolve overlapping semiderivative peaks, if the

Table 3.3 Averages and standard deviations of returned peak parameters and results of straight line fits of peak height to concentration for nearly classically reversible lsv data, constrained width [a,b,c]

	Cd			In			Pb					
Series	Potl.	Height	Width	Potl.	Height	Width	Potl.	Height	Width	Slope	Intercept	r^2
I	-.6902± 0.0005						-.4815± 0.0003	38.4± 0.5		4.52	-0.8	0.998
J	-.6930± 0.0009	39.2± 1.0		-.6528± 0.0009						6.16	2.2	0.999
K	-.6924± 0.0005			-.6532± 0.0006	37.4± 0.4					4.41	2.5	0.999
L	-.6894± 0.0004			-.6499± 0.0002	50.4± 0.9		-.4801± 0.0002	40.2± 0.4		4.30	4.0	0.999
A							-.4862± 0.0004		45.0± 0.9	5.09	0.4	0.999
B	-.6884± 0.0006		45.7± 2.0							4.36	-0.1	0.998
C				-.6517± 0.0004		36.4± 1.0				6.31	0.7	0.999

a) Slope, intercept and r^2 result from the least squares straight line fit of peak height to the concentration of added species in each series.
b) Units for slope and intercept are $\mu A/[V^{1/2} \times 1.0 \times 10^{-5} M]$ and $\mu A/V^{1/2}$, respectively.
c) Units for potential are V vs. the Ag/AgCl electrode, for height are $\mu A/V^{1/2}$, for width are mV.

kinetics of one of the systems are not completely classically reversible.

This is the case for standard addition series M. This series has the same background electrolyte as solutions F and G of Table 2.1. For a scan rate of 1.983 V/s the Cd component of solution F was found to be classically reversible, but the In component is kinetically controlled.

For s.v.c.f. to be judged effective in the resolution of the overlapped voltammograms of series M, returned peak parameters must match those found for the single peak solutions F and G. Also, standard deviations for returned potentials, widths and height of the non-added component must be small, and the intercept and regression coefficient from the peak height vs. concentration fit should be near 0.0 and 1.0, respectively.

Table 3.4 shows the averages and standard deviations of the returned peak potentials, widths, and height of the non-added component (Cd^{2+}) for series M. Also shown are the slope, intercept, and regression coefficient for the linear least squares fit of returned peak height to concentration of the added component (In^{3+}) for this series. At the bottom of the table are single peak parameters taken from Table 2.4.

S.v.c.f. is clearly not successful in resolving the two peaks. Peak potentials, heights, and widths are all very far from the single peak values. Standard deviations of these returned parameters are

Table 3.4 Averages and standard deviations of returned peak parameters and results of straight line fits of peak height to concentration for kinetically controlled systems [a,b,c]

	Cd			In				
Fitting Method	Potl.	Height	Width	Potl.	Width	Slope	Intercept	r^2
S.v.c.f.	-.6707± 0.0027	33.4± 4.8	53.8± 6.6	-.6338± 0.0012	30.8± 2.5	4.70	-3.4	0.941
Constrained Width S.v.c.f.	-.6798± 0.0027	22.2± 0.7		-.6456± 0.0013		5.09	0.4	0.999
Single Peak S.v.c.f.	-.6755	24.1	44.3	-.6431	54.5			

a) Slope, intercept and r^2 result from the least squares straight line fit of peak height to the concentration of added species in each series.
b) Units for slope and intercept are $\mu A/[V^{1/2} \times 1.0 \times 10^{-5} M]$ and $\mu A/V^{1/2}$, respectively.
c) Units for potential are V vs. the Ag/AgCl electrode, for height are $\mu A/V^{1/2}$, for width are mV.

extremely large. The regression coefficient for the fit of peak height to concentration is 0.941, a very small value, and the intercept is quite far from zero. S.v.c.f. cannot be used to separate overlapped kinetic peaks in lsv.

Much of the error in fitting the peaks could perhaps be avoided by the use of single peak parameters in fitting the semiderivatives. To this end, the constrained width curve fitting program CNWSBM was also used to fit the semiderivative data. Input peak widths to CNWSBM were the single peak widths, 44.3 mV for the Cd peak and 54.5 mV for the In peak. The results are also shown in Table 3.4, and are surprisingly good. Peak potentials are somewhat nearer to the single peak values, although the standard deviation does not improve. The average and standard deviation of the height for the Cd peak improve dramatically, as do the intercept and regression coefficient for the fit of peak height to concentration. It might be possible to do quantitative analysis of kinetically controlled systems using the constrained width s.v.c.f. procedure.

3.4.5 Effect of Residual Current

In Chapter 2 it was remarked that one of the problems in the application of s.v.c.f. to real lsv systems might be the effect of background, or residual, current. This is because it is usually very difficult to correct for the residual current in lsv, although (as mentioned) there are several approches to background correction in asv.

A study was made of the effects of background current on the application of s.v.c.f. to the nearly classically reversible data of Table 3.2. The voltammograms of series I, J, K and L were FT filtered, but not background subtracted, before the application of s.v.c.f. The results from s.v.c.f. to these data are shown in Table 3.5.

The results of Table 3.5 match the results of Table 3.2 closely. This indicates that the inclusion of the residual current, even at the low concentrations used in this work, does not affect the s.v.c.f. results greatly. The effect the residual current does have is shown in the results for series I, which is Pb^{2+} and Cd^{2+} in HCl, both already shown to be classically reversible. The average height of the Pb peak is increased slightly, but the major effect of the inclusion of residual current seems to be a broadening of the returned peak width. The slope and intercept of the straight line fit are hardly changed at all, which indicates that s.v.c.f. might be successful in doing quantitative analysis with linear sweep voltammograms that have not been background subtracted.

In fact, the inclusion of the background seems to improve results for the systems that contain In^{3+}. Probably the two errors, the slightly non-reversible kinetics and the background, are cancelling one another. This improvement is not to be looked for in the general case.

3.4.6 Multiple Peak Asv Systems

Table 3.5 Averages and standard deviations of returned peak parameters and results of straight line fits of peak height to concentration for nearly classically reversible lsv data without prior background subtraction [a,b,c]

	Cd			In			Pb					
Series	Potl.	Height	Width	Potl.	Height	Width	Potl.	Height	Width	Slope	Intercept	r^2
I	-.6896± 0.0008		56.2± 4.0				-.4807± 0.0003	40.6± 0.4	48.8± 0.8	4.51	-0.5	0.998
J	-.6914± 0.0013	39.6± 1.0	48.1± 0.9	-.6518± 0.0012		33.5± 1.4				5.97	2.0	0.999
K	-.6912± 0.0007		49.2± 1.0	-.6528± 0.0010	37.2± 0.9	34.7± 0.8				4.53	1.3	0.999
L	-.6887± 0.0011		47.9± 1.5	-.6493± 0.0004	50.7± 1.6	35.2± 0.6	-.4794± 0.0003	42.1± 0.5	49.5± 0.6	4.44	3.6	0.999

a) Slope, intercept and r^2 result from the least squares straight line fit of peak height to the concentration of added species in each series.
b) Units for slope and intercept are $\mu A/[V^{1/2} \times 1.0 \times 10^{-5} M]$ and $\mu A/V^{1/2}$, respectively.
c) Units for potential are V vs. the Ag/AgCl electrode, for height are $\mu A/V^{1/2}$, for width are mV.

The success of the s.v.c.f. technique in resolving the individual components of an anodic stripping voltammogram is to be judged in exactly the same way as it is for a linear sweep voltammogram. Table 3.6 shows the averages and standard deviations of returned peak potentials and widths, the average and standard deviation of the peak height of the component(s) not added, and the linear least squares fit parameters of the fit of concentration of added component to peak height for series N, O, and P. At the bottom of the table are results for the single peak series D and E studied in Chapter 2.

S.v.c.f. appears to be even more successful for the resolution of peaks in these a.s.v. systems than it was for the lsv systems. Although they are not shown for the individual voltammograms, returned coefficients of determination are close to one, and become larger and larger as the concentration of added component increases. Standard deviations of peak potentials are smaller than for the lsv systems, and average peak potentials for Tl and In are very near the single peak potentials. Except for the Tl component, standard deviations of peak widths are small. The large deviation in Tl peak widths is probably because the Tl peaks are much smaller than either the In or Cd peaks.

In contrast to the lsv results of Table 3.2, the asv peak widths for Cd in systems with In are very close to the theoretical 45.3 mV expected for this classically reversible system, and the peak widths for the In peak are close to those of the single peak width.

Table 3.6 Averages and standard deviations of returned peak parameters and results of straight line fits of peak height to concentration for a.s.v. data [a,b,c]

	Cd			In			Tl				
Series	Potl.	Height	Width	Potl.	Height	Width	Potl.	Width	Slope	Intercept	r^2
N	-.6934± 0.0001	17.19± 0.27	46.1± 0.2				-.5439± 0.0002	97.2± 2.1	1.12	0.34	0.999
O				-.6506± 0.0003	11.34± 0.49	28.6± 0.1	-.5415± 0.0016	87.2± 4.3	1.37	0.09	0.999
P	-.6937± 0.0006	9.28± 0.13	45.7± 0.4	-.6502± 0.0006	12.23± 0.23	29.0± 0.1	-.5428± 0.0010	90.3± 3.7	1.54	0.36	0.999
D							-.5440± 0.0002	93.4± 1.3	1.10	0.39	0.999
E				-.6488± 0.0002		29.0± 0.4			6.95	-3.17	0.999

a) Slope, intercept and r^2 result from the least squares straight line fit of peak height to the concentration of added species in each series.
b) Units for slope and intercept are $\mu A/[V^{1/2} \times 1.0 \times 10^{-7} M]$ and $\mu A/V^{1/2}$, respectively.
c) Units for potential are V vs. the Ag/AgCl electrode, for height are $\mu A/V^{1/2}$, for width are mV.

Intercepts for the straight line fits are all near zero. All of these results imply that s.v.c.f. works very well in the resolution of peaks in anodic stripping voltammetry.

References

1) K.J. Martin and I. Shain, Anal. Chem. 30, 1808 (1958)

2) A.M. Bond and B.S. Grabaric, Anal. Chem. 48, 1624 (1976)

3) R. Annino, Adv. Chromatogr. 15, 33 (1977)

4) D.W. Kirmse and A.W. Westerburg, Anal. Chem. 43, 1035 (1971)

5) B.S. Grabaric, R.J. O'Halloran and D.E. Smith, Anal. Chim. Acta 133, 349 (1981)

6) D.P. Binkley and R.E. Dessey, Anal. Chem. 52, 1335 (1980)

7) T.F. Brown and S.D. Brown, Anal. Chem. 53, 1410 (1981)

8) S.P. Perone and W.F. Gutknecht, Anal. Chem. 42, 906 (1970)

9) S.P. Perone and L.B. Sybrandt, Anal. Chem. 43, 382 (1971)

10) P.A. Boudreau and S.P. Perone, Anal. Chem. 51, 811 (1979)

11) F. Ammar and J.M. Saveant, J. Electroanal. Chem. 47, 215 (1973)

CHAPTER 4

A METHOD FOR THE NUMERICAL EVALUATION OF ELECTROCHEMICAL CONVOLUTION INTEGRALS USING TRANSFORM TECHNIQUES

4.1 INTRODUCTION

Convolution potential sweep voltammetry is based on the numerical evaluation of convolution integrals like those of (1.3.11) and (1.3.27). The methods used to evaluate these integrals are based on the knowledge of the exact form of the convolution integrals determined in the solutions to electrochemical boundary value problems. From the form of an integral a convoluting sequence is derived, and by a sequential convolution of the convoluting sequence with a sampled current sequence an approximation to the convolution integral is made.

The weakness of c.p.s.v. up to now is that the convolution integral can be obtained in a simple, analytic form only for a few very simple systems like the simple charge transfer, CE and EC mechanisms of Chapter 1. For systems with effects like non-infinite diffusion, or electrode adsorption isotherms, an analytic form of the convolution integral cannot be obtained, and c.p.s.v. as implemented previously cannot be applied to these systems.

For some systems, even if analytic forms of the convolution integral do not exist, analytic forms exist for the Laplace transformed concentration profile. Keller and Reinmuth (1) showed that for a system with finite diffusion, quasi-reversible electrode kinetics, and linear complications (first order kinetics, linear adsorption isotherms), the concentration profile in the Laplace domain is given by

$$\overline{C}_i(o,p) = \frac{C_i^*}{p} \pm \overline{i}(p)\overline{f}(p) \qquad (4.1.1)$$

where, for spherical diffusion,

$$\overline{f}(p) = -\frac{\text{hypf}\,(\ell\sqrt{p/D})}{nFA\,\sqrt{p/D}} \qquad (4.1.2)$$

The variable p is called the Laplace variable, l is the solution layer thickness for finite diffusion, and hypf is coth for a bounded system, and tanh for a non-bounded system. (A bounded system is a system with a solution layer of finite thickness.) Other symbols have the same meanings as in previous chapters. The function $\overline{f}(p)$ is commonly called a forcing function.

This paper proposes an alternate method for the numerical evaluation of the convolution integrals found in electrochemistry. This method does not depend on exact knowledge of the time domain convolution integral; instead, a convoluting sequence will be determined from knowledge of the Laplace domain forcing function $\overline{f}(p)$ of (4.1.1). The sequential convolution of this sequence with a sampled current sequence is equivalent to the methods used to evaluate the time domain convolution integral.

The method will be applied to the evaluation of the convolution integral encountered in the solution to the boundary value problem for classically reversible systems, i.e., the semiintegral. The

application of the method to more complex electrochemical systems will also be discussed.

4.2 BACKGROUND

This work involves the application of several mathematical techniques, including the Laplace transformation and the continuous and discrete Fourier transformations, that are not very well known to chemists. Another concept not well understood is that of convolution. For this reason, a short background of these ideas and techniques is presented in this section. For knowledge of all of these topics, the book by Bracewell (2) is very informative and presented in a manner that is easy to understand.

4.2.1 The Continuous Fourier Transform

Many references exist on the continuous Fourier transform. Besides the book by Bracewell, useful works have been written by Brigham (3) and Griffiths (4).

The continuous Fourier transform (CFT) $\overline{f}(s)$ of $f(t)$ is defined as

$$\overline{f}(s) = \int_{-\infty}^{\infty} f(t) \exp(-2\pi i s t)\, dt \qquad (4.2.1)$$

where s is a real number and is called the Fourier variable. The following definitions of the continuous Fourier transform are also often found:

$$\bar{f}(s) = \int_{-\infty}^{\infty} f(t) \exp(-ist)\, dt \qquad (4.2.2)$$

or

$$\bar{f}(s) = \frac{1}{(2\pi)^{1/2}} \int_{-\infty}^{\infty} f(t) \exp(-ist)\, dt \qquad (4.2.3)$$

The only difference among these is whether or not a factor of 2π or $(2\pi)^{1/2}$ is included in the definition of s. The definition (4.2.1) is assumed throughout this work.

The continuous Fourier transform exists if and only if the function f(t) fulfills the following criteria:

1) The integral of $|f(t)|$ from $t = -\infty$ to $+\infty$ exists.

2) Any discontinuities in f(t) are finite.

If f(t) is a physically observable quantity, then 1 and 2 must be true, and f(t) does have a continuous Fourier transform.

The back Fourier transform is defined as the operation on $\bar{f}(s)$ that returns the original function f(t). For the definition of $\bar{f}(s)$ given by (4.2.1), this is

$$f(t) = \int_{-\infty}^{\infty} \bar{f}(s) \exp(2\pi ist)\, dt \qquad (4.2.4)$$

There are a number of theorems relating to the continuous Fourier transform which derive directly from the definition (4.2.1). As some of these will be used later, it is best to review them now.

1) Similarity theorem: If $f(t)$ has the Fourier transform $\overline{f}(s)$, then $f(at)$ has the Fourier transform $|a|^{-1}\,\overline{f}(s/a)$.

2) Shift theorem: If $f(t)$ has the Fourier transform $\overline{f}(s)$, then $f(t-a)$ has the Fourier transform $\exp(-2\pi ias)\overline{f}(s)$.

3) Addition theorem: If $f(t)$ and $g(t)$ have the Fourier transforms $\overline{f}(s)$ and $\overline{g}(s)$, then the Fourier transform of $f+g$ is $\overline{f}+\overline{g}$.

The continuous Fourier transform has found much application in the analysis of electrical waveforms and filters, where a filter is to be understood in its electrical engineering sense as being some operation upon an input function that produces an output function. It has found many applications in image analysis. It is also, of course, familiar to students of elementary calculus as a tool in the solution of certain classes of differential equations.

There are some rather unusual functions that are often encountered in dealing with Fourier transforms. Several of these will be defined and discussed.

1) The rectangle function of unit height and width is defined as

$$\Pi(t) = \begin{cases} 1, & |t| < 1/2 \\ 1/2, & |t| = 1/2 \\ 0, & |t| > 1/2 \end{cases} \qquad (4.2.5)$$

Thus any finite segment of an infinite function can be represented as a product of the infinite function and a suitably multiplied and shifted rectangle function $\Pi(at-b)$.

2) The Heaviside function H(t), which is the unit step function, is defined by

$$H(t) = \begin{cases} 1, & t > 0 \\ 1/2, & t = 0 \\ 0, & t < 0 \end{cases} \qquad (4.2.6)$$

Any function with finite discontinuities can be decomposed into a continuous function plus a sum of shifted and multiplied Heaviside functions.

3) The filtering, or interpolating, function sinc (t) is defined by

$$\text{sinc } t = \frac{\sin \pi t}{\pi t} \qquad (4.2.7)$$

This function has the property sinc (0) = 1, sinc (1) = 0, and $\int_{-\infty}^{\infty}$ sinc (t) dt = 1.

The Fourier transform is not useful in the solution of those differential equations that describe mass transport in the

electrochemical systems of Chapter 1. To solve these problems, one must make use of a relative of the Fourier transform, the Laplace transform.

4.2.2 The Continuous Laplace Transform

The Laplace transformation is familiar to most electrochemists because of its power in the solution of electrochemical boundary value problems. Bracewell (2) has a chapter devoted to the Laplace transformation, and Bard and Faulkner (5) and Churchill (6) discuss the application of the Laplace transform to boundary value problems of the type encountered in electrochemistry.

The two-sided Laplace transform $\bar{f}(p)$ of $f(t)$ is defined by

$$\bar{f}(p) = \int_{-\infty}^{\infty} f(t) \exp(-pt)\, dt \qquad (4.2.8)$$

where p is the Laplace variable and is in general a complex number. From this definition, the Fourier transform is seen to be a special case of the Laplace transform, with p in (4.2.8) purely imaginary.

Usually one employs the Laplace transform with functions $f(t)$ such that $f(t) = 0$ for $t < 0$. This leads to the more commonly encountered definition of the Laplace transform, sometimes called the one-sided Laplace transform.

$$\overline{f}(p) = \int_{-\infty}^{\infty} f(t)\, \exp(-pt)\, dt \qquad (4.2.9)$$

The back Laplace transformation of a function $\overline{f}(p)$ is

$$f(t) = \frac{1}{2\pi i} \int_{c-i\infty}^{c+i\infty} \overline{f}(p)\, \exp(pt)\, dp \qquad (4.2.10)$$

where c is some real constant.

It is the real part of p that makes the Laplace transform necessary for the solution of electrochemical boundary value problems. Consider the solution to the simple charge transfer reaction, given in Appendix II. One of the first step in the solution involves the integration by parts of the integral

$$\int_0^{\infty} \frac{\partial C_{ox}}{\partial t} \exp(-pt)\, dt = C_{ox}(x,t)\, \exp(-pt)\Big|_{t=0}^{t=\infty} + p \int_0^{\infty} C_{ox} \exp(-pt)\, dt \qquad (4.2.11)$$

Up to this point in the solution the Fourier transform could have been used. At this point the argument is made that $C_{ox}(x,t)\exp(-pt)$ at $t = \infty$ is equal to zero. This is true only if the real part of $p > 0$; if the Fourier transform is used, so that $\exp(-pt) = \exp(-ist)$, then the exponential term does not go to zero, and is in fact undefined. The Laplace transform must be used for the elimination of this term. In

general, the purpose of the real part of p is to force the convergence of (4.2.9) at large t for a given time domain function f(t).

The similarity of the Laplace transform to the Fourier transform results in an identity of theorems for both transformations. All of the similarity, shift, and addition theorems apply to the Laplace transformation as well as to the Fourier.

There is one very important theorem that remains to be discussed, and also applies equally to both Fourier and Laplace transformations. This is the convolution theorem. The importance of this theorem will become more obvious after a discussion of convolution.

4.2.3 Convolution

The concept of convolution is central to many concepts in the analysis of real signals. Bracewell (2) gives a very thorough discussion of convolution in his work. The idea of convolution describes variously the familiar data manipulation techniques of smoothing, peak sharpening, auto- and cross-correlations and many others. The convolution of two functons f(t) and g(t), denoted by the asterisk notation f(t)*g(t), is defined as

$$h(t) = f(t)*g(t) = \int_{-\infty}^{\infty} f(u)g(t-u)\,du \qquad (4.2.12)$$

Convolution is commutative, associative and distributive; that is,

$$\begin{aligned} f*g &= g*f \\ (f*g)*h &= f*(g*h) \\ f*(g+h) &= f*g + f*h \end{aligned} \qquad (4.2.13)$$

One way to perceive convolution is the following. The function h(t) is an integral, and as such can be understood as the area under the curve f(u)g(t-u). For example: consider the convolution of two functions f(t) = Π(t), g(t) = Π(t). The convolution of these two functions is easy to determine, since both are non-zero only for $|t| \leq 1/2$. The convolution h(t) of these two functions is depicted graphically in Figure 4.1.

In this convolution the function f(u), by (4.2.12), remains centered at the origin of the u axis. The convolution h(t) is performed by reversing the g(u) function, and moving the g(t-u) function along the u axis for each value of t. At each value of t, the product f(u)g(t-u) is determined and gives h(t). In Figure 4.1, the value of f(u)g(t-u) for a given t is the area of the intersection of the two Π functions, which is indicated by cross-hatching. This area is h(t) for the given t. The convolution function h(t) is shown for all t at the bottom of Figure 4.1. The convolution function is a triangle, which is well known to be the convolution of a rectangle function with itself.

Convolution is sometimes easier to understand if one considers the convolution of two sequences of numbers. Bracewell (2) discusses

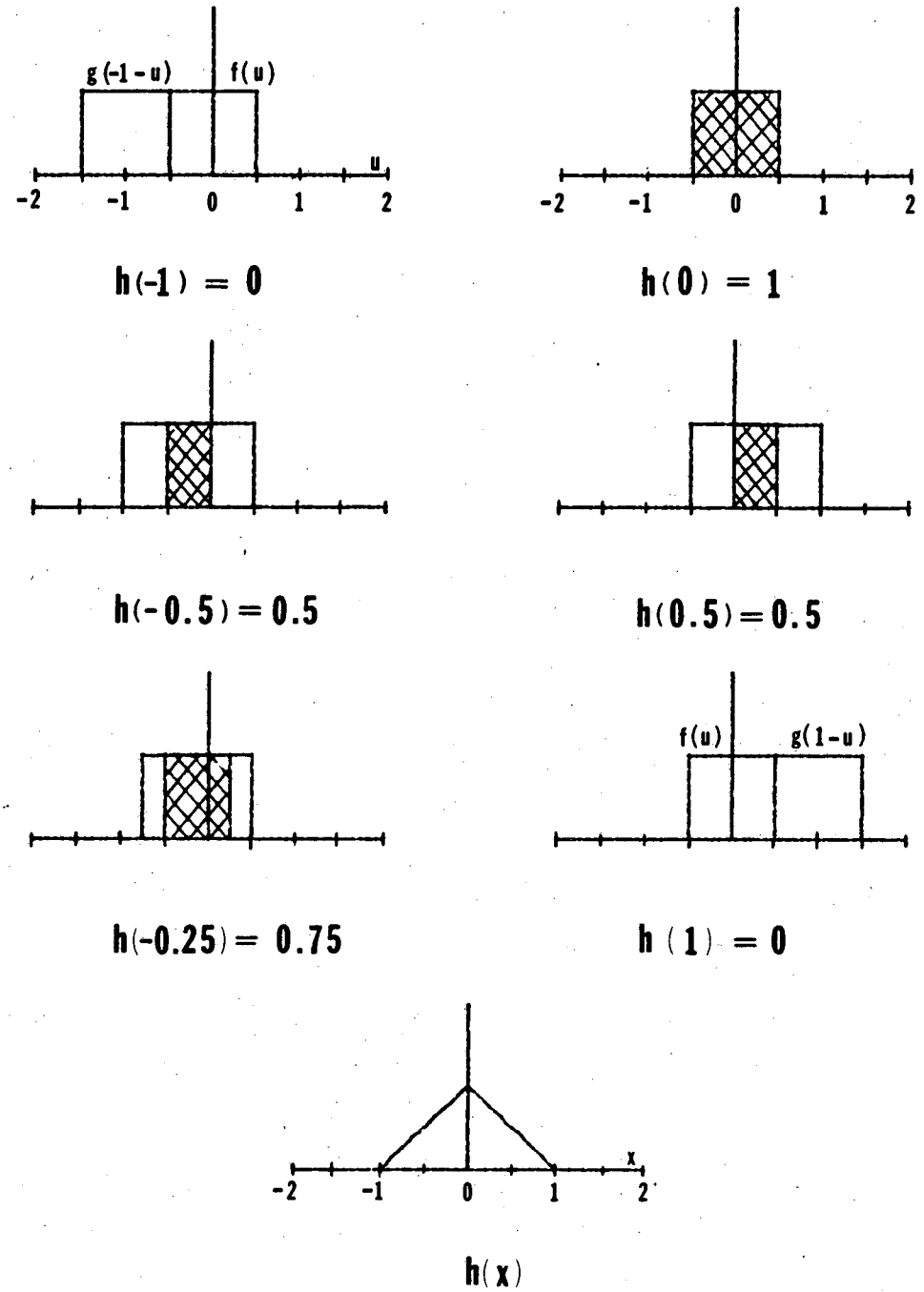

Figure 4.1: Convolution h(x) of two rectangle functions. Cross hatches indicate overlap of f(u) and g(x-u) for different x, and consequently h(x).

at length sequential convolution, which he calls the serial product of two sequences. The sequence f^N is defined as an ordered set of values ($f^N(0)$ $f^N(1)$ $\cdots$ $f^N(N-1)$), and the sequence g^N as ($g^N(0)$ $g^N(1)$ $\cdots$ $g^N(N-1)$). This notation for a sequence of numbers, and for the elements of a sequence, will be used throughout this work.

Figure 4.2 shows the convolution of two sequences f^4 and g^4. The first step in the sequential convolution $f^4 * g^4$ is the reversal of g^4, and the positioning of the erstwhile first element (now last) of g^4 under the first element of f^4. The sequence g^4 is called the convoluting sequence. The two elements $f^4(0)$ and $g^4(0)$ are multiplied, and the product $h^7(0)$ is the first element of the resultant convolution sequence. The reversed g^4 sequence is moved over one space, and the first two elements of f^4 are multiplied by the last two elements of the reversed g^4 sequence and summed to get the second element $h^7(1)$ of the convolution sequence. The process is repeated as shown in Figure 4.2 until the last element in f^4 is multiplied by the first element of the reversed g^4 convoluting sequence. The result is a seven element convolution sequence h^7. In general, the convolution of two N element sequences results in a 2N-1 element convolution sequence.

Convolution in nature takes many forms. For scientists, perhaps the most important instance of convolution is in the description of mechanisms that cause the broadening of spectral peaks or lines. One type of broadening familiar to all analytical chemists is the broadening of a peak in an atomic or molecular spectrum due to the

$f^4 = (3 \quad 1 \quad 2 \quad 0)$

$g^4 (1 \quad 1 \quad 0 \quad 1)$

$$\begin{array}{llll} & 3 & 1 & 2 & 0 \\ \underline{1} & \underline{0} & \underline{1} & \underline{1} & \end{array}$$

$h^7(0) = (3)(1) = 3$

$$\begin{array}{llll} 3 & 1 & 2 & 0 \\ \underline{1} & \underline{0} & \underline{1} & \underline{1} \end{array}$$

$h^7(3) = (0)(1) + (2)(1) + (1)(0) + (3)(1) = 5$

$$\begin{array}{llll} & 3 & 1 & 2 & 0 \\ & \underline{1} & \underline{0} & \underline{1} & \underline{1} \end{array}$$

$h^7(1) = (1)(1) + (3)(1) = 3$

$$\begin{array}{llll} 3 & 1 & 2 & 0 \\ & \underline{1} & \underline{0} & \underline{1} & \underline{1} \end{array}$$

$h^7(4) = (0)(1) + (2)(0) + (1)(1) = 1$

$$\begin{array}{llll} & 3 & 1 & 2 & 0 \\ \underline{1} & \underline{0} & \underline{1} & \underline{1} & \end{array}$$

$h^7(2) = (2)(1) + (1)(1) + (3)(0) = 3$

$$\begin{array}{llll} 3 & 1 & 2 & 0 \\ & & \underline{1} & \underline{0} & \underline{1} & \underline{1} \end{array}$$

$h^7(5) = (0)(0) + (2)(1) = 2$

$$\begin{array}{llll} 3 & 1 & 2 & 0 \\ & & \underline{1} & \underline{0} & \underline{1} & \underline{1} \end{array}$$

$h^7(6) = (0)(1) = 0$

$h^7 = (3 \quad 3 \quad 3 \quad 5 \quad 1 \quad 2 \quad 0)$

Figure 4.2: Sequential convolution of two sequences. The convolution begins at upper left, proceeds down the left hand column, continues at upper right, and proceeds down the right hand column.

finite resolving power of a monochromator (7,8). The observed spectrum $S(\lambda)$ is not the true spectrum $T(\lambda)$ but is rather a convolution of the true spectrum with the broadening function $B(\lambda)$ of the monochromator:

$$S(\lambda) = \int_{-\infty}^{\infty} T(\lambda')B(\lambda-\lambda')\, d\lambda' \qquad (4.2.14)$$

The function $B(\lambda)$ is commonly called the slit function. Many methods exist for the retrieval of $T(\lambda)$ from $S(\lambda)$ (9-11); this results in a sharpening of the peaks in a spectrum, and hence enhances resolution.

Other instances of convolution include, for example, the averaging process which an analog to digital converter performs to obtain a digital data point, or the effect of mixing chambers in chromatography. In almost any conceivable experiment an observed signal is the result of the convolution of the true signal with some instrument function. This makes an understanding of convolution important for nearly all scientists.

Convolution enters into the study of electrochemistry very directly. Consider again the solution of the boundary value problem for the reversible charge transfer system, which is given in Appendix II. One of the final steps in the solution is the transformation of the concentration profile $\overline{C}_i(0,p)$, which is in terms of the transform variable p, to a solution in terms of the time variable t. In Appendix II this occurs between (A.II.12) and (A.II.14). This transformation is made by means of the convolution theorem, which is

the last, and perhaps most important, of the transform theorems.

The convolution theorem, which holds for both Laplace and Fourier transforms, says that if f(t) has the transform $\bar{f}(p)$ (or $\bar{f}(s)$), and g(t) has the transform $\bar{g}(p)$ (or $\bar{g}(s)$), then the transform of the product f(t)g(t) is the convolution $\bar{f}(p)*\bar{g}(p)$ (or $\bar{f}(s)*\bar{g}(s)$). In mathematical terms, for the Laplace transformation,

$$\int_{-\infty}^{\infty} f(t)g(t)\exp(-pt)\,dt = \int_{-\infty}^{\infty} \bar{f}(p')\bar{g}(p-p')\,dp' \qquad (4.2.15)$$

There is an equivalent theorem for the product of two transforms,

$$\frac{1}{2\pi i}\int_{c-i\infty}^{c+i\infty} \bar{f}(p)\bar{g}(p)\exp(pt)\,dp = \int_{0}^{t} f(\tau)g(t-\tau)\,d\tau \qquad (4.2.16)$$

Similar equations obtain for the Fourier transform (2). In equation A.II.14, the inverse transform of $\bar{i}(p)$ is i(t), while it is known that the inverse transform of $p^{-1/2}$ is $(t/\pi)^{-1/2}$. The concentration profile equations A.II.14 follow immediately from (4.2.16).

4.2.4 Discrete Fourier Transform

Because experimental data is always obtained as a finite set of points, one cannot analyze data with either the continuous Fourier transform or the continuous Laplace transform. To allow the transform analysis of discrete data, several discrete transforms have been developed. One of these is the discrete Fourier transform (DFT).

A great deal of work has been done with the aid of the DFT in the last fifteen years. Undoubtedly this is due to Cooley and Tukey (12), who developed an algorithm for the rapid computation of the discrete Fourier transform, the so-called Fast Fourier transform. A number of references exist on the discrete Fourier transform (2-4, 13-16). Only in the last few years have chemists appreciated the great differences between the discrete and continuous Fourier transforms, probably because it is only in the last few years that electrical engineers have written explanations of the DFT that chemists have understood.

By definition, the forward discrete Fourier transform of a sequence of points $f^N = (f^N(0)\ f^N(1) \cdots f^N(N-1))$ is

$$\bar{f}^N(\nu/N) = N^{-1} \sum_{\tau=0}^{N-1} f^N(\tau) \exp(-2\pi i \nu\tau/N) \qquad (4.2.17)$$

where ν also ranges from 0 to N-1, so that $\bar{f}^N(\nu/N)$ is part of the sequence $\bar{f}^N = (\bar{f}^N(0)\ \bar{f}^N(1/N) \cdots \bar{f}^N((N-1)/N)$. The backward discrete Fourier transformation is

$$f^N(\tau) = \sum_{\nu=0}^{N-1} \bar{f}^N(\nu/N) \exp(2\pi i \nu\tau/N) \qquad (4.2.18)$$

The DFT can be derived from the CFT. It is instructive to present the derivation, since it shows the correspondence between discrete and continuous transforms. The derivation, which follows, is

taken from Cooley, et al. (14).

Suppose that the function f(t) has the CFT $\overline{f}(s)$. Next, suppose that f(t) is sampled at intervals of length Δt. To represent this, let $t = \tau\Delta t$, $\tau = 0, 1, 2, \ldots$ Substituting $t = \tau\Delta t$ into (4.2.4),

$$f(\tau\Delta t) = \int_{-\infty}^{\infty} \overline{f}(s) \exp(2\pi i s\tau\Delta t)\, ds \qquad (4.2.19)$$

One may represent (4.2.19) as

$$f(\tau\Delta t) = \sum_{k=-\infty}^{\infty} \int_{k/\Delta t}^{(k+1)/\Delta t} \overline{f}(s) \exp(2\pi i s\tau\Delta t)\, ds \qquad (4.2.20)$$

Because τ is an integer, $\exp(2\pi i s\tau\Delta t)$ is a periodic function of s with period $1/\Delta t$. Since the function $\exp(2\pi i s\tau\Delta t)$ is periodic over the intervals of integration, one may write the sum of (4.2.20) as

$$f(\tau\Delta t) = \int_{0}^{k/\Delta t} \left(\ldots+\overline{f}(s)+\overline{f}(s+1/\Delta t) + \overline{f}(s+2/\Delta t)+\ldots\right) \exp(2\pi i s\tau\Delta t)\, ds \qquad (4.2.21)$$

Letting

$$\overline{f}_p(s) = \sum_{k=-\infty}^{\infty} \overline{f}(s+k/\Delta t) \qquad (4.2.22)$$

one obtains

$$f(\tau\Delta t) = \int_0^{1/\Delta t} \bar{f}_p(s)\, \exp(2\pi i s\tau\Delta t)\, dt \qquad (4.2.23)$$

where $\bar{f}_p(s)$ is the periodic function formed by the superposition of the non-periodic function $\bar{f}(s)$, shifted by all multiples of a fundamental period $1/\Delta t$.

The Fourier series expansion of any periodic function $g(t)$ with period T is

$$g(t) = \frac{1}{T} \sum_{j=-\infty}^{\infty} a_i\, \exp(-2\pi i j t/T) \qquad (4.2.24)$$

where

$$a_i = \int_0^T g(t)\, \exp(2\pi i j t/T)\, dt \qquad (4.2.25)$$

so that, for the periodic function $\bar{f}_p(s)$ with period $1/\Delta t$, one can represent $\bar{f}_p(s)$ as

$$\bar{f}_p(s) = \Delta t \sum_{\tau=-\infty}^{\infty} f(\tau\Delta t)\, \exp(-2\pi i s\tau\Delta t) \qquad (4.2.26)$$

Consider the values of $\bar{f}_p(s)$ at N equally spaced points between 0 and $1/\Delta t$. Making a substitution $s = \nu/(N\Delta t) = \nu\Delta s$,

$$\overline{f}_p(\nu\Delta s) = \Delta t \sum_{\tau=-\infty}^{\infty} f(\tau\Delta t)\, \exp(-2\pi i\nu j/N) \qquad (4.2.27)$$

Since $\exp(-2\pi i\nu\tau/N)$ is a periodic function of τ with period N, one may make the argument as was done with $\overline{f}_p(s)$, and say

$$\overline{f}_p(\nu\Delta s) = \Delta t \sum_{\tau=-\infty}^{N-1} f_p(\tau\Delta t)\, \exp(-2\pi i\nu\tau/N) \qquad (4.2.28)$$

where

$$f_p(\tau\Delta t) = \sum_{\ell=-\infty}^{\infty} f(\tau\Delta t+\ell N\Delta t) \qquad (4.2.29)$$

The function $f_p(\tau\Delta t)$ is a periodic function with period $N\Delta t$. For this reason, one may apply the same arguments just used to obtain (4.2.28) to obtain

$$f_p(\tau\Delta t) = \frac{1}{N\Delta t} \sum_{\nu=0}^{N-1} \overline{f}_p(\nu\Delta s)\, \exp(2\pi i\nu\tau/N) \qquad (4.2.30)$$

If Δt is taken as one, the relations (4.2.28) and (4.2.30) reduce to (4.2.17) and (4.2.18).

The periodic nature of the functions $\overline{f}_p(\nu\Delta s)$ and $f_p(\tau\Delta t)$ lead to

a great difference in the application of the CFT and DFT. Suppose that $\Delta t = 1$. The periodic nature of $f_p(\tau)$ means that $f_p(\tau) = f_p(\tau + N)$. This means, for example, that for an N-point sequence that $f_p(\tau = -1) = f_p(\tau = N-1)$; i.e., the last point in the transform is actually right next to the first point. This is equally true for a frequency domain sequence.

The periodic nature of both time and frequency domain sequences explains many effects found in the practical application of the DFT. For example, consider a paper about the use of the Fast Fourier Transform (FFT) in the filtering of high frequency noise from electrochemical data (17). High frequency noise is eliminated from the data by taking the FFT of the data, setting all the high frequency terms after a certain frequency equal to zero, (e.g., setting $\overline{f}_p(\nu/N) = 0$ for $|\nu| > 20$, and $N = 512$) and taking the back transform. Because the high frequency components are mostly noise, this process should return electrochemical data with significantly less noise than the original data, as indeed it does.

Reference 17 states, however, that if the data does not begin and end at the baseline, that this process produces large, sinusoidal waves in the back transformed filtered data. The effect is removed by subtracting a straight line from the data prior to the initial transformation, so that the subtracted data file does begin and end at the baseline, and adding the straight line back in at the end of the process. The large, sinusoidal waves originally superimposed upon the data are ascribed to some kind of aliasing effect.

The cause of this aliasing effect is obvious if the DFT is understood in the cyclic sense. If the first and last points of the data file are not nearly equal, there is a large discontinuity between $f_p(\tau = -1)$, which is also $f_p(\tau = N-1)$, and $f_p(\tau = 0)$. This discontinuity is described, in the frequency domain, (i.e., in the function $\overline{f}_p(\nu/N)$), by high frequency terms, so that if all high frequency terms are set to zero, many of the terms that describe the discontinuity vanish. The result is the degradation of the data at the endpoints.

The background presented in this section is sufficient for an understanding of the rest of this work. A method will be derived for the numerical evaluation of time domain convolution integrals from knowledge of the forcing function $\overline{f}(p)$ in Laplace space. To do this, it is necessary to examine how the numerical convolution has been done in the past.

4.3 NUMERICAL EVALUATION OF CONVOLUTION INTEGRALS

Up to now c.p.s.v. has relied on the numerical integration of the convolution integral

$$m(t) = \frac{1}{\sqrt{\pi}} \int_0^t \frac{i(\tau)d\tau}{\sqrt{t-\tau}} \qquad (4.3.1)$$

by means of a sequential convolution like that described in Section 4.2.3. This section will describe the derivation of the convoluting sequence used most commonly in the past to evaluate (4.3.1). A

derivation of a different convoluting sequence for the evaluation of (4.3.1) will be proposed. This latter sequence will be shown to give identical results in the approximation of the semiintegral for a classically reversible charge transfer system. This section will also develop a method for the evaluation of more general convolution integrals.

4.3.1 Derivation of Convoluting Sequences for the Semiintegral

The semiintegral of (4.3.1) has the form of the Riemann-Liouville definition of an integral of fractional order -1/2 (18-20). This definition can be shown (21) to be equivalent to the Grunwald definition of a semiintegral (22), so that one has

$$\frac{1}{\sqrt{\pi}} \int_0^t \frac{i(\tau)d\tau}{\sqrt{t-\tau}} = \frac{1}{\sqrt{\pi}} \lim_{N\to\infty} \left\{ \delta^{1/2} \sum_{j=0}^{N-1} \frac{\Gamma(j+1/2)}{\Gamma(j+1)} i(t-\delta j) \right\} \qquad (4.3.2)$$

where Γ is the Euler gamma function, $i(t-\delta j)$ is the $(N-j)^{th}$ current point, and N is the number of subdivisions of equal width $\delta = t/N$ into which the interval from $\tau = 0$ to $\tau = t$ is divided. The integral is approximated (for N large enough) simply by dropping the limit in (4.3.2), so that

$$\frac{1}{\sqrt{\pi}} \int_0^t \frac{i(\tau)d\tau}{\sqrt{t-\tau}} \approx \left\{ \frac{\delta^{1/2}}{\sqrt{\pi}} \sum_{j=0}^{N-1} \frac{\Gamma(j+1/2)}{\Gamma(j+1)} i(t-\delta j) \right\} \qquad (4.3.3)$$

This is known to be a good approximation to the actual semiintegral.

(See the previous chapters of this work, and the references contained therein.)

There are many possible approaches to the evaluation of m(t), however. Equation 4.3.3 is inconvenient because it employs Γ functions, which are impossible to represent as simple analytic functions. Another approach can be made by using the more general definition of an integral. Because convolution is commutative, (4.3.1) can be written as

$$m(t) = \frac{1}{\sqrt{\pi}} \int_0^t \frac{i(t-\tau)d\tau}{\sqrt{\tau}} \tag{4.3.4}$$

Using the definition of an integral as the limit of a sum, if the interval from $\tau = 0$ to $\tau = t$ is divided into N subintervals of equal length δ, one has

$$\frac{1}{\sqrt{\pi}} \int_0^t \frac{i(t-\tau)d\tau}{\sqrt{\tau}} = \lim_{N\to\infty} \left\{ \delta \sum_{j=0}^{N-1} \frac{1}{\sqrt{\tau_j}}\, i(t-\tau_j) \right\} \tag{4.3.5}$$

where τ_j is some point such that $\delta j \leq \tau_j \leq \delta(j+1)$. The approximation is achieved by dropping the limit, so that

$$\frac{1}{\sqrt{\pi}} \int_0^t \frac{i(t-\tau)d\tau}{\sqrt{\tau}} \approx \delta \sum_{j=0}^{N-1} \frac{1}{\sqrt{\tau_j}}\, i(t-\tau_j) \tag{4.3.6}$$

It was found by us that for large j

$$\frac{\Gamma(j+1/2)}{\Gamma(j+1)} \approx \frac{1}{\sqrt{1/\pi+j}} \tag{4.3.7}$$

Therefore if one chooses (as is possible, for large enough N),

$$\frac{1}{\sqrt{\tau_j}} = \frac{1}{\delta^{1/2}\sqrt{1/\pi+j}} \qquad i(t-\tau_j)=i(t-\delta j) \tag{4.3.8}$$

The final approximation to m(t) is

$$m(t) \approx \frac{\delta^{1/2}}{\sqrt{\pi}} \sum_{j=0}^{N-1} \frac{1}{\sqrt{1/\pi+j}}\ i(t-\delta j) \tag{4.3.9}$$

This is the approximation used by Suprenant et al. (23), which was given by them without any justification.

Both (4.3.3) and (4.3.9) are examples of time domain sequential convolution as described in Section 4.2.3. In the implementation of (4.3.3), a convoluting sequence $C^N = (C^N(0)\ C^N(1) \cdots C^N(N-1))$ is created by setting $C(0) = \delta^{1/2}$, and deriving a recursion relation using the properties of the gamma function, so that for $j > 1$,

$$C^N(j+1) = \frac{(j-1/2)}{j} C^N(j) \tag{4.3.10}$$

The convoluting sequence C^N is then sequentially convolved with an N point current sequence to obtain the semiintegral.

The implementation of (4.3.9) is simpler: a convoluting sequence C^N is constructed from

$$C^N(j) = \frac{\delta^{1/2}}{\sqrt{\pi}} (1/\pi + j)^{-1/2} \qquad (4.3.11)$$

for j = 0 to j = N-1, and subsequently is sequentially convolved with the current.

Figure 4.3 shows two semiintegrals of an artificial lsv wave of a classically reversible system. The semiintegrals were made by a FORTRAN program called SEMI, which sequentially convolved the sequences defined by (4.3.10) and (4.3.11) with the artificial linear sweep voltammogram. The voltammogram was created by means of the digital simulation program DIGIT, which is described in Section 1.5.1. The computer system used to run these programs, and all other programs discussed in this work, is the LSI-11/23 system described in Section 2.4.3.

The semiintegrals created by the two different approximations are seen to be superimposed. This implies that (4.3.9) is as good an approximation to the semiintegral as is the approximation of (4.3.3).

4.3.2 Derivation of Convoluting Sequences for General Convolution Integrals

One would like to derive approximations to the convolution integrals of more complex systems. Suppose a system is of the type such that the Laplace domain concentration profile (4.1.1) may be obtained. Suppose also that the inverse transform of $\overline{f}(p)$ is f(t);

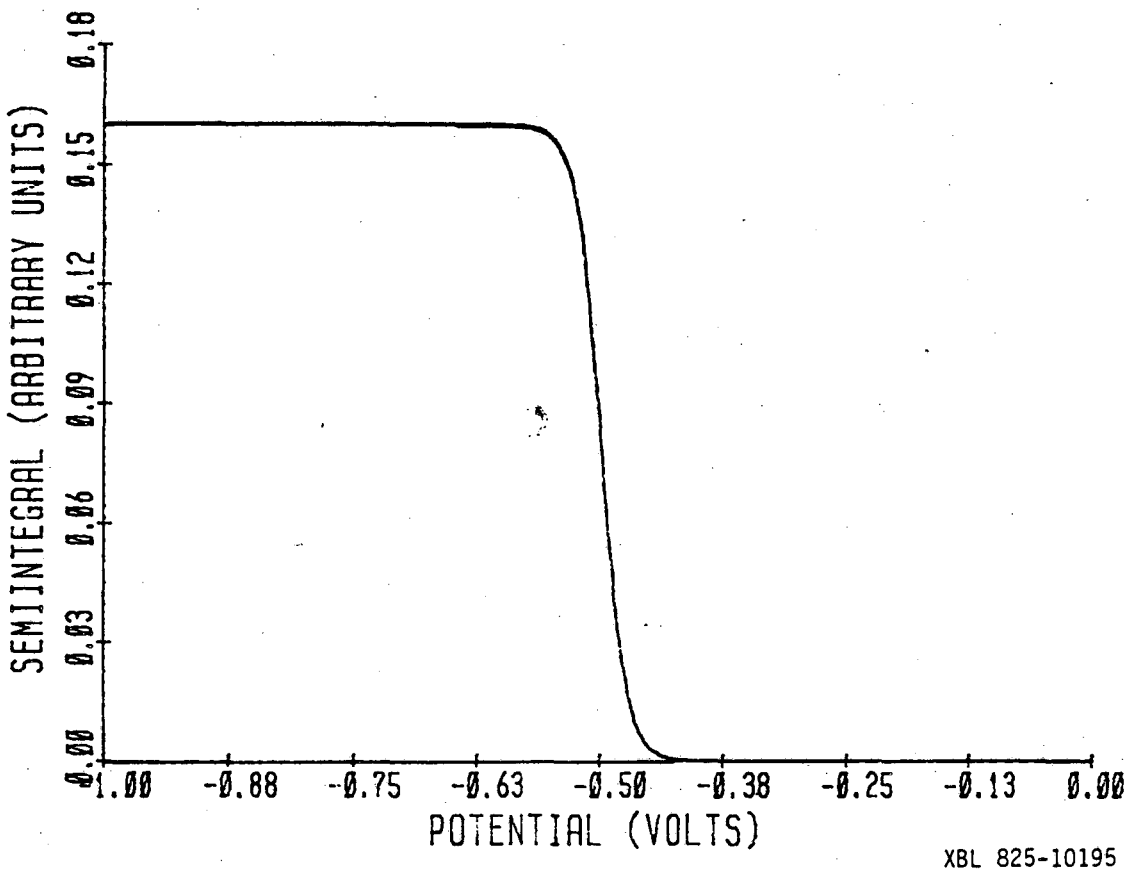

Figure 4.3: Semiintegrals of a voltammogram of a classically reversible system created by the sequential convolutions of (4.3.3) and (4.3.9).

$f(t)$ certainly exists, although it is probably not a simple function, and possibly is not even describable by an analytic function. If the inverse transform of $\bar{f}(p)$ is $f(t)$, then (4.2.15) implies that

$$C_i(0,t) = C_i^* \pm \int_0^t f(t-\tau)i(\tau)\, d\tau \qquad (4.3.12)$$

and it is seen that integrals of the form

$$h(t) = \int_0^t f(t-\tau)i(\tau)\, d\tau \qquad (4.3.13)$$

must be approximated.

For N large enough, one may make the same approximation used in deriving (4.3.9), and derive

$$\int_0^t f(t-\tau)i(\tau)d\tau \approx \delta \sum_{j=0}^{N-1} f(\tau_j)i(t-\tau_j) \qquad (4.3.14)$$

The approximation is again a convolution of the current sequence i^N by a convolution sequence C^N, where the individual element $C^N(j)$ in this sequence is given by

$$C(j) = f(\delta(a+j)) \qquad (4.3.15)$$

and where a is some constant $0 \leq a \leq 1$ to be determined. For N very large, the choice of a does not matter.

The next section will describe how the convolution sequence C^N, defined by (4.3.15), may be derived from the Laplace equation 4.1.1.

4.4 DERIVATION OF CONVOLUTING SEQUENCES FROM LAPLACE EQUATIONS

One would like to be able to derive a sequence C^N like that defined by (4.3.15) from the Laplace equation (4.1.1). This must involve three steps. One must first derive from the continuous Laplace domain function (4.1.2) a continuous Fourier domain function that represents the sampled convolution function (4.3.15). Using this Fourier domain function, one must next construct a sequence in the discrete Fourier domain corresponding to the DFT of the time domain convolution sequence $\overline{C}^N$. Finally, one must take the back DFT to obtain the sequence C^N. One must go from the continuous Laplace domain, to the continuous Fourier domain, to the discrete Fourier domain, and lastly to the time domain.

4.4.1 Derivation of the Correct Laplace Function

The forcing function $\overline{f}(p)$ in (4.1.1) does not represent the Laplace transformation of the function f of (4.3.15) that is sampled at times $t = \delta(a+j)$, $j = 0, 1, \ldots, N-1$ in the derivation of a convoluting sequence. This is because $\overline{f}(p)$ represents in the time domain a function f(t) that extends from $t = 0$ to $t = \infty$. Because of the periodic nature of the function $f_p(\tau)$ of (4.2.29), the function f(t) must be truncated.

Consider this in a slightly different way. We hope to derive from the Laplace transform equation (4.1.1) convolution seqences C^N that are given by (4.3.15). The very last step in this derivation will be to take the DFT of some sequence $\overline{C}^N$ to obtain C^N. What must the continuous function C(t) corresponding to C^N be in order to achieve this? As was seen in Section 4.2.4, C^N is related to C(t) by

$$C^N(\tau) = \sum_{k=-\infty}^{\infty} C(\tau + kN\delta) \qquad (4.4.1)$$

If C^N is to represent, for example, the sampling of the function C(j) = f(δ(a+j)) of (4.3.15) from j = 0 to j = N-1, the function f(δ(a+j)) must be equal to zero for j < 0, j > N-1. Otherwise (4.4.1) implies that C^N will be in error due to the superpositioning of terms for j < 0 and j > N-1.

The function f(δ(a+j)) must be truncated at j = 0 and j = N-1. This truncation can be represented by the rectangle function Π(t), so that

$$C(t) = \Pi\left(\frac{t - \delta/2(N-1)}{\delta(N-1)}\right) f(a\delta+t) \qquad (4.4.2)$$

The Laplace transform function that describes the truncated function is not $\overline{f}(p)$, but is rather

$$\overline{C}(p) = \int_0^\infty \Pi\left(\frac{t - \delta/2(N-1)}{\delta(N-1)}\right) f(a\delta+t)\exp(-pt)dt \qquad (4.4.3)$$

By the Laplace transform shift theorem this is

$$\overline{C}(p) = \exp(a\delta p) \int_0^\infty \Pi\left(\frac{t}{\delta(N-1)} - \frac{(2a+N-1)}{2(N-1)}\right) f(t)\exp(-pt)dt \qquad (4.4.4)$$

Equation 4.2.15 says that the transform of a product is the convolution of the transforms. The Laplace transform of f(t) is $\overline{f}(p)$ of (4.1.2). The Laplace transform of the rectangle function is sinh(p/2)/(p/2), and by the shift and similarity theorems the Laplace transform of the rectangle function of (4.4.4) is

$$\int_0^\infty \Pi\left(\frac{t}{\delta(N-1} - \frac{(2a+N-1)}{2(N-1)}\right) \exp(-pt)dt =$$

$$\exp\left(-\frac{(2a+N-1)p\delta}{2}\right) \frac{\sinh(p\delta(N-1)/2)}{(p\delta(N-1)/2)}\, \delta(N-1) \qquad (4.4.5)$$

Then the Laplace transform convolution theorem (4.2.15) says

$$\overline{C}(p) = \frac{\exp(p\delta a)}{2\pi i} \int_{c-i\infty}^{c+i\infty} \delta(N-1)\exp\left(-\frac{(2a+N-1)\delta p'}{2}\right) \frac{\sinh(\delta(N-1)p'/2)}{(\delta(N-1)p'/2)}$$

$$\overline{f}(p-p')dp' \qquad (4.4.6)$$

4.4.2 Derivation of the Convoluting Sequence C^N From $\overline{C}(p)$

One would like to derive from (4.4.6) a relation for $\overline{C}(s)$, the Fourier transform of the truncated convolution function $C(t)$. If this can be done, then (4.2.22) can be used to obtain the discrete Fourier transform pair of the convolution sequence C^N.

The relation between Laplace and Fourier transformations is as follows. Consider a function $f(t)$, that has both Laplace and Fourier transformations $\overline{f}(s)$ and $\overline{f}(p)$. Taking the back transforms of both $\overline{f}(s)$ and $\overline{f}(p)$,

$$\int_{-\infty}^{\infty} \overline{f}(s)\exp(2\pi ist)ds = f(t) = \frac{1}{2\pi i}\int_{c-i\infty}^{c+i\infty} \overline{f}(p)\exp(pt)dt \qquad (4.4.7)$$

Then, substituting $p = c + 2\pi is'$, c real, in the integral of the r.h.s.,

$$\int_{-\infty}^{\infty} [\overline{f}(s)]\exp(2\pi ist)ds = \int_{-\infty}^{\infty} [\overline{f}(c+2\pi is')\exp(ct)]\exp(2\pi is't)ds' \qquad (4.4.8)$$

This implies that Laplace and Fourier transform functions are related by

$$\overline{f}(s) = \overline{f}(c+2\pi is')\exp(ct) \qquad (4.4.9)$$

The choice of c remains to be determined. The purpose of c in the Laplace transformation is to force the Laplace integral of (4.2.9)

to convergence as $t\to\infty$; in other words, c must be chosen large and positive enough to force $f(t)\exp(-pt)$ to go to zero as $t\to\infty$. In general, then, c cannot be chosen to be zero.

In this particular instance, however, the function f(t) is a truncated function and is itself equal to zero for t greater than some finite value. In this case the Laplace integral is convergent for any c, since f(t) itself is zero as $t\to\infty$. Therefore c can be chosen to be zero, and (4.4.9) reduces to

$$\overline{f}(s) = \overline{f}(2\pi i s') \tag{4.4.10}$$

The Fourier transform $\overline{C}(s)$ of the truncated convoluting function is obtained by substituting $p = 2\pi i s$ in $\overline{C}(p)$. The Fourier transform of the truncated convolution function C(t) is

$$\overline{C}(s) = \exp(2\pi i s a\delta) \int_{-\infty}^{\infty} \delta(N-1)\exp(-i\pi s'(2a+N-1)) \operatorname{sinc}(\pi s'\delta(N-1))\overline{f}(2\pi i(s-s'))ds' \tag{4.4.11}$$

Since one knows $\overline{f}(p)$ from the solution of the boundary value problem (4.1.1), one can solve for $\overline{C}^N$ as the periodic summation of the integral (4.4.11). From this, the convolution sequence C^N can be determined from (4.2.18).

4.5 EXAMPLE FOR REVERSIBLE SYSTEMS

4.5.1 Derivation of the Convolution Function

To show that the procedure suggested by Section 4.4 works, consider the application of this method to a simple reversible charge transfer system. For such a system the Laplace domain concentration profile is

$$\overline{C}(0,p) = \frac{C^*}{p} + \frac{\overline{\Gamma}(p)}{nFADp^{1/2}} \qquad (4.5.1)$$

so that the forcing function $\overline{f}(p)$ is $p^{-1/2}$. From the last section, the Fourier transform function $\overline{f}(s)$ equivalent to $\overline{f}(p)$ is $\overline{f}(s) = (2\pi is)^{-1/2}$. Substituting this into (4.4.11), one obtains

$$\overline{C}(s) = \exp(2\pi isa\delta) \int_{-\infty}^{\infty} \delta(N-1)\exp(-i\pi s'(2a+N-1)) \cdot \operatorname{sinc}(\pi s'\delta(N-1))(2\pi i(s-s'))^{-1/2} ds' \qquad (4.5.2)$$

If one assumes $a = 1/\pi$, as in (4.3.11), then

$$\overline{C}(s) = \frac{1}{\sqrt{\pi}} \exp(2is\delta) \int_{-\infty}^{\infty} \delta(N-1)\exp(-i\pi s'(2/\pi+N-1)) \cdot \operatorname{sinc}(\pi s'\delta(N-1))(2i(s-s'))^{-1/2} ds' \qquad (4.5.3)$$

Because the function $(2i(s-s'))^{-1/2}$ does have an analytic Fourier transformation, (4.5.3) can be simplified. Because the forward and backward Fourier transformations are inverse operators, (4.5.3) can be

written as

$$= \frac{\exp(2is\delta)}{\sqrt{\pi}} \int_{-\infty}^{\infty} \exp(-2\pi ist) \int_{-\infty}^{\infty} \exp(2\pi ist) \int_{-\infty}^{\infty} \delta(N-1)...ds' \; ds \; dt$$

$$= \frac{\exp(2is\delta)}{\sqrt{\pi}} \int_{-\infty}^{\infty} \exp(-2\pi ist) \int_{-\infty}^{\infty} \delta(N-1)\exp(-i\pi s'(2\pi+N-1)) \; \mathrm{sinc}(\pi s'\delta(N-1))$$

$$\left[\int_{-\infty}^{\infty} (2i(s-s'))^{-1/2}\exp(2\pi ist)ds\right] ds'dt \qquad (4.5.4)$$

The term in brackets is the inverse Fourier transform of $(2i(s-s'))^{-1/2}$. The Fourier transform of the function f(t) such that

$$f(t) = \begin{cases} t^{1/2}, & t \geq 0 \\ 0, & t < 0 \end{cases} \qquad (4.5.5)$$

is $(2is)^{-1/2}$. Therefore, the inverse transform of $(2i(s-s'))^{-1/2}$ is, by the shift theorem, $\exp(2\pi is't)f(t)$. Then

$$\overline{C}(s) = \frac{\exp(2is\delta)}{\sqrt{\pi}} \int_{-\infty}^{\infty} \exp(-2\pi ist)f(t)\left[\int_{-\infty}^{\infty} \delta(N-1)\exp(-i\pi s'((2/\pi+N-1))\right.$$

$$\left.\exp(2\pi is't)ds'\right] dt \qquad (4.5.6)$$

The term in brackets is the inverse Fourier transform of the Fourier

transform of the rectangle function $\Pi\left(\frac{t}{\delta(N-1)} - \frac{(2/\pi+N-1)}{2(N-1)}\right)$, and so

$$\overline{C}(s) = \frac{\exp(2is\delta)}{\sqrt{\pi}} \int_{-\infty}^{\infty} \Pi \frac{t}{\delta(N-1)} - \frac{(2/\pi+N-1)}{2(N-1)} f(t)\exp(-2\pi ist)dt \tag{4.5.7}$$

This is just

$$\overline{C}(s) = \frac{\exp(2is\delta)}{\sqrt{\pi}} \int_{\delta/\pi}^{\delta(1/\pi+N-1)} \frac{1}{\sqrt{t}} \exp(-2\pi ist)dt \tag{4.5.8}$$

Making the substitution $u^2 = 2\pi ist$,

$$\overline{C}(s) = \frac{\exp(2is\delta)}{\sqrt{\pi}(2\pi is)^{1/2}} \int_{(2is\delta)^{1/2}}^{(2\pi is\delta(1/\pi+N-1))^{1/2}} \exp(-u^2)du \tag{4.5.9}$$

From the definition of the error function

$$\overline{C}(s) = \frac{\exp(2is\delta)}{\sqrt{\pi}(2is)^{1/2}} \operatorname{erf}((2\pi is\delta(1/\pi+N-1))^{1/2}) - \operatorname{erf}((2is\delta)^{1/2}) \tag{4.5.10}$$

Following Section 4.2.4, and substituting $s = \nu/N\delta$ in (4.5.10), one obtains the final form of $\overline{C}(s)$ as

$$\bar{C}(\nu/N\delta) = \left(\frac{N\delta}{\pi}\right)^{1/2} \frac{\exp(2i\nu/N)}{(2i\nu)^{1/2}} \left[\mathrm{erf}\left((2\pi i(\nu/N)(1/\pi+N-1)\right)^{1/2}\right) - \mathrm{erf}\left((2i\nu/N)^{1/2}\right)\right] \qquad (4.5.11)$$

One then uses the definition of $\bar{C}_p(\nu/N\delta)$ of (4.2.22) to determine the DFT $\bar{C}^N$ of the convoluting sequence C^N.

In the practical application of this method, it is of course impossible to sum (4.2.22) from $k = -\infty$ to $k = \infty$. However, because of the $\nu^{-1/2}$ factor in (4.5.11), the function $\bar{C}(\nu/N\delta)$ is band-limited, and $\bar{C}(\nu/N\delta) \to 0$ as $\nu \to \infty$. A function

$$\bar{C}_p(\nu/N\delta) = \sum_{k=-\ell}^{\ell} \bar{C}\left((\nu/N+k)/\delta\right) \qquad (4.5.12)$$

will, for large enough ℓ, approximate the true $\bar{C}_p(\nu/N\delta)$ closely.

4.5.2 Construction of the Convolution Sequence C^N

Using (4.5.12) and (4.5.10) one can now construct the discrete Fourier transform pair of the convoluting sequence. This is done by means of the FORTRAN program FDOMSI.

In the program FDOMSI, for a given value of k, starting with k = 0, the values of $\bar{C}((\nu/N + k)/\delta)$ are calculated for $\nu = 0,1,\ldots, N-1$, where N is the number of points in the convolution sequence and for this work is set equal to 512. After all of the values of $\bar{C}((\nu/N + k)/\delta)$ have been calculated for a given k, the function $\bar{C}_p(\nu/N\delta)$ is

constructed by means of (4.5.11). One property of the CFT speeds the calculation of $\overline{C}_p(\nu/N\delta)$. If a time domain function f(t) is wholly real, as the function C(t) must be, since the concentration $C_i(o,t)$ to which it is related is physically observable, then the CFT of f(t), $\overline{f}(s)$, has the properties (2):

1) $\text{Re } \overline{f}(s) = \text{Re } \overline{f}(-s)$

2) $\text{Im } \overline{f}(s) = -\text{Im } \overline{f}(-s)$

Thus, after all of the $\overline{C}((\nu/N + k)/\delta)$ have been calculated for a given k, the $\overline{C}_p(\nu/N\delta)$ function is created by

$$\text{Re } \overline{C}_p\left(\frac{\nu}{N\delta}\right) = \text{Re } \overline{C}_p\left(\frac{\nu}{N\delta}\right) + \text{Re } \overline{C}\left(\frac{\nu}{N\delta} + \frac{k}{\delta}\right) + \text{Re } \overline{C}\left(\frac{N-\nu}{N\delta} + \frac{k}{\delta}\right)$$

$$\text{Im } \overline{C}_p\left(\frac{\nu}{N\delta}\right) = \text{Im } \overline{C}_p\left(\frac{\nu}{N\delta}\right) + \text{Im } \overline{C}\left(\frac{\nu}{N\delta} + \frac{k}{\delta}\right) - \text{Im } \overline{C}\left(\frac{N-\nu}{N\delta} + \frac{k}{\delta}\right) \quad (4.5.13)$$

This summation sums over the negative k as well as over the positive k, without explicitly calculating $\overline{C}((\nu/N + k)/\delta)$ for negative values of k. After the summation has been made, the process begins anew for k incremented by one. The process terminates when k reaches a limiting number of iterations ℓ, which is input to the program.

The error function terms in $\overline{C}((\nu/N + k)/\delta)$ are not calculated directly: instead, two different series approximations to the error functions are made. The absolutely convergent series approximation to the error function (24)

$$\text{erf}(x) = \frac{2}{\sqrt{\pi}}\left(x - \frac{x^3}{3} + \frac{x^5}{5\cdot 2!} - \frac{x^7}{7\cdot 3!} + \ldots\right) \qquad (4.5.14)$$

is used to approximate the error function term $\text{erf}((2i\nu/N)^{1/2})$.

For the numerical calculation of the discrete Fourier transform, the function $\overline{C}_p(\nu/N\delta)$ in (4.5.12) must be separated into real and imaginary parts. Letting $v = 2\nu/N$, and substituting $x = (iv)^{1/2}$ into (4.5.13), one has

$$\text{Re}\left[\left(\frac{\delta}{\pi}\right)^{1/2} \frac{\exp(iv)}{(iv)^{1/2}}\ \text{erf}\ ((iv)^{1/2})\right]$$

$$\frac{2\delta^{1/2}}{\pi}\left\{\cos v\left(1 - \frac{v^2}{5\cdot 2!} + \frac{v^4}{9\cdot 4!} - \ldots\right) + \sin v\left(\frac{v}{3} - \frac{v^3}{7\cdot 3!} + \frac{v^5}{11\cdot 5!} - \ldots\right)\right\}$$

$$\text{Im}\left[\left(\frac{\delta}{\pi}\right)^{1/2} \frac{\exp(iv)}{(iv)^{1/2}}\ \text{erf}\ ((iv)^{1/2})\right] =$$

$$\frac{2\delta^{1/2}}{\pi}\left\{\sin v\left(1 - \frac{v^2}{5\cdot 2!} + \frac{v^4}{9\cdot 4!} - \ldots\right) - \cos v\left(\frac{v}{3} - \frac{v^3}{7\cdot 3!} + \frac{v^5}{11\cdot 5!} - \ldots\right)\right\}$$

(4.5.15)

The series (4.5.14) is useful for small x, but for large x it is often impossible to evaluate because of computer roundoff error. Instead, for large x the folowing asymptotic approximation to erf(x) must be used (24)

$$\operatorname{erf}(x) = 1 - \frac{\exp(-x^2)}{\sqrt{\pi}\, x}\left(1 - \frac{1}{2x^2} + \frac{1\cdot 3}{(2x^2)^2} - \frac{1\cdot 3\cdot 5}{(2x^2)^3} + \ldots\right) \tag{4.5.16}$$

This series was used to evaluate the $\operatorname{erf}((2\pi i s(\nu/N)(1/\pi+N-1))^{1/2})$ term. Letting $w = 2\pi(\nu/N)(1/\pi+N-1)$, and substituting $x = (iw)^{1/2}$ into (4.5.16), one obtains

$$\operatorname{Re}\left[\left(\frac{\delta}{\pi}\right)^{1/2} \frac{\exp(iv)}{(iv)^{1/2}} \operatorname{erf}(iw)^{1/2}\right]$$

$$= \left(\frac{\delta}{\pi v}\right)^{1/2} \{\cos v\, \Sigma\,(1) - \sin v\, \Sigma\,(2)\}$$

$$\operatorname{Im}\left[\left(\frac{\delta}{\pi}\right)^{1/2} \frac{\exp(iv)}{(iv)^{1/2}} \operatorname{erf}(iw)^{1/2}\right]$$

$$= \left(\frac{\delta}{\pi v}\right)^{1/2} \{\sin v\, \Sigma\,(1) + \cos v\, \Sigma\,(2)\} \tag{4.5.17}$$

where

$$\Sigma(1) = \frac{1}{\sqrt{2}} + \frac{1}{\sqrt{\pi w}}\left\{\sin w\left(1 - \frac{1\cdot3}{(2w)^2} + \frac{1\cdot3\cdot5\cdot7}{(2w)^4} - \ldots\right)\right.$$
$$\left. - \frac{\cos w}{2w}\left(1 - \frac{1\cdot3\cdot5}{(2w)^2} + \frac{1\cdot3\cdot5\cdot7\cdot9}{(2w)^4} - \ldots\right)\right\}$$

$$\Sigma(2) = \frac{1}{\sqrt{2}} + \frac{1}{\sqrt{\pi w}}\left\{\cos w\left(1 - \frac{1\cdot3}{(2w)^2} + \frac{1\cdot3\cdot5\cdot7}{(2w)^4} - \ldots\right)\right.$$
$$\left. - \frac{\sin w}{2w}\left(1 - \frac{1\cdot3\cdot5}{(2w)^2} + \frac{1\cdot3\cdot5\cdot7\cdot9}{(2w)^4} - \ldots\right)\right\}$$

(4.5.18)

The entire $\overline{C}((\nu/N + k)/\delta)$ function for a given ν, k is the difference between (4.5.17) and (4.5.15).

After the discrete Fourier transform sequence was created by FDOMSI, the backward DFT of the sequence was taken and written to disk. The subroutine used to perform the back DFT was a Fast Fourier transform subroutine written in FORTRAN by Mertz (25). The back transform is the approximation to the convoluting sequence C^N defined by (4.3.11). The sequence created by FDOMSI for $\ell = 8$ is plotted as a function of τ in Figure 4.4. This sequence should be close to that defined by (4.3.11), and does appear to go as $t^{-1/2}$ except for the first and last points, which are too small. These latter points are in fact almost exactly half of the values of the convoluting sequence C^N defined by (4.3.11) at these points. This is an artifact of the method used to approximate the sequence. The rectangle function $\Pi(t)$

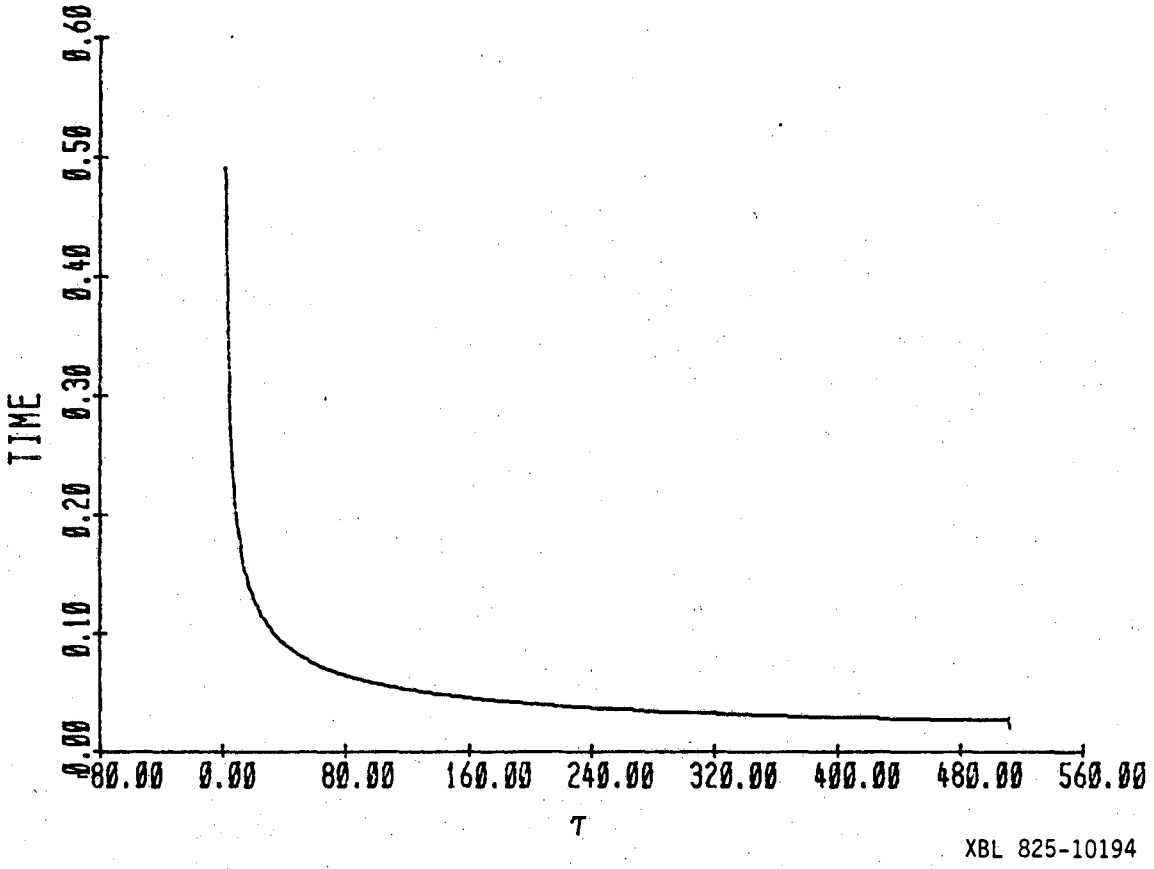

Figure 4.4: Convolution sequence C^N created by FDOMSI for $\ell = 8$.

was defined in Section 4.2.1 as being equal to 1/2 at $|t| = 1/2$; thus, the first and last points of the sequence are 1/2 of what they should be. This is easily rectified by multiplying the first and last points by two.

The best way to check the method is to use the convoluting sequences created by FDOMSI for different values of ℓ to semiintegrate voltammetric data by the process of sequential convolution. Figure 4.5 shows the semiintegral approximated by the sequential convolution of the sequence created by FDOMSI, with $\ell = 16$, and a simulated voltammogram of a classically reversible system. Also shown is the semiintegral created from the sequential convolution of the simulated voltammogram with the convoluting sequence defined by (4.3.11). It is seen that for $\ell = 16$, the convoluting sequences created by the method outlined in Section 4.4 result in a semiintegral that is indistinguishable from the semiintegral created by sequential convolution with the convoluting sequence defined by (4.3.11). The method of Section 4.4 works in the evaluation of the semiintegral.

4.6 CONSIDERATION OF MORE COMPLEX SYSTEMS

For systems like the reversible charge transfer, where the inverse Fourier transform of $\overline{f}(2\pi is)$ does exist, the method outlined in Section 4.4 is not necessary: for these systems one may derive an integral equation representation of the concentration profile in the time domain. For more complex systems, one must depend on the direct evaluation of (4.4.11) to determine the DFT of the convolution

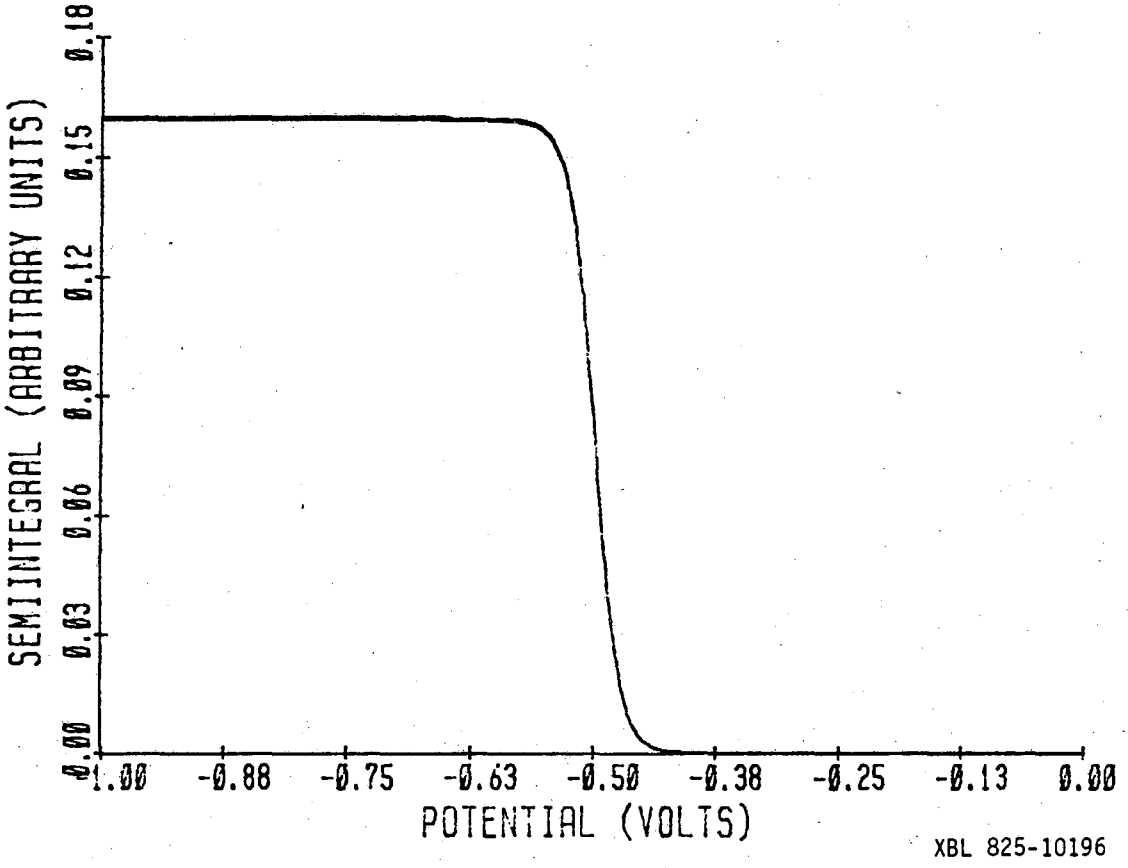

Figure 4.5: Semiintegrals of the voltammogram of Figure 4.3, created by sequential convolution with the sequence C^N of Figure 4.4, and by the sequential convolution of (4.3.9).

sequence C^N. This integral is impossible to evaluate directly since it contains a singularity at s' = s, and does not possess one of the special forms necessary for the application of Gaussian quadrature.

Equation 4.4.11 can be simplified, however. From (4.1.2), it is seen that the function $\overline{f}(p)$ of (4.1.1) has the form $\overline{f}(p)/p^{1/2}$. This means that (4.4.11) reduces to

$$\overline{C}(s) = \exp(2\pi isa\delta) \int_0^{\infty} \delta(N-1)$$

$$\exp(-i\pi s'(2a+N-1))\operatorname{sinc}(\pi s'\delta(N-1)) \frac{\overline{f}(2\pi i(s-s'))}{(2\pi i(s-s'))^{1/2}}\, ds \qquad (4.6.1)$$

Letting $\ell = \pi(2a+N-1)$, $m=\pi\delta(N-1)$, $n = 2\pi a\delta$, substituting for $\exp(-i\ell s')$ using de Moivre's theorem, and separating the integral into two integrals at s' = s, one obtains

$$\overline{C}(s) = \frac{\exp(ins)}{\pi\sqrt{2\pi i}}\left\{\int_{-\infty}^{s} \frac{\cos(\ell s')\sin(ms')\overline{f}(2\pi i(s-s'))ds'}{s'\sqrt{s-s'}}\right.$$

$$- i\int_{-\infty}^{s} \frac{\sin(\ell s')\sin(ms')\overline{f}(2\pi i(s-s'))ds'}{s'\sqrt{s-s'}}$$

$$- \int_{s}^{\infty} \frac{\sin(\ell s')\sin(ms')\overline{f}(2\pi i(s-s'))ds'}{s'\sqrt{s'-s}}$$

$$\left. - i\int_{s}^{\infty} \frac{\cos(\ell s')\sin(ms')\overline{f}(2\pi i(s-s'))ds'}{s'\sqrt{s'-s}}\right\} \qquad (4.6.2)$$

Making the substitution $u = (s-s')^{1/2}$ for the first two integrals, and $u = (s'-s)^{1/2}$ for the second two, one obtains

$$\overline{C}(s) = \frac{2\delta(N-1)\exp(ins)}{\pi\sqrt{2\pi i}} \left\{ \int_0^\infty \frac{\cos(\ell(s-u^2))\sin(m(s-u^2))\overline{f}(2\pi i u^2)du}{m(s+u^2)} \right.$$

$$- i \int_0^\infty \frac{\sin(\ell(s-u^2))\sin(m(s-u^2))\overline{f}(2\pi i u^2)du}{m(s+u^2)}$$

$$- i \int_0^\infty \frac{\cos(\ell(s+u^2))\sin(m(s+u^2))\overline{f}(-2\pi i u^2)du}{m(s+u^2)}$$

$$\left. - \int_0^\infty \frac{\sin(\ell(s+u^2))\sin(m(s+u^2))\overline{f}(-2\pi i u^2)du}{m(s+u^2)} \right\} \qquad (4.6.3)$$

Since $\overline{f}$ is known from (4.1.2), it looks to be possible to determine $\overline{C}(s)$ for many electrochemical systems using (4.6.3). None of the integrals in (4.6.3) have a singularity, and since the integrand goes as $(s+u^2)^{-1}$, it should be possible to truncate the evaluation of the integrals at some large u. This calculation is not suitable for a microcomputer like the LSI-11/23 used in this work, however. Further verification of the method outlined in this work awaits the calculation of (4.6.3) on some main frame computer.

4.7 CONCLUSIONS

This work has presented a method for the evaluation of convolution integrals in electrochemistry for systems in which the

form of the convolution integral is not known exactly. That this method works for the simple charge transfer system is shown by Figure 4.5, in which the semiintegral calculated by means of the transform method outlined in this work is seen to be identical to the semiintegral calculated by means of the time domain approximation used previously. This implies, for N large enough, that (4.6.1) can be used to evaluate convolution integrals of very complex systems. It then becomes possible to extend the benefits of convolutive voltammetric curve fitting, as described in Chapter 1, to these more complex systems. This extension is at present not possible by any other means.

It remains to be seen whether or not the implementation of (4.6.1) proves practical on a routine basis. At the present time, it is probably not practical for implementation on a small laboratory microcomputer. In the future, however, as laboratory microcomputers are interfaced to larger computers, or if the increases in the power of laboratory microcomputers continue, the transform method used in this work may prove suitable for the enhancement of the analysis of complex electrochemical systems.

References

1) H.E. Keller and W.H. Reinmuth, Anal. Chem. 44, 435 (1972)

2) R.N. Bracewell, "The Fourier Transformation and its Applications," 2nd ed., McGraw-Hill, New York, 1978

3) E.O. Brigham, "The Fast Fourier Transform," Prentice-Hall, New Jersey, 1974

4) P.R. Griffiths, ed., "Transform Techniques in Chemistry," Plenum Press, New York, 1978

5) A.J. Bard and L.R. Faulkner, "Electrochemical Methods," Wiley and Sons, New York, 1980

6) R.V. Churchill, "Operational Mathematics," 2nd ed., McGraw-Hill, New York, 1958

7) D.A. Ramsay, J. Am. Chem. Soc. 74, 72 (1952)

8) L. de Galan and J.D. Winefordner, Spectrochim. Acta B, 23, 277 (1968)

9) A. den Harder and L. de Galan, Anal. Chem. 46, 1464 (1974)

10) D.W. Kirmse and A.W Westerburg, Anal. Chem. 43, 1035 (1971)

11) A.L. Khidir and J.C. Decius, Spectrochim. Acta 18, 1629 (1962)

12) J.W. Cooley and J.W. Tukey, Math. Comput. 19, 297 (1965)

13) G.D. Bergland, I.E.E.E. Spectrum 6(7), 41 (1969)

14) J.W. Cooley, P.A. Lewis and P.D. Welch, IEEE Audio Trans. 15, 79 (1967)

15) A. Antoniou, "Digital Filters: Analysis and Design," McGraw-Hill, New York, 1979

16) R.B. Lam, R.C. Wieboldt and T.L. Isenhour, Anal. Chem. 53, 889A (1981)

17) J. W. Hayes, D.E. Glover, D.E. Smith and M.W. Overton, Anal. Chem. 45, 277 (1973)

18) J. Liouville, J. Ecole Polytechn. 13, 71 (1832)

19) M. Reisz, Acta Math. 81, 1 (1949)

20) B. Riemann, "The Collected Works of Bernhard Riemann," H. Weber, ed., 2nd ed., Dover, New York, 1953

21) K.B. Oldham and J. Spanier, "The Fractional Calculus," Vol. 111 in Mathematics in Science and Engineering Series, Academic Press, New York, 1974

22) A.K. Grunwald, Z. Angew. Math. Phys. 12, 441 (1867)

23) H.L. Suprenant, T.H. Ridgeway and C.N. Reilly, J. Electroanal. Chem. 75, 125 (1977)

24) B.O. Pierce and R.M. Foster, "A Short Table of Integrals," Ginn and Co., Boston , Mass., 1957

25) L. Mertz, Appl. Optics 10, 386 (1971)

POSTSCRIPT:

GENERAL CONCLUSIONS

This work has tried to show the advantages of the application of sophisticated data analysis techniques to digitized electrochemical data. The acquisition of such data is dependent upon the existence of cheap, fast, laboratory microcomputers, so that the author is grateful to the computer people in Silicon Valley and elsewhere, although he doubts that the advances in computer technology have been made purely for his benefit.

In this work methods have been outlined for the determination of system parameters for simple electrochemical systems. One of the methods outlined, semiderivative voltammetric curve fitting, has been shown to be effective in fitting waves of several electrochemical systems. The next logical step is to apply other convolutive voltammetric curve fitting techniques to the determination of system parameters for other systems. This will prove (or disprove) the theories of Nicholson and Shain (1) and Saveant and Vianello (2) about the behavior of linear sweep voltammetric systems in several limiting cases of kinetic behavior.

S.v.c.f. has been shown to be effective in the resolution of some overlapped lsv and asv waves. Although it was stated to be impossible to use other c.v.c.f. techniques in the resolution of overlapped voltammetric waves, it may in fact be possible, only very difficult. Certainly it will require the use of a mainframe computer. This may not be a severe handicap, however, and some work could be done on this problem, especially on using c.v.c.f. techniques to resolve waves of systems for which some parameters (such as rate

constants and equilibrium constants) are known from single peak investigations.

To the author, the most interesting part of this work is the fourth chapter. This is because the method outlined in this chapter allows, in theory, the extension of c.v.c.f. techniques to many more electrochemical systems than has been previously possible. The next step in the development of the methods of Chapter 4 is the evaluation of equations like (4.4.11) for systems described by (4.1.1), and applying the evaluation methods to real data. If the method is found to be useful for these real systems, the scope of future applications for this method is virtually unlimited.

References

1) R.S. Nicholson and I. Shain, Anal. Chem. 36, 706 (1964)

2) J.M. Saveant and E. Vianello, Electrochem. Acta 12, 629 (1967)

APPENDIX I: Glossary

A.I.1 Glossary of Symbols

A	Surface area of electrode
C_i	Concentration of component i
C_i^*	Bulk concentration of component i
D_i	Diffusion constant
e	Semiderivative
E	Potential
E	Standard potential
$E^{o'}$	Formal potential
$E^r_{1/2}$	Reversible half-wave potential
E_i	Initial potential
E_p	Potential at peak maximum
$E_{p/2}$	Potential at half peak maximum
$\overline{f}(p)$	Laplace transform pair of function f(t)
$\overline{f}(s)$	Fourier transform pair of function f(t)
f^N	Sequence of N values
$f^N(\tau)$	τ^{th} element of a sequence of N values
$\overline{f}^N$	Discrete Fourier transform pair of a sequence of N values
F	Faraday constant
i	Current, square root of -1
i^*	Limiting current
i_p	Current at peak maximum
i_f	Faradaic current
i_c	Capacitive current

k^o	Charge transfer rate constant
k_f	Forward homogeneous rate constant
k_b	Backward homogeneous rate constant
K	Equilibrium constant
ℓ	Solution layer thickness
m	Semiintegral
m^*	Limiting value of semiintegral
n	Number of electrons
p	Laplace variable
r^2	Linear least squares regression coefficient
R	Gas constant
R^2	Coefficient of determination
s	Fourier variable
s^2	Variance of linear least squares fit
S(a)	Error sum of squares
t	Time
T	Temperature
x	Distance from electrode surface
α	Transfer coefficient
λ	Dimensionless homogeneous rate constant
Λ	Dimensionless charge transfer rate constant
ν	Scan rate, index for frequency domain sequence
χ	Dimensionless distance variable
τ	Dimensionless time variable, index of time domain sequence
Γ	Euler Gamma function

A.I.2 Glossary of Abbreviations

asv	Anodic stripping voltammetry
CFT	Continuous Fourier transform
c.p.s.v.	Convolutive potential sweep voltammetry
c.v.c.f.	Convolutive voltammetric curve fitting
DEC	Digital Equipment Corporation
DFT	Discrete Fourier transform
lsv	Linear sweep voltammetry
HMDE	Hanging mercury drop electrode
PAR	Princeton Applied Research (Corp.)
S/N	Signal to noise ratio
s.v.c.f.	Semiderivative voltammetric curve fitting

APPENDIX II: SOLUTION TO BOUNDARY VALUE PROBLEMS

A.II.1: Solution for the simple charge transfer system.

Restatement of the problem:

For the charge transfer reaction

$$Ox + ne^- \overset{k^o}{=} Red \qquad \text{(A.II.1)}$$

if it is assumed that mass transport is due solely to diffusion, and that diffussion can be assumed to be linear, then the Fick's second law equations are

$$\frac{\partial C_{ox}}{\partial t} = D_{ox} \frac{\partial^2 C_{ox}}{\partial x^2}$$

$$\frac{\partial C_{red}}{\partial t} = D_{red} \frac{\partial^2 C_{red}}{\partial x^2} \qquad \text{(A.II.2)}$$

Two boundary conditions are, with the assumption of semi-infinite diffusion,

$$C_{ox}(x,t=0) = C_{ox}(x=\infty,t) = C_{ox}^*$$

$$C_{red}(x,t=0) = C_{red}(x=\infty,t) = 0 \qquad \text{(A.II.3)}$$

Another boundary condition results from Fick's first law

$$D_{ox}\left(\frac{\partial C_{ox}}{\partial x}\right)_{x=0} = -D_{red}\left(\frac{\partial C_{red}}{\partial x}\right)_{x=0} = \frac{i(t)}{nFA} \qquad \text{(A.II.4)}$$

The first step in the solution of the boundary value problem is the Laplace transformation of (A.II.2). A review of the Laplace transformation as applied to the solution of electrochemical boundary value problems is given in Bard and Faulkner (Ref. 75 in Chapter 1). The definition of the Laplace transformation $\bar{f}(p)$ of a function $f(t)$ is

$$\bar{f}(p) = \int_0^\infty f(t)\, e^{-pt}\, dt \qquad \text{(A.II.5)}$$

so that the Laplace transformation of the first equation of (A.II.2) is

$$\int_0^\infty \frac{\partial C_{ox}}{\partial t}\, e^{-pt}\, dt = D_{ox}\int_0^\infty \frac{\partial^2 C_{ox}}{\partial x^2}\, e^{-pt}\, dt$$

Since the integral on the r.h.s. is independent of x, one may rewrite this latter equation as

$$\int_0^\infty \frac{\partial C_{ox}}{\partial t}\, e^{-pt}\, dt = D_{ox}\frac{\partial}{\partial x^2}\left\{\int_0^\infty C_{ox}\, e^{-pt}\, dt\right\}$$

But the term in brackets is just the Laplace transformation of the concentration $\overline{C}_{ox}$, so that

$$\int_0^\infty \frac{\partial C_{ox}}{\partial t} e^{-pt} dt = D_{ox} \frac{\partial^2 \overline{C}_{ox}}{\partial x^2} \qquad \text{(A.II.6)}$$

The integral on the l.h.s. is evaluated by integration by parts.

$$D_{ox} \frac{\partial^2 \overline{C}_{ox}}{\partial x^2} = C_{ox}(x,t)\, e^{-pt} \Big|_{t=0}^{\infty} + p \int_0^\infty C_{ox}\, e^{-pt} dt$$

At $t = \infty$, $\exp(-pt) = 0$; from (A.II.3), $C_{ox}(x,t=0) = C_{ox}^*$. Therefore

$$D_{ox} \frac{\partial^2 \overline{C}_{ox}}{\partial x^2} = -C_{ox}^* + p\, \overline{C}_{ox} \qquad \text{(A.II.7)}$$

Similarly, one can derive for the reduced species

$$D_{red} \frac{\partial^2 \overline{C}_{red}}{\partial x^2} = p\, \overline{C}_{red} \qquad \text{(A.II.8)}$$

These last two equations reveal the utility of the Laplace transformation technique: the partial differential equations in time and space are reduced to ordinary differential equations in space alone. The solution to (A.II.7) is

$$\bar{C}_{ox} = \frac{C^*_{ox}}{p} - \left(\frac{D_{ox}}{p}\right)^{1/2} \left(\frac{\partial \bar{C}_{ox}}{\partial x}\right)_{x=0} \exp\left(-\left(\frac{p}{D_{ox}}\right)^{1/2} x\right) \qquad \text{(A.II.9)}$$

and to (A.II.8) is

$$\bar{C}_{red} = -\left(\frac{D_{red}}{p}\right)^{1/2} \left(\frac{\partial \bar{C}_{red}}{\partial x}\right)_{x=0} \exp\left(-\left(\frac{p}{D_{red}}\right)^{1/2} x\right) \qquad \text{(A.II.10)}$$

One is interested in the surface concentration of both species, and so, substituting x = 0 in (A.II.9) and (A.II.10)

$$\bar{C}_{ox}(x=0,p) = \frac{C^*_{ox}}{p} - \left(\frac{D_{ox}}{p}\right)^{1/2} \left(\frac{\partial \bar{C}_{ox}}{\partial x}\right)_{x=0} \qquad \text{(A.II.11)}$$

$$\bar{C}_{red}(x=0,p) = -\left(\frac{D_{red}}{p}\right)^{1/2} \left(\frac{\partial \bar{C}_{red}}{\partial x}\right)_{x=0}$$

Taking the Laplace transformation of (A.II.4), and substituting this into (A.II.11), one obtains

$$\bar{C}_{ox}(0,p) = \frac{C^*_{ox}}{p} - \frac{\bar{i}(p)}{\sqrt{D_{ox}p}\ nFA} \qquad (A.II.12)$$

$$\bar{C}_{red}(0,p) = \frac{\bar{i}(p)}{\sqrt{D_{red}p}\ nFA}$$

where $\bar{i}(p)$ is the Laplace transformation of the current $i(t)$.

The solution for the surface concentrations of Ox and Red can then be found by taking the back transform of (A.II.12). The back transform of $\bar{C}_{ox}(o,p)$ is $C_{ox}(o,t)$, the back transform of $\bar{C}_{red}(o,p)$ is $C_{red}(o,t)$, and the back transform of C^*_{ox}/p is C^*_{ox}. The back transforms of the other terms are found indirectly, by means of the convolution theorem. The Laplace transform convolution theorem says that if two functions $\bar{f}(p)$ and $\bar{g}(p)$ have back transforms $f(t)$ and $g(t)$ respectively, then the product $\bar{f}(p)\bar{g}(p)$ has the back transform $f(t)*g(t)$, where this latter expression is called the convolution of f and g and is defined by

$$f*g = \int_0^t f(\tau)g(t-\tau)d\tau = \int_0^t f(t-\tau)g(\tau)d\tau \qquad (A.II.13)$$

Since the transform of $\bar{i}(p)$ is $i(t)$, and $p^{-1/2}$ has the transform $t^{-1/2}$,

$$C_{ox}(0,t) = C^*_{ox} - \frac{1}{\sqrt{D_{ox}}\, nFA} \int_0^t \frac{i(\tau)d\tau}{\sqrt{t-\tau}}$$

$$C_{red}(0,t) = \frac{1}{\sqrt{D_{red}}\, nFA} \int_0^t \frac{i(\tau)d\tau}{\sqrt{t-\tau}} \qquad \text{(A.II.14)}$$

Making the change of variable $\gamma = E_i - \nu\tau$, and substituting in $E = E_i - \nu t$,

$$C_{ox}(0,E) = C^*_{ox} - \frac{1}{nFA\,\sqrt{D_{ox}\nu}} \int_E^{E_i} \frac{i(\gamma)d\gamma}{\sqrt{\gamma-E}}$$

$$C_{red}(0,E) = \frac{1}{nFA\,\sqrt{D_{red}\nu}} \int_E^{E_i} \frac{i(\gamma)d\gamma}{\sqrt{\gamma-E}} \qquad \text{(A.II.15)}$$

A.II.2: Solution for the CE mechanism.

Restatement of the problem:

Consider a reaction

$$C \underset{k_b}{\overset{k_f}{\rightleftharpoons}} Ox$$

$$Ox + ne^- = Red \qquad \text{(A.II.16)}$$

Assuming semi-infinite, linear diffusion, the partial differential equations describing this system are

$$\frac{\partial C_c}{\partial t} = D_c \frac{\partial^2 C_c}{\partial x^2} + k_b C_{ox} - k_f C_c$$

$$\frac{\partial C_{ox}}{\partial t} = D_{ox} \frac{\partial^2 C_{ox}}{\partial x^2} - k_b C_{ox} + k_f C_c \qquad \text{(A.II.17)}$$

$$\frac{\partial C_{red}}{\partial t} = D_{red} \frac{\partial^2 C_{red}}{\partial x^2}$$

with boundary conditions

$$C_{ox}(x,t=0) = C_{ox}(x=\infty,t) = C_{ox}^*$$

$$C_{red}(x,t=0) = C_{red}(x=\infty,t) = 0 \qquad \text{(A.II.18)}$$

$$C_c(x,t=0) = C_c(x=\infty,t) = C_c^* = \frac{C_{ox}^*}{K}$$

where $K = k_f/k_b$. The last boundary condition is the Fick's first law equation

$$\left(\frac{\partial C_c}{\partial x}\right)_{x=0} = 0, \quad D_{ox}\left(\frac{\partial C_{ox}}{\partial x}\right)_{x=0} = -D_{red}\left(\frac{\partial C_{red}}{\partial x}\right)_{x=0} = \frac{i(t)}{nFA} \qquad \text{(A.II.19)}$$

The solution of (A.II.17) is made simpler by a change of variable. Letting

$$f(x,t) = C_{ox}(x,t) + C_c(x,t)$$

$$g(x,t) = C_c(x,t) \qquad \text{(A.II.20)}$$

and substituting (A.II.20) into (A.II.17), and (for simplicity) assuming $D = D_c = D_{ox} = D_{red}$, one obtains upon rearrangement

$$\frac{\partial f}{\partial t} = D \frac{\partial^2 f}{\partial x^2}$$

$$\frac{\partial g}{\partial t} = D \frac{\partial^2 g}{\partial x^2} - kg \qquad \text{(A.II.21)}$$

$$\frac{\partial C_{red}}{\partial t} = D \frac{\partial^2 C_{red}}{\partial x^2}$$

where $k = k_f + k_b$.

Taking the Laplace transformation of each of (A.II.21), one obtains

$$\frac{\partial^2 \bar{f}}{\partial x^2} = \frac{p}{D} \bar{f} - \frac{C_c^* + C_{ox}^*}{D}$$

$$\frac{\partial^2 \bar{g}}{\partial x^2} = \frac{p+k}{D} \bar{g} \qquad \text{(A.II.22)}$$

$$\frac{\partial^2 \bar{C}_{red}}{\partial x^2} = \frac{p}{D} \bar{C}_{red}$$

The solutions to these differential equations are

$$\bar{f} = -\left(\frac{D}{p}\right)^{1/2}\left(\frac{\partial \bar{f}}{\partial x}\right)_{x=0} \exp\left(-\left(\frac{p}{D}\right)^{1/2} x\right) + \frac{C_c^* + C_{ox}^*}{p}$$

$$\bar{g} = -\left(\frac{D}{p+K}\right)^{1/2}\left(\frac{\partial \bar{g}}{\partial x}\right)_{x=0} \exp\left(-\left(\frac{p+k}{D}\right)^{1/2} x\right) \qquad \text{(A.II.23)}$$

$$C_{red} = -\left(\frac{D}{p}\right)^{1/2}\left(\frac{\partial \bar{C}_{red}}{\partial x}\right)_{x=0} \exp\left(-\left(\frac{p}{D}\right)^{1/2} x\right)$$

The desired solution is in terms of $\bar{C}_{ox}$. From (A.II.20), and because the Laplace transformation operator is linear, $\bar{C}_{ox} = \frac{K}{K+1}(\bar{f} - \bar{g})$. So

$$\bar{C}_{ox} = \frac{K}{K+1}\left\{\frac{C_c^* + C_{ox}^*}{p} - \left(\frac{D}{p}\right)^{1/2}\left(\frac{\partial \bar{f}}{\partial x}\right)_{x=0} \exp\left(-\left(\frac{p}{D}\right)^{1/2} x\right)\right.$$

$$\left. + \left(\frac{D}{p+k}\right)^{1/2}\left(\frac{\partial \bar{g}}{\partial x}\right)_{x=0} \exp\left(-\left(\frac{p+k}{D}\right)^{1/2} x\right)\right\} \qquad \text{(A.II.24)}$$

But (A.II.19) implies that

$$\left(\frac{\partial \bar{f}}{\partial x}\right)_{x=0} = \left(\frac{\partial \bar{C}_{ox}}{\partial x}\right)_{x=0} = -K\left(\frac{\partial \bar{g}}{\partial x}\right)_{x=0}$$

Therefore

$$\overline{C}_{ox} = \left(\frac{K}{K+1}\right)\frac{C_c^* + C_{ox}^*}{p} + \frac{K}{K+1}\left(\frac{\partial \overline{C}_{ox}}{\partial x}\right)_{x=0}\left\{-\left(\frac{D}{p}\right)^{1/2}\exp\left(-\left(\frac{p}{D}\right)^{1/2}x\right)\right.$$

$$\left. - \frac{1}{K}\left(\frac{D}{p+k}\right)^{1/2}\exp\left(-\left(\frac{p+k}{D}\right)^{1/2}x\right)\right\} \qquad \text{(A.II.25)}$$

Then $\overline{C}_{red}$ (o,p) and $\overline{C}_{ox}$ (o,p) are

$$\overline{C}_{ox}(0,p) = \left(\frac{K}{K+1}\right)\frac{C_c^* + C_{ox}^*}{p} + \frac{K}{K+1}\left(\frac{\partial \overline{C}_{ox}}{\partial x}\right)_{x=0}\left\{-\left(\frac{D}{p}\right)^{1/2} - \frac{1}{K}\left(\frac{D}{p+k}\right)^{1/2}\right\} \qquad \text{(A.II.26)}$$

$$\overline{C}_{red}(0,p) = -\left(\frac{D}{p}\right)^{1/2}\left(\frac{\partial \overline{C}_{red}}{\partial x}\right)_{x=0}$$

From (A.II.19), and since $C_c^* = C_{ox}^*/K$,

$$\overline{C}_{ox}(0,p) = \frac{C_{ox}^*}{p} + \frac{K}{K+1}\,\frac{\overline{i}(p)}{DnFA}\left\{-\left(\frac{D}{p}\right)^{1/2} - \frac{1}{K}\left(\frac{D}{p+k}\right)^{1/2}\right\} \qquad \text{(A.II.27)}$$

$$\overline{C}_{red}(0,p) = \frac{\overline{i}(p)}{nFA\sqrt{Dp}}$$

The shift theorem for Laplace transformations says that if $\overline{f}(p)$ has the inverse Laplace transform f(t), then $\overline{f}(p + a)$ has the inverse transform exp(-at) f(t). Therefore the inverse transform of $(p + k)^{-1/2}$ is $\exp(-kt)\, t^{-1/2}$. Then, using the convolution theorem as before to find the back transform of (A.II.27),

$$C_{ox}(0,t) = C^{*}_{ox} - \frac{1}{\sqrt{D}\, nFA} \int_{0}^{t} \left\{ \frac{K}{K+1} + \frac{\exp[-k(t-\tau)]}{K+1} \right\} \frac{i(\tau)d\tau}{\sqrt{t-\tau}}$$

(A.II.28)

$$C_{red}(0,t) = \frac{1}{\sqrt{D}\, nFA} \int_{0}^{t} \frac{i(\tau)d\tau}{\sqrt{t-\tau}}$$

Substituting $\gamma = E_i - \nu\tau$, and $E = E_i - \nu t$, one has

$$C_{ox}(0,E) = C^{*}_{ox} - \frac{1}{nFA\sqrt{D\nu}} \int_{E}^{E_i} \left\{ \frac{K}{K+1} + \frac{\exp\left[-\lambda\left(\frac{nF}{RT}\right)(\gamma-E)\right]}{K+1} \right\} \frac{i(\gamma)d\gamma}{\sqrt{\gamma-E}}$$

$$C_{red}(0,E) = \frac{1}{nFA\sqrt{D\nu}} \int_{E}^{E_i} \frac{i(\gamma)d\gamma}{\sqrt{\gamma-E}} \qquad \text{(A.II.29)}$$

TECHNICAL INFORMATION DEPARTMENT
LAWRENCE BERKELEY LABORATORY
UNIVERSITY OF CALIFORNIA
BERKELEY, CALIFORNIA 94720